



Norwegian University of
Science and Technology

Improved Energy Efficiency with Solar Panels in Combinations with Cooling / Heating System

Chengyang Jiang

Sustainable Energy

Submission date: December 2017

Supervisor: Trygve Magne Eikevik, EPT

Norwegian University of Science and Technology
Department of Energy and Process Engineering

Preface

Nowadays, with the unceasing human population growth and fast economic development, the global energy demand is also increasing unceasingly. Meanwhile, the increasing carbon dioxide emission has become a significant environmental problem. According to the International Energy Outlook 2017 written by U.S. Energy Information Administration (EIA), world energy consumption increases from 370 quadrillion British thermal units (Btu) in 1990 to 660 quadrillion Btu by 2030 then to 740 quadrillion Btu by 2040. Based on the model of EIA, most of the increase in energy consumption will come from developing countries which have strong economic growth and quickly growing populations.

At the same time, the world energy-related carbon dioxide emissions are expected to have an average 0.6% per year growth from 2015 to 2040 while the average growth is 1.3% per year between 1990 and 2015.

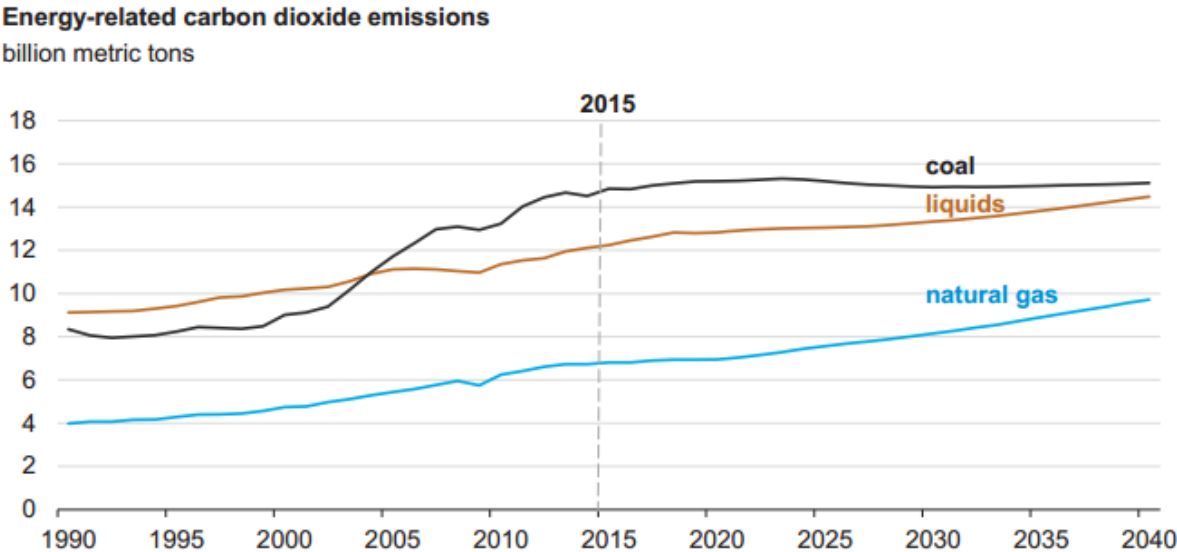


Fig. 1 World total carbon dioxide emissions of coal, liquids and natural gas by EIA (2017)

There are two main reasons which slow down the growth of energy-related carbon dioxide emissions, the first one is the increasing energy efficiency because of the new science and technology, the second one is the gradual shift from coal toward natural gas and renewable energy sources, which is indicated by Fig. 1.

As shown in Fig. 2, although China has reduced the use of coal and started using natural

gas, nuclear power and renewable energy, China remains the world’s largest user of coal. As a big responsible nation, China insists the Common but Differentiated Responsibility Principle, and assumes the responsibility for reducing carbon dioxide emissions. In this case, we have to not only develop new technologies to improve the energy efficiency but also improve the proportion of renewable energy like solar energy, wind power.

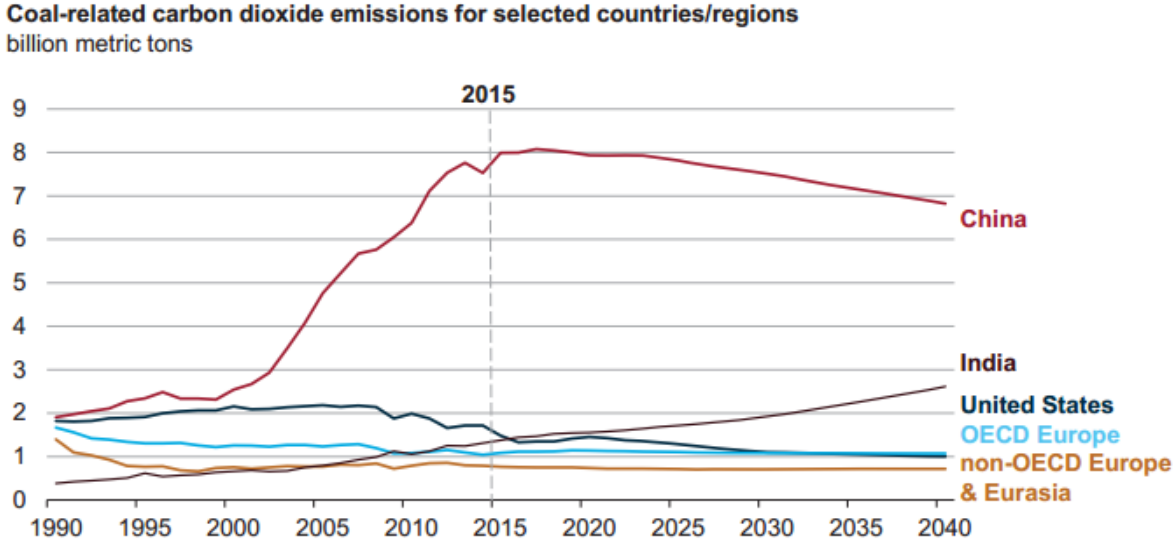


Fig. 2 Coal-related carbon dioxide emissions of some countries/regions by EIA (2017)

Fig. 3 shows the energy consumption of three main sectors, industrial sector, transportation sector and building sector. The industrial sector, which includes agriculture, construction, manufacturing and mining, is the world’s largest energy-consuming sector. Building energy has now accounted for about 20% of the primary energy consumption all over the world, and in some developed regions, the number may reach 45%. According to the report, world industrial sector energy use rises by 0.7% per year from 2015 to 2040, while the increase for transportation is 1.0% per year and the increase for buildings is 1.1% per year. Therefore, building energy consumption will account for more and more proportion in the future. In 2009, the building energy consumption accounted 23.39% of the primary energy consumption in China, and this number will increase in the future because of the fast growing building area.

In particular, building sector has the largest potential of energy saving among all sectors. We don’t have to do many changes to make our buildings more energy efficient. Replacing traditional light bulbs with LED lights, Upgrading HVAC systems can save much energy. What’s more, many places in China are still using coal for domestic heating, which is inefficient

and environmentally unfriendly. With the development of heat pump technology, we can use heat pump for domestic hot water producing and space heating in the near future.

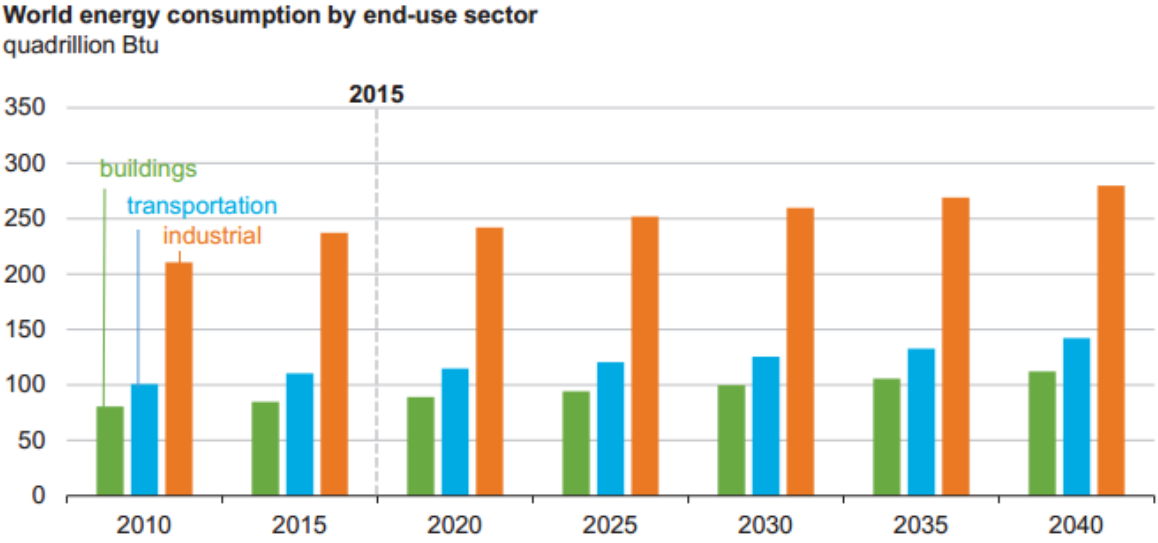


Fig. 3 World energy consumption of different sectors by EIA (2017)

Solar energy is an important source of renewable energy and its technologies are broadly characterized as either passive solar or active solar depending on how they capture and distribute solar energy or convert it into solar power. In 2011, the IEA (International Energy Agency) said that "the development of affordable, inexhaustible and clean solar energy technologies will have huge longer-term benefits. It will increase countries' energy security through reliance on an indigenous, inexhaustible and mostly import-independent resource, enhance sustainability, reduce pollution, lower the costs of mitigating global warming, and keep fossil fuel prices lower than otherwise. These advantages are global. Hence the additional costs of the incentives for early deployment should be considered learning investments; they must be wisely spent and need to be widely shared".

China has advantageous solar energy resources compared with other countries which share the same latitude. Fig. 4 shows the solar energy distribution in China, the annual sunshine duration of over 2/3 national area is more than 2000 hours. The annual solar irradiance of most cities in China is over $5.86 \times 10^6 \text{ kJ/m}^2$. Therefore, in China, the comprehensive utilization of solar has great development potential and it can optimize the energy structure and contribute to environmental protection. With the support from government, solar energy is uniquely advantageous in various ways and has broad market prospect. Actually, China is the world's

largest market for both solar thermal energy and photovoltaics.

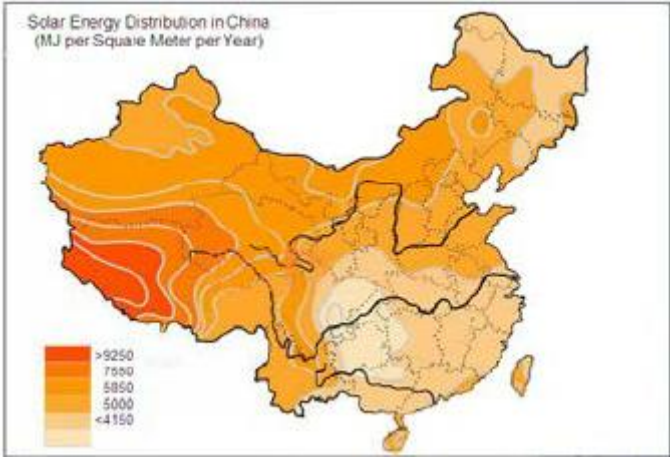


Fig. 4 Solar energy distribution in China

Since 2013, China has become the global leading installer of solar photovoltaic. Two years later, China narrowly surpassed Germany and became the world’s largest producer of photovoltaic power. By the end of 2016, total capacity reached 77.4GW, and in 2017 China was the first country to pass 100GW. Meanwhile, by the end of 2014, the solar water heating capacity of China was 290GWth, accounting for about 70% of the total world capacity. Rooftop solar water heaters are ubiquitous in China.

The idea of this thesis came from comprehensive utilization of solar photovoltaic and solar thermal power. By combining PV panel and refrigeration system, it can not only improve the panel conversion efficiency by reducing the cell temperature but also produce domestic hot water by recovering the thermal power from the solar radiation which is not converted into electricity.

Acknowledgement

First of all, I'd like to show my sincere appreciation for the guidance from my two supervisors Trygve Magne Eikevik and Yanjun Dai throughout the project. Professor Dai taught me the basic knowledge about heat pump and solar energy utilization which played an important role in my project. Professor Eikevik helped me learn more knowledge about the components of refrigeration systems and system design. He also introduced the importance of natural refrigerants as a future alternative in heat pump and refrigeration. When I met some problems, professor Eikevik could always give me a good solution. What's more, since I'm a foreign student from China, Professor Eikevik also cared about my life in Norway.

I also want to express my thanks to Inge Havard Rekstad and Zhequan Jin. Inge Havard Rekstad is a senior engineer from EPT and Zhequan Jin was a PhD candidate of NTNU. They always helped out when I needed support with my test rig or any problems during the experiments. Inge Havard Rekstad gave me some good suggestions when I built my test rig and the discussion between us helped me have a better understanding of my project.

Technicians from the Lab like Lars Konrad Sorensen, Aleksander Mosand should also be thanked for helping me build up the test rig. Sometimes I just changed my plans and they always helped me with great patience.

A thanks should also be given to SJTU and NTNU. It is a great honor to have the chance to participate in this joint master program. Studying and living in Norway for one year has been one of the most wonderful experiences in my life.

Finally, I would like to thank my family and my friends for their continuous support throughout my education.

Summary

Nowadays, with the unceasing human population growth and fast economic development, the global energy demand is also increasing unceasingly. Meanwhile, the increasing carbon dioxide emission has become a significant environmental problem. Building energy has now accounted for about 1/5 of the primary energy consumption all over the world. The number in China was 23.39% in 2009 and it is still growing fast. In particular, building sector has great potential of energy saving. With the development of renewable energy like solar energy and wind power, the energy structure in China can be more reasonable. What's more, part of the heating demand can be covered by heat pump whose efficiency is much higher than electric heating and gas heating.

The conversion efficiency of a photovoltaic (PV) cell is greatly influenced by its temperature. According to experimental results, every 1°C rise in cell temperature reduces the conversion efficiency by about 0.4% for multi-crystalline cells. Therefore, many researches have been done to decrease the PV panel temperature to increase the performance. Different types of PV/T collectors were developed to realize the comprehensive utilization of solar photovoltaic/thermal (PV/T) energy. The main difference of these collectors is working media which can be air, water, refrigerant and heat pipe.

When the air or the water was used as working media of PV/T collectors, it was usually heated to a high temperature for direct heating usage. This was actually on the opposite direction of conversion efficiency improvement. In this thesis, a PV panel was combined with a heat pump system. The refrigerant used in this work is propane (R290) and it is an environmental friendly working fluid whose ODP and GWP is 0 and 3. The evaporator of the heat pump was fixed under the PV panel. This combination, which is called PV evaporator in the following, can improve the conversion efficiency by cooling the PV cells and absorb solar thermal energy to produce hot water with the help of heat pump at the same time. What's more, the temperature of refrigerant is constant and relatively low during evaporation, this is good for the performance of PV cells.

Based on the concepts above, a test rig of PV/T heat pump system was designed and built.

Experimental researches were taken under summer weather conditions of Trondheim. According to the experimental results, the conversion efficiency of the PV panel can reach 15.5% in the best case, it was increased by 6.9% compared with the nominal value. The efficiency was influenced by solar radiation, ambient temperature and angle of incidence. A higher ambient temperature leads to a lower efficiency. The influence of the solar irradiance is complicated, ordinarily, a higher solar radiation may cause a decline in efficiency. The PV evaporator can absorb heat both from solar radiation and environment, the heat-collecting efficiency ranged from 0.45 to 0.77 in the tests. The COP of the heat pump is greatly influenced by the condenser supply water temperature. COP decreases with the increasing condenser supply water temperature. Solar radiation and ambient temperature have a positive impact on COP. The average COP of the heat pump can reach 4.3 when the water was heated from 14.8°C to 50.6°C. The fractional errors of the measured conversion efficiency, COP are 5% and 5.2%.

Simulation of the test rig was made by EES to study the performance of PV/T heat pump system at different places and climates. The effectiveness of the simulation was validated by comparing the simulated results and experimental results. Daily performance analysis on April 30 in Shanghai was done, and it indicated that a higher air temperature leads to a better comprehensive performance. Annual operation simulated results in Shanghai, Oslo, New Delhi were analyzed. Monthly average value of air temperature, solar radiation and wind speed was adopted as the rated condition for annual performance evaluation. The annual average COP in Shanghai, Oslo, New Delhi are 3.5, 2.8 and 4.4, respectively. And the annual average conversion efficiency in Shanghai, Oslo, New Delhi are 16.4%, 17.3%, 15.5%. An air evaporator in parallel and an inverter compressor can be used to improve the performance in cold environment without sufficient sunlight.

Content

Preface	i
Acknowledgement.....	v
Summary	vi
Content	1
List of Figures	1
List of Tables	4
Nomenclature	5
1 Introduction	1
2 Objectives.....	2
3 Literature review	3
3.1 Photovoltaic(PV) Panel.....	3
3.2 PV/T collector	5
3.3 Heat pump	6
3.3.1 Refrigerants	6
3.3.2 classification.....	7
3.4 PV solar assisted heat pump.....	8
3.5 Plate heat exchanger.....	12
3.5.1 Geometry.....	12
3.5.2 Correlations for single phase heat transfer.....	14
3.5.3 Correlations for condensation heat transfer	16
4 Theory	19
4.1 Mathematical model.....	19
4.1.1 Heat flow at the PV panel	19
4.1.2 Compressor.....	21
4.1.3 Evaporator	21
4.1.4 Thermostatic expansion valve.....	22
4.1.5 Water-cooled condenser	23

4.2 Performance indicators.....	23
4.3 Chapter summary	24
5 Experimental investigation.....	25
5.1 Description of the test rig	25
5.1.1 Test rig design	25
5.1.2 Test rig build-up	31
5.1.3 Instrumentation.....	33
5.2 Experimental scheme	36
5.2.1 Overall view of the test rig performance.....	36
5.2.2 Test procedure in laboratory	37
5.2.3 Test procedure outside laboratory	38
5.3 Experimental results and analysis	39
5.3.1 Tests in laboratory	39
5.3.2 Experimental results before modification	40
5.3.3 Problems and modification of the test rig	45
5.3.4 Experimental results after modification	50
5.3.5 Error analysis.....	55
5.4 Chapter summary	56
6 Simulation	57
6.1 Simulation tool EES	57
6.2 Computation method	57
6.3 Simulation model validation	59
6.4 Performance analysis in different cities	62
6.4.1 Daily performance in Shanghai	62
6.4.2 Annual performance analysis	64
6.5 Chapter summary	69
7 Discussions.....	70
7.1 Problems and improvements of the experiment.....	70
7.2 Problems and improvements of the simulation	71

7.3 The feasibility for commercial use.....	71
8 Conclusion.....	72
9 Further work.....	73
Reference.....	74
Appendix 1	78
Appendix 2	80
Appendix 3	81
Appendix 4.....	85

List of Figures

FIG. 1 WORLD TOTAL CARBON DIOXIDE EMISSIONS OF COAL, LIQUIDS AND NATURAL GAS BY EIA (2017).....	I
FIG. 2 COAL-RELATED CARBON DIOXIDE EMISSIONS OF SOME COUNTRIES/REGIONS BY EIA (2017).....	II
FIG. 3 WORLD ENERGY CONSUMPTION OF DIFFERENT SECTORS BY EIA (2017)	III
FIG. 4 SOLAR ENERGY DISTRIBUTION IN CHINA.....	IV
FIG. 3- 1 ENERGY CONSERVATION FOR PV PANEL.....	4
FIG. 3- 2 REAL-TIME FLUCTUATIONS OF SOLAR IRRADIANCE AND PV PANEL TEMPERATURE	5
FIG. 3- 3 SCHEMATIC OF THE FLAT PLATE PV/T COLLECTOR	6
FIG. 3- 4 A GENERALIZED CLASSIFICATION OF THE RECENT DEVELOPMENT IN HEAT PUMP TECHNOLOGIES.....	7
FIG. 3- 5 SECTIONAL VIEW CUTTING OFF FROM A PV EVAPORATOR MODULE	9
FIG. 3- 6 CROSS-SECTION VIEW OF TWO PV/T COLLECTOR/EVAPORATORS.....	10
FIG. 3- 7 CROSS-SECTION VIEW OF AN LCPV/T-HP MODULE AND ITS RELATIVE POSITIONING WITH A PARABOLIC CONCENTRATOR.....	11
FIG. 3- 8 SCHEMATIC DIAGRAM OF THE PV/T COLLECTOR/EVAPORATOR	11
FIG. 3- 9 EXPLODED VIEW OF PLATE HEAT EXCHANGER.....	13
FIG. 3- 10 SCHEMATIC VIEW OF PLATE.....	13
FIG. 3- 11 AVERAGE HEAT TRANSFER COEFFICIENT ON R290-SIDE VS. REFRIGERANT MASS FLUX.....	18
FIG. 3- 12 EFFECT OF VAPOR SUPER-HEATING ON AVERAGE HEAT TRANSFER COEFFICIENT ON R290-SIDE	18
FIG. 4- 1 SKETCHES OF THE PV/T EVAPORATOR PANEL	19
FIG. 5- 1 SCHEMATIC DIAGRAM OF THE TEST RIG.....	26
FIG. 5- 2 INSTALLATION OF THE GRID TIE INVERTER	28
FIG. 5- 3 DIAGRAM OF THE PV/T EVAPORATOR	29
FIG. 5- 4 DRAFT OF THE TEST RIG	31
FIG. 5- 5 A) FRAME OF THE TEST RIG; B) ALUMINUM PLATE WITH COPPER COILS;.....	32

FIG. 5- 6 A) ELECTRIC CABINET B) GRID TIE INVERTER.....	33
FIG. 5- 7 REFRIGERANT CHARGE	33
FIG. 5- 8 HUKSEFLUX PYRANOMETER	35
FIG. 5- 9 HIOKI LR8400-20 DATA LOGGER.....	35
FIG. 5- 10 ARTIFICIAL SUN	37
FIG. 5- 11 BIRD’S EYE VIEW OF THE TEST FACILITIES	38
FIG. 5- 12 TEST RIG OUTSIDE LABORATORY.....	39
FIG. 5- 13 WEATHER DATA ON MAY 11, 2017.....	41
FIG. 5- 14 PULSE SIGNAL FROM THE PULSE GENERATOR WATER METER	41
FIG. 5- 15 VARIATION OF HEATING CAPACITY AND SOLAR IRRADIANCE ON MAY 11, 2017	42
FIG. 5- 16 VARIATION OF CONDENSER SUPPLY WATER TEMPERATURE AND COMPRESSOR POWER ON MAY 11, 2017.....	43
FIG. 5- 17 VARIATION OF PV ELECTRICITY OUTPUT AND CONVERSION EFFICIENCY ON MAY 11, 2017	44
FIG. 5- 18 VARIATION OF TEMPERATURE OF DIFFERENT POINTS ON PV PANEL ON MAY 11, 2017	44
FIG. 5- 19 VARIATION OF COP, AVERAGE COP, F_{EN} AND $F_{EN,A}$ OF THE SYSTEM ON MAY 11, 2017.....	45
FIG. 5- 20 SUPERHEAT AND PRESSURE DROP OF THE TEST RIG BEFORE MODIFICATION	46
FIG. 5- 21 VARIATION OF REFRIGERANT TEMPERATURE AFTER EVAPORATOR BEFORE MODIFICATION	47
FIG. 5- 22 SECTION VIEW OF NEW DISTRIBUTOR A) PART1 B) PART2 C) ASSEMBLY	48
FIG. 5- 23 TEMPERATURE DISTRIBUTION ON PV PANEL A) IN THE LAB; B) OUTSIDE WHEN THE HEAT PUMP WASN’T RUNNING; C) OUTSIDE WHEN THE HEAT PUMP WAS RUNNING.	49
FIG. 5- 24 WEATHER DATA ON MAY 29, 2017.....	50
FIG. 5- 25 VARIATION OF PV ELECTRICITY OUTPUT AND CONVERSION EFFICIENCY ON MAY 29, 2017	51
FIG. 5- 26 VARIATION OF CONDENSER SUPPLY WATER TEMPERATURE AND COMPRESSOR POWER ON MAY 29, 2017	52
FIG. 5- 27 VARIATION OF SYSTEM PERFORMANCE WITH CONDENSER SUPPLY WATER TEMPERATURE ON MAY 11, 2017 ...	53
FIG. 5- 28 VARIATION OF SOLAR IRRADIANCE AND COP ON JUN 7, 2017 AND JUN 8, 2017	53
FIG. 6- 1 FLOW CHART OF THE COMPUTATION PROCESS FOR SYSTEM MODEL	58
FIG. 6- 2 MEASURED AND SIMULATED DATA OF COMPRESSOR POWER AND AVG. WATER TEMPERATURE ON MAY 29, 2017	60
FIG. 6- 3 MEASURED AND SIMULATED DATA OF COP AND AVERAGE COP ON MAY 29, 2017	60

FIG. 6- 4 MEASURED AND SIMULATED DATA OF PV POWER AND PV EFFICIENCY ON MAY 29, 2017.....	61
FIG. 6- 5 SOLAR IRRADIANCE DATA ON APR 30, 2017 IN SHANGHAI.....	62
FIG. 6- 6 MONTHLY AVERAGE WATER TEMPERATURE IN SHANGHAI	63
FIG. 6- 7 VARIATION OF COP AND CONVERSION EFFICIENCY ON APR 30, 2017 IN SHANGHAI.....	64
FIG. 6- 8 MONTHLY AVERAGE WATER TEMPERATURE IN DIFFERENT CITIES	65
FIG. 6- 9 OPERATING INTERFACE OF THE SOFTWARE NAMED METEONORM.....	65
FIG. 6- 10 MONTHLY AVERAGE SOLAR IRRADIANCE IN DIFFERENT CITIES.....	66
FIG. 6- 11 MONTHLY AVERAGE AMBIENT TEMPERATURE IN DIFFERENT CITIES.....	67
FIG. 6- 12 MONTHLY AVERAGE WIND SPEED IN DIFFERENT CITIES.....	67
FIG. 6- 13 MONTHLY AVERAGE COP _a IN DIFFERENT CITIES	68
FIG. 6- 14 MONTHLY AVERAGE CONVERSION EFFICIENCY AND ENERGY GENERATION FACTOR.....	69

List of Tables

TABLE 5- 1 SPECIFIC FEATURES OF THE PV PANEL	26
TABLE 5- 2 COMPONENT LIST	28
TABLE 5- 3 GEOMETRIC CHARACTERISTICS OF THE BRAZED PLATE HEAT EXCHANGER	30
TABLE 5- 4 INSTRUMENT LIST.....	34
TABLE 5- 5 EXPERIMENTAL RESULTS ON DIFFERENT DAYS	54
TABLE 6- 1 COMPARISON BETWEEN EXPERIMENTAL RESULTS AND SIMULATED RESULTS	61
TABLE 6- 2 PERFORMANCE COMPARISON IN TRONDHEIM AND NORWAY.....	64

Nomenclature

A_f	Solar panel frame area
A_p	Solar panel surface area
$ACRC$	Air conditioning and refrigeration center
b	Corrugation depth
C	Constant
COP	Coefficient of the performance
COP_a	Average coefficient of the performance
C_p	Specific heat capacity of the PV/T panel
C_{TEV}	Characteristic constant of the valve
C_w	Specific heat capacity of the water
D_h	Hydraulic diameter
d_i	Internal diameter
e	Evaporation enhancement coefficient
E	PV Output power
f_{en}	Energy generation factor
$f_{en,a}$	Average energy generation factor
FF	Fill factor
G_{eff}	Effective solar radiation
G_s	Incoming solar irradiance
GWP	Global warming potential
h_{conv}	Forced convection coefficient
h_e	Average heat transfer coefficient
h_l	Heat transfer coefficient in liquid state
h_{NB}	Boiling heat transfer coefficient
h_r	Heat transfer coefficient on refrigerant side
h_w	Heat transfer coefficient on water side
I_m	Nominal power current
I_{sc}	Short circuit current
k	Adiabatic compression index
L	Length of the evaporator
$LMTD$	Log-mean temperature difference
M	Molecular weight of refrigerant
m_p	Mass of PV/T panel
m_r	Mass flow of the refrigerant
m_w	Mass flow of the water

N_{in}	Input power consumption of the compressor
N_{th}	Theoretical power consumption of the compressor
ODP	Ozone depression potential
p	Corrugation pitch
P_c	Condensing pressure
P_{crit}	Critical pressure of refrigerant
P_d	Discharge gas pressure
P_e	Evaporation pressure
P_m	Nominal power
P_r	Pressure of refrigerant
P_{red}	Reduced pressure
P_s	Suction gas pressure
q	Heat flux in evaporator
Q_c	Condensing capacity
Q_{conv}	Convective heat exchange
Q_{rad}	Long-wave radiation heat exchange
Q_{loss}	Heat loss
Q_e	Removed heat through evaporator
Re	Reynolds number
Re_l	Reynolds number in liquid state
R_p	Surface roughness
R_{plate}	Thermal resistance of the plate
RPM	Rotating speed of the motor
S	Boiling depression factor
T_{al}	Temperature of the aluminum plate
T_{amb}	Ambient temperature
T_c	Solar cell temperature
T_{cond}	Condensing temperature
TCR	Thermal contact resistance
T_{eva}	Evaporating temperature
$T_{h,w}$	Final water temperature
$T_{i,w}$	Inlet water temperature
$T_{l,w}$	Initial water temperature
$T_{o,w}$	Outlet water temperature
T_p	Solar panel temperature
T_r	Refrigerant temperature
T_{ref}	Reference solar cell temperature
T_{sky}	Sky temperature

T_w	Wall temperature
V_{dis}	Displacement of the compressor
V_m	Nominal power voltage
V_{oc}	Open circuit voltage
v_{wind}	Wind speed
x	Inlet quality of refrigerant
X_{tt}	Martinelli parameter
α	Absorptivity of the PV/T panel
β	Chevron angle
β_{ref}	Temperature coefficient of the PV panel
γ	Solar radiation coefficient
δ_{bs}	Thickness of the back sheet
δ_{gl}	Thickness of the glass
δ_{ins}	Thickness of the insulation material
ε_p	Emissivity of the panel
ε_f	Emissivity of the frame
η_c	Conversion efficiency
η_i	Indicated efficiency
η_{inv}	Efficiency of the grid tie inverter
η_m	Mechanical efficiency
η_{mo}	Motor efficiency
η_p	Heat-collecting efficiency
η_{power}	Electricity-generation efficiency of a coal-fired power plant
η_{ref}	Nominal electrical efficiency
λ_{bs}	Thermal conductivity of the back sheet
λ_{gl}	Thermal conductivity of the glass
λ_{ins}	Thermal conductivity of the insulation material
λ_v	Volumetric efficiency of the compressor
μ_g	Viscosity of the refrigerant in gas state
μ_l	Viscosity of the refrigerant in liquid state
ρ_g	Density of the refrigerant in gas state
ρ_l	Density of the refrigerant in liquid state
ρ_s	Density of the suction gas
σ	Stefan-Boltzmann's constant
ϕ	Surface enlargement factor
ϕ_l	Two-phase multiplier
ω	Acentric factor

1 Introduction

Solar energy is one of the most important renewable energy and its technologies are widely used to generate electricity and capture thermal energy. Active solar techniques use photovoltaics, concentrated solar power, solar thermal collectors, pumps, and fans to convert sunlight into useful outputs. According to International Energy Agency, solar power is anticipated to become the world's largest source of electricity by 2050. In the last two decades, photovoltaics (PV), also known as solar PV, has evolved from a pure niche market of small scale applications towards becoming a mainstream electricity source. Solar energy is also widely used for water heating. As of 2007, the total installed capacity of solar hot water systems was approximately 154 thermal gigawatt (GW_{th}).

Heat pump has become a mature technology over the past two decades. With raising cost of fuel and raising concern of global warming, the interest in HP as a means of energy recovery appears to have been resurrected. Heat pumps offer one of the most practicable solutions to the greenhouse effect. It is the only known process that recirculates environmental and waste heat back into a heat production process; offering energy efficient and environmentally friendly heating and cooling in applications ranging from domestic and commercial buildings to process industries. Practical studies have shown the potential of heat pumps to drastically reduce greenhouse gases, in particular CO_2 emissions, in space heating and heat generation. The positive impact on environment depends on the type of heat pump and driving power used (Chua et al., 2010).

Solar panels have a decreasing efficiency with increasing operating cell temperature. Therefore, combining solar panels with heat pump systems can not only decrease the operating cell temperature but also recover the thermal energy wasted. What's more, using solar energy as the heat source of heat pumps can be a better choice compared with air source heat pumps in some operating conditions, because solar assisted heat pumps can have a higher evaporating temperature in sunny days which is good to the performance of heat pumps.

2 Objectives

The main objectives of this project are

1. Design and build a test rig of PV/T heat pump system. A PV panel was combined with a refrigeration system to improve the conversion efficiency and recover solar thermal energy.
2. Plan tests of the PV/T heat pump system. Experiments should be done both in the lab and outside. Fix the problems of the test rig found during the operation
3. Establish a computer simulation model using EES. The simulated results should be compared with the experimental results to demonstrate the effectiveness of the model. Investigate the performance of the system at different places and climates. Give suggestions to optimize the system.
4. Suggest other ideas, designs and concepts for further work.

3 Literature review

Solar photovoltaic(PV) panel is designed to absorb the sun's rays as a source of energy for generating electricity. The performance of the PV panel decreases with increasing temperature, fundamentally owing to increased internal carrier recombination rates, caused by increased carrier concentrations(Dubey et al., 2013). In this chapter, the researches on the photovoltaic panel, PV/T collector, heat pump, PV solar assisted heat pump, plate heat exchanger will be introduced

3.1 Photovoltaic(PV) Panel

The performance of the PV panel is related to the plate temperature and many studies have been carried out for finding out the effect of temperature on the electrical efficiency of a PV cell/module. The output electrical power of the PV panel can be calculated by the following equation:

$$P_m = I_m V_m = (FF) I_{sc} V_{oc} \quad (3.1)$$

FF is fill factor, I_{sc} is short circuit current, V_{oc} is open circuit voltage and subscript m refers to the maximum power point in the modules I-V curve. The open circuit voltage and the fill factor decrease substantially with temperature but short-circuit current increases slightly(Zondag, 2008).

The effect of temperature on the electrical efficiency of a PV cell/module can be obtained by using fundamental equation:

$$\eta_c = \eta_{ref} \left[1 - \beta_{ref} (T_c - T_{ref}) + \gamma \log_{10} T(t) \right] \quad (3.2)$$

The temperature coefficient β_{ref} and the solar radiation coefficient γ are mainly decided by the material properties and the solar radiation coefficient is usually taken as zero(Evans, 1981), so the above equation reduces to:

$$\eta_c = \eta_{ref} \left[1 - \beta_{ref} (T_c - T_{ref}) \right] \quad (3.3)$$

In order to calculate the efficient of the PV panel, the evaluation of panel temperatures is necessary. The panel temperature is determined by a function of weather variables such as

radiation, ambient temperature, local wind speed, glazing-cover transmittance, plate absorptance, etc(Skoplaki and Palyvos, 2009). Fig. 3- 1 shows the energy conservation for PV panel. Jones and Underwood used the energy balance of PV cells to calculate the module temperature, where cooling strategies of short-wave radiation, long-wave radiation and convection were all considered(Jones and Underwood, 2001).

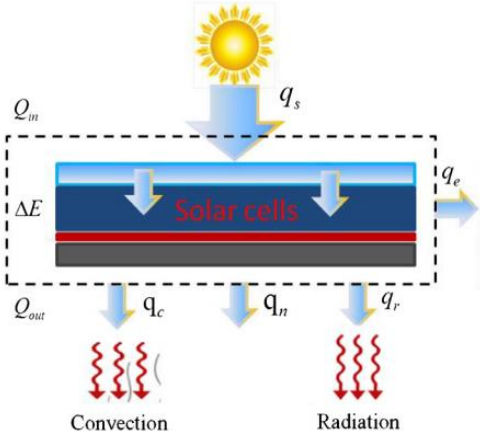


Fig. 3- 1 Energy conservation for PV panel

Yanping and Christopher(Du et al., 2016) developed theoretical models for evaluating temperature of PV panels in realistic scenarios, analyzed the characteristics of temperature variations in different conditions and assessed the heating effect on electrical efficiency of solar cells based on real-time temperature measurements in the current field test. According to their results, for a solar cell with an absorption rate of 70%, the predicted temperature is as high as 60°C under a solar irradiance of 1000W/m² when the wind speed is 0m/s. Fig. 3- 2 shows the real-time fluctuations of solar irradiance and PV panel temperature. The panel temperature is around 31°C when the ambient temperature is 15°C.

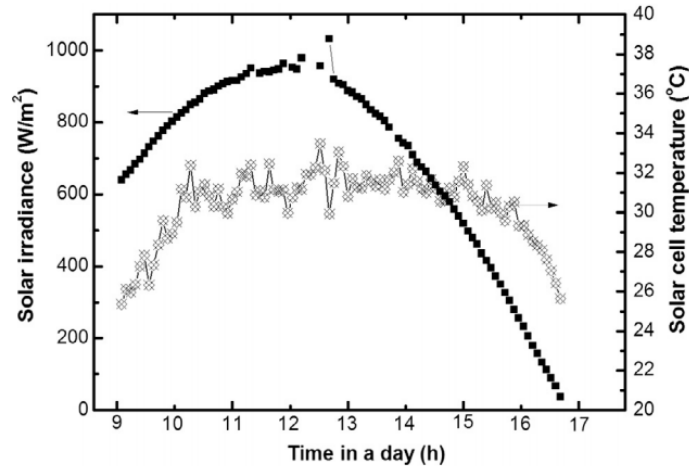


Fig. 3- 2 Real-time fluctuations of solar irradiance and PV panel temperature

3.2 PV/T collector

Hybrid photovoltaic/thermal system was proposed not only to improve the electrical efficiency of the PV panel, but also to utilize the thermal energy gathered from the sun. A PV/T system can be segregated into two parts; the photovoltaic technology which derived from solar cell technology and convert into electricity, and thermal solar technology derived from the thermal collector and convert the solar energy into heat(Zondag, 2008).

There have been significant technological advancements concerning all types of PV/T collectors during the past few years. Some commercial products show up in the market. There are four main types of PV/T collectors, and the main difference between them is working media. It can be air, water, refrigerant and heat pipe(Chen et al., 2018).

In this project, a PV/T collector was designed and used as the evaporator of the heat pump system. The structure of the collector is very similar to the flat plate PV/T collectors which are usually used to generate domestic hot water. Fig. 3- 3 shows the schematic of the typical flat plate PV/T collector. Cold water goes through the pipes to absorb heat and cool the PV cells.

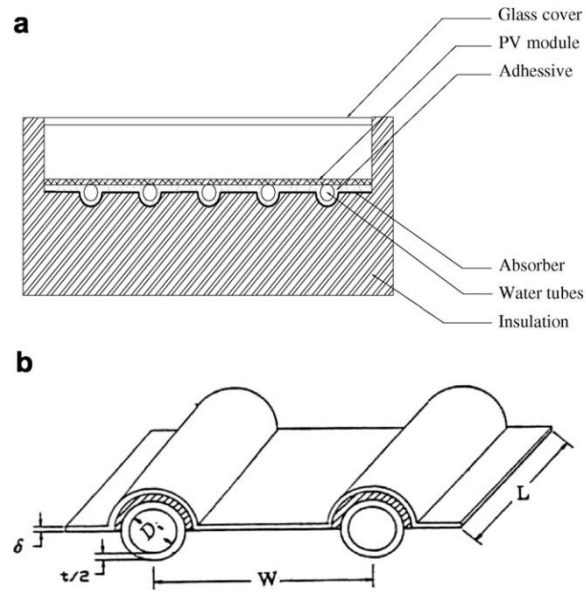


Fig. 3- 3 Schematic of the flat plate PV/T collector

The working media used in this project is propane (R290) and the structure of the collector will be introduced in section 5.

3.3 Heat pump

A heat pump is a device that provides heat energy from a source of heat to a destination called a "heat sink". Heat pumps are designed to move thermal energy opposite to the direction of spontaneous heat flow by absorbing heat from a cold space and releasing it to a warmer one. A heat pump uses some amount of external power to accomplish the work of transferring energy from the heat source to the heat sink.

3.3.1 Refrigerants

Refrigerants are the working fluid used in heat pump system, they undergo phase transitions from liquid to gas and back again in most cycles. Different refrigerants are used for different applications relating to their thermodynamic properties, prices and safety regulations.

However, many refrigerants can cause some environmental problems, like global warming and ozone depletion. The GWP of CO₂ is 1 and the ODP of R12 is 1, the GWP and ODP of other refrigerants are given relative to the value of CO₂ and R12. Many halons, chlorofluorocarbons (CFC), and hydro chlorofluorocarbons (HCFC), particularly CFC-11 and CFC-12 were preferred refrigerants for many years because of their nonflammability and

nontoxicity. However, they have very high GWP and ODP because of their stability in atmosphere. The popular alternative refrigerants like R134a still have GWP thousands of times greater than CO₂. More environment-friendly refrigerants should be used in the future.

In this project, propane (R290) was used as the working fluid. Propane is an environmental friendly working fluid, its ODP and GWP is 0 and 3. What’s more, propane has excellent thermodynamic properties, similar to those of R22. It has been used successfully as working media in large refrigeration plant for many years, notably in the petrochemical process industry(Lorentzen, 1995). However, propane is highly flammable and explosive. It can be used without limitation as long as refrigerant charge do not exceed 0.15kg.

3.3.2 classification

Heat pump has evolved to become a mature technology over the past two decades(Chua et al., 2010). Fig. 3- 4 shows a generalized classification of the recent development in heat pump technologies. The integration of heat pump with solar technology presents a novel hybrid system whereby the performance of the heat pump can be significantly enhanced by taking heat from a natural source solar energy(Mohanraj et al., 2009).

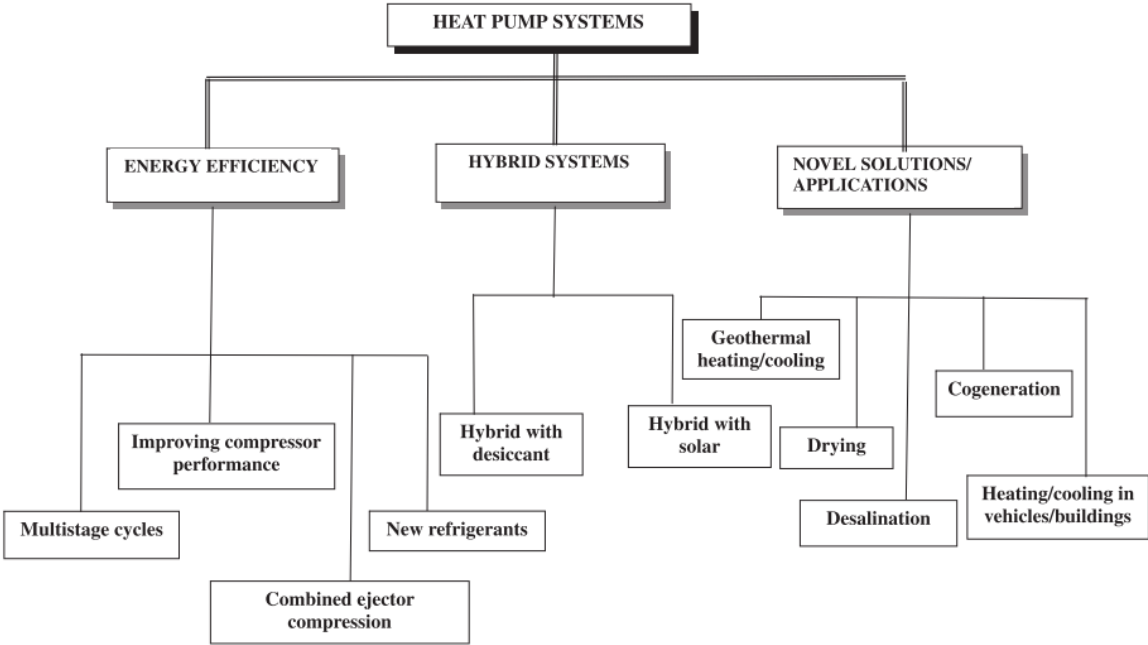


Fig. 3- 4 A generalized classification of the recent development in heat pump technologies

Many works on solar assisted heat pump (SAHP) were conducted in recent years. Among the works, direct expansion system was investigated by many people(Sporn and Ambrose, 1955,

Kong et al., 2011, Fernández-Seara et al., 2012, Moreno-Rodríguez et al., 2012, Molinaroli et al., 2014, Sun et al., 2014, Jiang and Dai, 2016) and the DX-SAHP water heater has a better performance compared with the air source heat pump water heater(Sun et al., 2015). Meanwhile, new ideas related to the integrations of solar-thermal, photovoltaic (PV) and heat pump have been conceived to yield novel hybrid systems. In this project, a PV/T heat pump test rig will be designed, built and tested.

3.4 PV solar assisted heat pump

The concept of solar assisted heat pump was first proposed by Sporn and Ambrose(Sporn and Ambrose, 1955). The concept of the PV/T solar collector was put forward by Kern and Russell(Russell and Kern, 1979), TRNSYS simulation of PV/T collector heat pump system for residence in New York and Fort Worth climates in their work, and analysis of the technical and economic results are discussed. The outcome brought a great lift to the overall efficiency of solar energy. Since then the progress of the technology had been slow.

The direct conversion of solar energy into electricity by means of photovoltaic modules has received much attention since 1990s(Ji et al., 2008b). However, the electricity conversion efficiency of a PV cell in the commercial market is currently not more than 20%(Huang et al., 2001). The majority of the solar radiation on the PV module is converted into heat, which results in an increase of the PV panel temperature and a decrease of electrical efficiency. However, in the Rankine refrigeration cycle operation, the solar energy absorbed by the refrigerant at the collector will be released later on at the condenser with a higher working temperature. What's more, a higher evaporating temperature leads to higher COP and the electrical efficiency of the PV panel will increase too.

Ito et al.(Ito et al., 1997, Ito et al., 2005) constructed SAHP systems with PV/T evaporators based on this principle. They developed different kinds of PV/T evaporators. In 1997, flat-plate solar collectors which were insulated on the back and bonded with PV modules on the upper surfaces were used. The experimental results indicated that the COP of the heat pump could be as high as 6.0, when 40°C water was supplying to the condenser. However, the COP became 2 when there was little solar radiation. They also found the PV modules on the collectors did not

appreciably influence the performance of the heat pump. In 2005, aluminum roll-bond panel with PV modules on the surface was used. A smaller pressure drop of the refrigerant flow at the evaporator was realized after the modification and the collector efficiency factor could reach 0.9. However, the PV or the overall PV/T performance in the system was not covered in their publications.

Ji et al.(Ji et al., 2008a, Ji et al., 2008b, Pei et al., 2009) constructed a novel PV-SAHP system with PV cells laminated onto the evaporator-collector plate. Fig. 3- 5 shows the sectional view cutting off from a PV evaporator module. The experimental rig was set up in Hefei, China. The tests of four different operating modes with condenser supply water temperature at 20°C, 30°C,40°C and 50°C respectively were conducted in a 4-day period in November 2005. During the testing period the weather conditions were relatively the same, with the average values of solar radiation, ambient temperature and wind velocity around 606 W/m², 13.7°C and 3.2m/s respectively. The max COP, max COP_{p/t}, average COP, average COP_{p/t}, and average photovoltaic efficiency were determined as 10.4, 16.1, 5.4, 8.3, and 13.4% respectively. Mathematical model was developed and numerical simulation was performed based on the distributed parameters approach. The simulated results were found in good agreement with the experimental results.

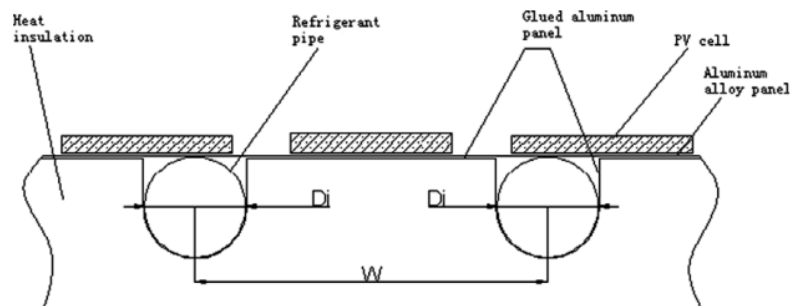


Fig. 3- 5 Sectional view cutting off from a PV evaporator module

Xu et al.(Xu et al., 2008) developed a novel PV/T integrated heat pump system for electricity generation and domestic hot water heating. PV modules were directly laminated on the surface of solar thermal collector, to the back of which evaporator tubes was adhered. Two different structures, which is shown in Fig. 3- 6, of PV/T evaporators applying conventional copper tube and multi-port flat extruded tube were designed and investigated. The latter

structure had a better performance according to the simulated results. The simulated results based on 150L water heating load showed the system could produce 50°C hot water with a COP ranged from 4.23 to 5.54 all year around in Nanjing, China.

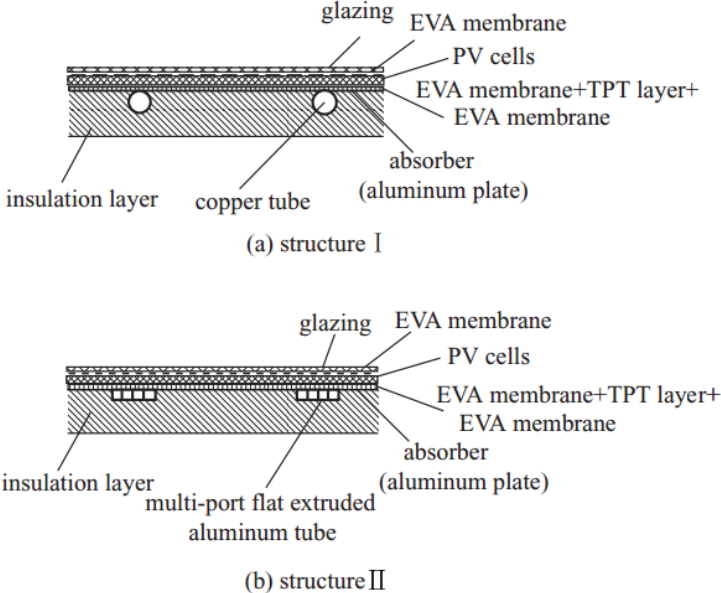


Fig. 3- 6 Cross-section view of two PV/T collector/evaporators

Xu et al.(Xu et al., 2011) developed a novel low-concentrating solar PV/T integrated heat pump system(LCPV/T-HP). The LCPV/T solar collector had a surface area of 1.584m²(1320×1200mm), and consisted of six flat strips of PV/T modules (62.5×1200mm) with truncated parabolic concentrators fixed on both sides of a PV/T module, as shown in Fig. 3- 7. Two LCPV/T solar collectors were mounted in parallel with a tilt angle of 30° in this work. Experiments were carried out in Nanjing, China and experiment results showed that the LCPV/T-HP system achieved an average COP of 4.8 for heating water from 30°C to 70°C on a sunny summer day, with an output electrical efficiency of 17.5%, 1.36times higher than that of the LCPV system.

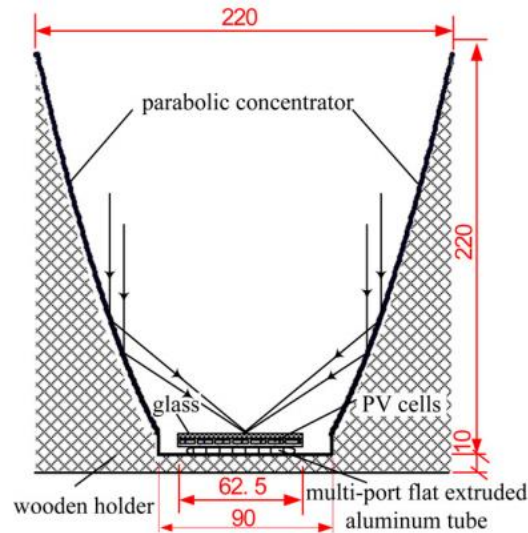


Fig. 3- 7 Cross-section view of an LCPV/T-HP module and its relative positioning with a parabolic concentrator

Fu et al.(Fu et al., 2012) designed a heat pump with heat-pipe PV/T collectors and the hybrid system is called the photovoltaic solar assisted heat pump/heat-pipe (PV-ASHP/HP) system. The system could operate in three different modes, the heat-pipe, solar-assisted heat pump and air-source heat pump. The novel heat pipe PV/T collector/evaporator is shown in Fig. 3- 8. The results showed that the PV-SAHP/HP system could reach a daily average energy efficiency of 61.1-82.1% and an exergy efficiency of 8.3-9.1% when operating in the solar-assisted heat-pump mode. The daily average heat-pump COP could reach 4.01 when solar radiation was strong.

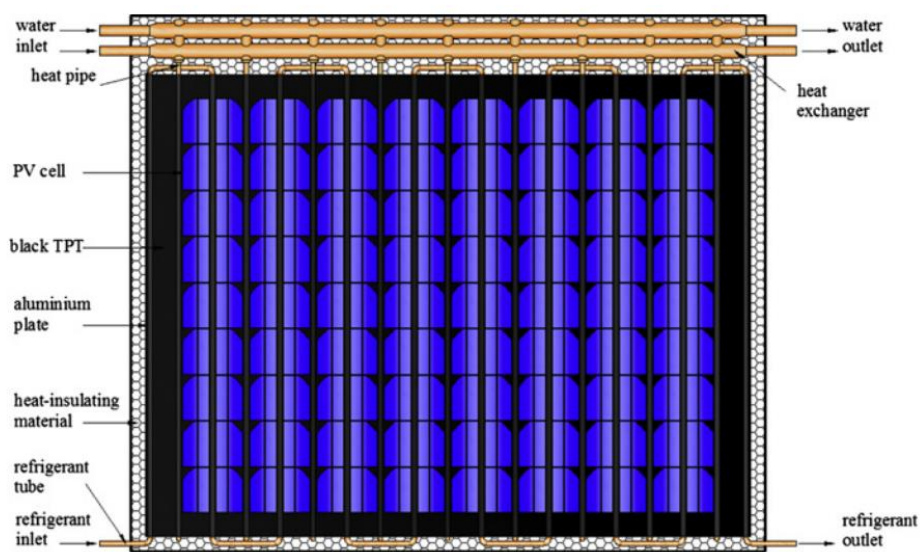


Fig. 3- 8 Schematic diagram of the PV/T collector/evaporator

Tsai et al.(Tsai, 2015) developed a novel model for a refrigerant-based photovoltaic/thermal assisted heat pump water heater (PVT-HPWH) system. The proposed model which took the interactive effect of surrounding conditions on PV characteristics into consideration matched the experiment results well.

3.5 Plate heat exchanger

Plate heat exchangers were initially introduced for use within the dairy industry as a result of the need to clean the surfaces regularly for hygienic reasons. The pressing depths of the plates were small, which means the hydraulic diameters of the channels between the plates were small. So plate heat exchangers were one of the very first type of mini-channel heat exchanger (Palm and Claesson, 2006).

Over the past 30 years, it has become possible to manufacture brazed heat exchangers. The condenser used in this work is a brazed plate heat exchanger. Brazed plate heat exchangers are manufactured by placing a copper (or nickel) foil in between each of the stainless steel plates and placing the pile of plates in furnace just above the melting temperature of copper. Capillary forces draw the copper to the points of contact between adjacent plates, thereby connecting each couple not only at the edges but at a large number of points across the heat transfer area. Due to this, the brazed plate heat exchangers have the advantage of tolerating high pressures, a typical rating being 30 bar. They have become very popular as evaporators and condensers in liquid chillers and heat pumps.

Plate heat exchangers are extremely compact compared to most types of heat exchangers. They have large heat transfer surface while the volume is small. There are some calculation methods for the prediction of heat transfer and pressure drop, but it is difficult to choose the most appropriate models among these calculation methods. Especially the predictions by using different correlations for boiling and condensation give quite different results.

3.5.1 Geometry

The plate patterns of almost all plate heat exchangers are chevron-shaped, as shown in Fig. 3-9. Normally, each plate has an identical pattern, but every second plate is rotated 180° so that the pattern of adjacent plates points in opposite directions.

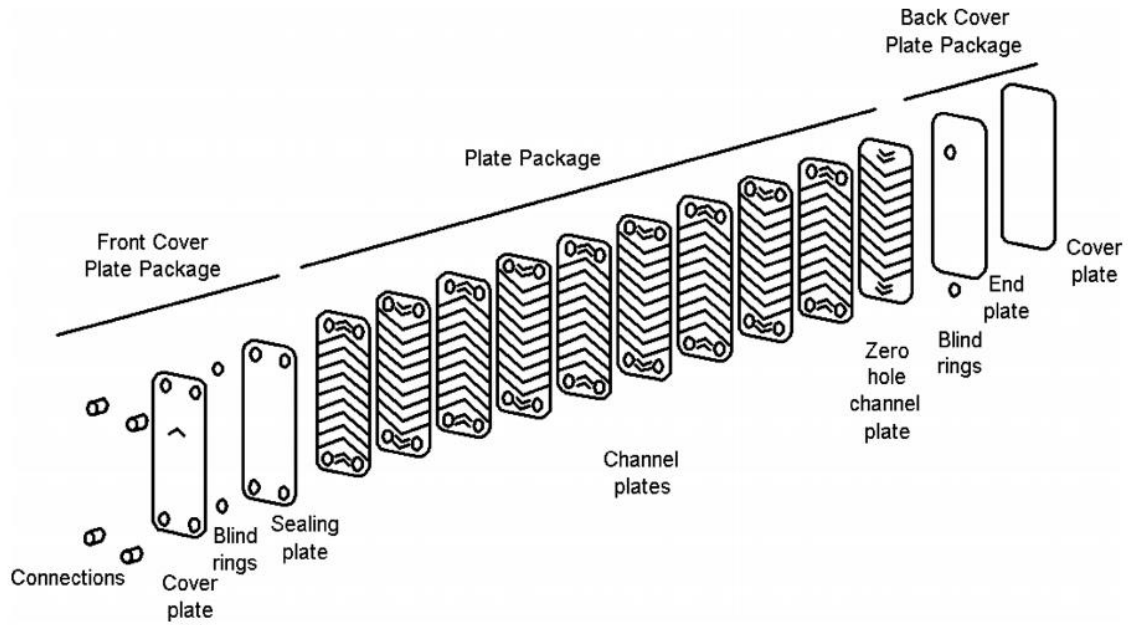


Fig. 3- 9 Exploded view of plate heat exchanger

The geometry of the unit cell within the structure is determined by shape and size of the corrugations. The schematic view of the plate is shown in Fig. 3- 10 (Longo, 2010). The corrugation is usually close to sinusoidal and can be identified by the following parameters: the chevron angle, the pressing depth, the corrugation pitch.

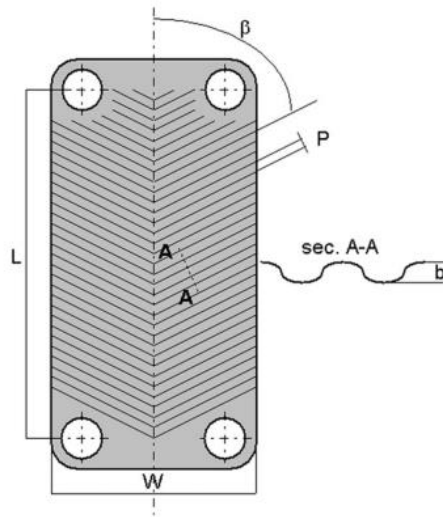


Fig. 3- 10 Schematic view of plate

Most plate heat exchangers on the market have similar pressing depths and corrugation pitch, while the chevron angles vary depending on the application (Palm and Claesson, 2006).

Table 3- 1 Typical min and max values for unit cell parameters

Parameter	Min	Max	Unit
Chevron angle	30	65	°
Pressing depth	1.2	5	mm
Corrugation pitch	7	15	mm

It is important to define a hydraulic diameter of the channel for the non-dimensional representation of heat transfer and pressure drop. There are two different definitions of the hydraulic diameter which are used in the literature (Claesson, 2005). The most common definition used is similar to the definition of two wide parallel plates, hence

$$D_h = 2b \quad (3.1)$$

The other definition is defined according to the non-circular tube definition of the hydraulic diameter:

$$D_h = \frac{2b}{\phi} \quad (3.2)$$

Where ϕ is surface enlargement factor.

In the following, the first definition is used without special instruction

3.5.2 Correlations for single phase heat transfer

There are many investigators working on the single phase heat transfer and pressure drop in plate heat exchangers. However, it is difficult to find a general theory or correlation to solve this problem because there are lots of combination of geometric parameters. Therefore, each investigation should be regarded as a special case and the results only applicable for the specific geometry tested.

The Wilson plot method is a widely used method to determine convection coefficients based on measured experimental data and the subsequent construction of appropriate correlation equations (Fernández-Seara et al., 2007). After the formulation of Wilson, general correlation equations for the analysis of internal forced convection based on Reynolds analogy have appeared in the literature. Early modifications of the Wilson plot method assumed a general correlation for the convection coefficient in which the mass flow is varied as a power of the Reynolds and Prandtl numbers instead of fluid velocity. In this format, the exponents of

Reynolds number and Prandtl number in Eq. (3.3) have to be assumed.

$$Nu = C_1 \cdot Re^{C_2} Pr^{C_3} \quad (3.3)$$

Focke et al. studied the effect of the corrugation inclination angle on the thermohydraulic performance of plate heat exchangers (Focke et al., 1985). The correlation used in this study was in the format of Eq. (3.3) in which $C_3=0.5$. The value of C_1 and C_2 and the application range can be found in Table 3- 2.

Table 3- 2 Value of constants and application range

Corrugation angle	C_1	C_2	Application range
0°	0.021	0.868	$8000 \leq Re \leq 56000$
30°	0.77	0.54	$120 \leq Re \leq 1000$
	0.44	0.64	$1000 \leq Re \leq 42000$
45°	1.67	0.44	$45 \leq Re \leq 300$
	0.405	0.7	$300 \leq Re \leq 2000$
	0.84	0.6	$2000 \leq Re \leq 20000$
60°	1.89	0.46	$20 \leq Re \leq 150$
	0.57	0.7	$150 \leq Re \leq 600$
	1.112	0.6	$600 \leq Re \leq 16000$

Muley et al. did the experimental study of turbulent flow heat transfer and pressure drop in a plate heat exchanger with chevron plates (Muley and Manglik, 1999). A specific set of experimental water to water tests is carried out on the condenser to determine the calibration correlation for heat transfer on the water-side. The experimental data for $Re \geq 1000$, $30^\circ \leq \beta \leq 60^\circ$, and $\phi=1.29$ can be correlated as

$$Nu = [0.2668 - 0.006967\beta + 7.244 \times 10^{-5} \beta^2] \times Re^{[0.728 + 0.0543 \sin[(\pi\beta/45) + 3.7]]} Pr^{1/3} (\mu / \mu_w)^{0.14} \quad (3.4)$$

According to the study of Yan et al., the single phase water to water heat transfer test for the plate heat exchanger was carried out. The chevron angle of the heat exchanger is 60° . The convection heat transfer coefficient in the cold side was correlated by the least square method as (Yan et al., 1999)

$$Nu = 0.2121 Re^{0.78} Pr^{1/3} \quad (3.5)$$

Hayes et al. investigated the carbon dioxide condensation in chevron plate heat exchangers. For the single-phase analysis, data was taken using hot and cold water flow through the middle and side channels, respectively. Three brazed plate heat exchanger with different interior configuration were tested (Hayes and Jokar, 2009, Hayes et al., 2011).

Yang et al. investigated the single-phase heat transfer for nine brazed-plate heat exchanger with different geometric parameters (Yang et al., 2017). A generalized ACRC correlation includes 22 different plate heat exchangers, 25 various correlations from 1985 to 2015 with a wide range of geometric parameters and working conditions: $50 \leq Re \leq 8000$; $2 \leq Pr \leq 290$; $27^\circ \leq \beta \leq 63^\circ$; $1.16 \leq \phi \leq 1.464$; $0.557 \leq 2b/p \leq 1.290$. This correlation has the accuracy of 50% and is given as follows:

$$Nu = (-1.342 \times 10^{-4} \cdot \beta^2 + 1.808 \times 10^{-2} \cdot \beta - 0.0075) \cdot Re^{(-7.956 \times 10^{-5} \cdot \beta^2 + 9.687 \times 10^{-3} \cdot \beta + 0.3155)} \cdot Re^{\phi/\beta} \cdot Re^{2b/p \cdot \beta} \cdot Pr^{1/3} \cdot \left(\frac{\mu}{\mu_w}\right)^{0.14} \quad (3.6)$$

3.5.3 Correlations for condensation heat transfer

Typical values of water film heat transfer coefficient are 8000 to 10000 whilst the refrigerant heat transfer coefficient is less than 5000. Thus the main heat transfer resistance is on the refrigerant side (Claesson, 2005). Condensation in plate heat exchangers has been reported in the literature.

Copper discussed the application of plate heat exchangers as condensers for steam (Cooper, 1974). He used the correlation by Lockhart-Martinelli for pressure drop and a simple condensate heat transfer correlation by Ananiev, shown to be successful to predict local heat transfer coefficients during condensation in plate heat exchangers.

$$h_r = h_l \cdot \sqrt{\frac{\rho_l}{\rho_{tp}}} \quad (3.7)$$

Baskin investigated the literature for plate heat exchanger in heat pumps (Baskin, 1991). He stated that heat transfer for condensation should be calculated as

$$\bar{h}_r = 13.8 \frac{\lambda_l}{D_h} Pr^{1/3} \left(\frac{\Delta h_g}{C_p \Delta t} \right)^{1/6} \left[Re \left(\frac{\rho_l}{\rho_g} \right)^{0.5} \right]^{0.2} \quad (3.8)$$

If $1000 < Re \left(\frac{\rho_l}{\rho_g} \right)^{0.5} < 2000$ and for $2000 < Re \left(\frac{\rho_l}{\rho_g} \right)^{0.5} < 10000$ as

$$\bar{h}_r = 0.1 \frac{\lambda_l}{D_h} \text{Pr}^{1/3} \left(\frac{\Delta h_{lg}}{C_p \Delta t} \right)^{1/6} \left[\text{Re} \left(\frac{\rho_l}{\rho_g} \right)^{0.5} \right]^{2/3} \quad (3.9)$$

Yan et al. investigated R134a condensing in a plate heat exchanger (Yan et al., 1999). At higher vapor quality, the heat transfer and pressure drop were also higher. Higher heat flux does not significantly increase heat transfer. Increasing system pressure slightly decreases the heat transfer, however the effect was rather small. The heat transfer was correlated as

$$h_r = \frac{\lambda_l}{D_h} \cdot 4.118 \cdot \text{Re}_{eq}^{0.4} \text{Pr}_l^{1/3} \quad (3.10)$$

Where

$$\text{Re}_{eq} = \frac{G \left[(1-x) + x \cdot \left(\frac{\rho_l}{\rho_g} \right)^{0.5} \right] \cdot D_h}{\mu_l} \quad (3.11)$$

Palmer measured Nusselt numbers for R22, R290, R290/600a, and R32/152a undergoing evaporation and condensation in a brazed plate heat exchanger (Palmer et al., 2000). The refrigerant experienced wavy, stratified flow at low heat and mass fluxes, 1.3 kW/m² to 9.3 kW/m² and 1.6 kg/m²s to 19 kg/m²s, respectively. The condenser correlations for R290 is:

$$Nu_r = Nu_l^{0.387} \phi_l^{0.0824} Ga^{0.346} P_{red}^{1.5} \omega^{1.5} \quad (3.12)$$

Where

$$Nu_l = C_1 \cdot \text{Re}_l^{C_2} \text{Pr}_l^{C_3} \quad (3.13)$$

$$\text{Re}_l = \frac{GD_h(1-x)}{\mu_l} \quad (3.14)$$

$$\phi_l = \sqrt{1 + \frac{12}{X_u} + \frac{1}{X_u^2}} \quad (3.15)$$

$$X_u = \left(\frac{1-x}{x} \right)^{0.9} \left(\frac{\rho_g}{\rho_l} \right)^{0.5} \left(\frac{\mu_l}{\mu_g} \right)^{0.1} \quad (3.16)$$

$$P_{red} = \frac{P}{P_c} \quad (3.17)$$

$$\omega = -\log(P_{red}) \quad (3.18)$$

Longo investigated the heat transfer coefficients and pressure drop measured during HC-600a, HC-290 and HC-1270 saturated vapor condensation inside a brazed plate heat exchanger

(Longo, 2010). The heat transfer coefficients show weak sensitivity to saturation temperature and great sensitivity to mass flux and fluid properties. There exists a transition point when the mass flux is around 15-18 kg/m²s. The brazed plate heat exchanger used here has a chevron angle of 60° and a corrugation pitch of 2mm. Fig. 3- 11 shows the average heat transfer coefficient on R290-side vs. refrigerant mass flux.

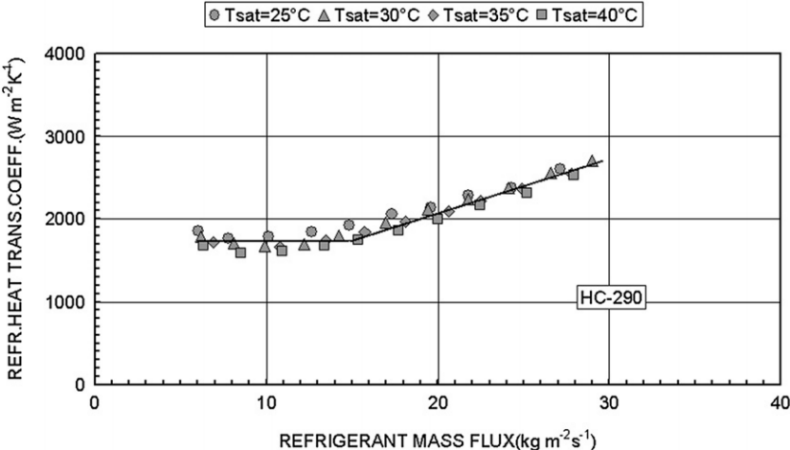


Fig. 3- 11 Average heat transfer coefficient on R290-side vs. refrigerant mass flux

Longo also investigated the effect of vapor super-heating on hydrocarbon refrigerant 600a, 290, 1270 condensation inside a brazed plate heat exchanger (Longo, 2011). Vapor super-heating can increase heat transfer coefficient. The super-heating temperature used here is around 10°C. Fig. 3- 12 shows effect of vapor super-heating on average heat transfer coefficient on R290-side.

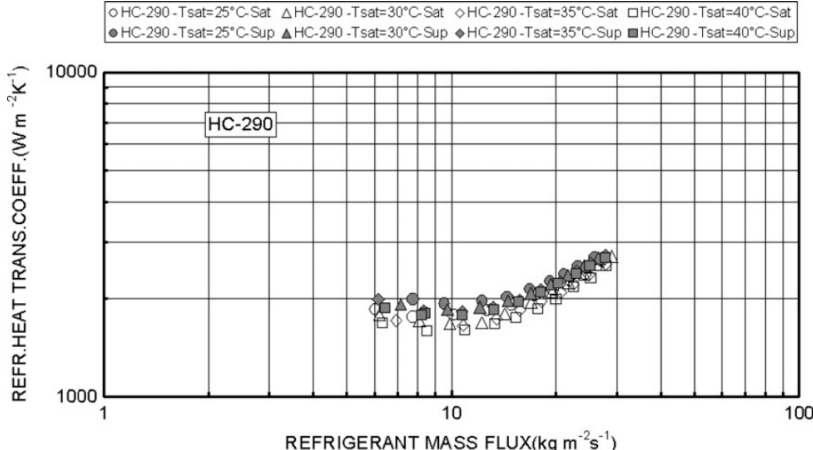


Fig. 3- 12 Effect of vapor super-heating on average heat transfer coefficient on R290-side

4 Theory

In this chapter, the mathematical model and the performance indicator of the PV/T heat pump system will be introduced

4.1 Mathematical model

4.1.1 Heat flow at the PV panel

Fig. 4- 1 shows the sketches of the PV/T evaporator panel. It includes 3.2mm solar glass with anti-reflection surface treatment, multi-crystalline solar cells, 0.5mm PET back sheet, 8mm aluminum back plate, 3/16” copper tube and 25mm insulation material. There are three energy transfer mechanisms involved in the PVT evaporator(Tsai, 2015): PV effect that converts solar energy into electricity, thermal transportation that conveys solar thermal radiation into PV/T evaporator panel and heat exchange with ambient environment which includes convection and radiation, and heat recovery that evaporates the refrigerant within the coil for the evaporation of heat pump system.

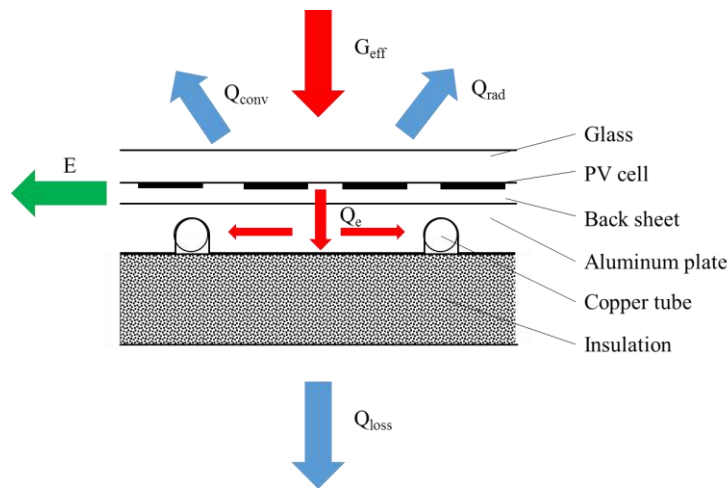


Fig. 4- 1 Sketches of the PV/T evaporator panel

The thermodynamic equation of the PV/T evaporator panel is given by:

$$m_p C_p \frac{\partial T_p}{\partial t} = G_{eff} - E - Q_{conv} - Q_{rad} - Q_{loss} - Q_e \quad (4. 1)$$

Where m_p is the mass of the PV/T panel, C_p is the specific heat capacity of the PV/T panel, T_p is the temperature of the PV/T panel, t is the operating time, G_{eff} is the effective solar radiation the PV/T panel can absorb, E is the output electric power, Q_{conv} is the convective heat

exchange between PV panel front surface and ambient air, Q_{rad} is the long-wave radiation heat exchange in the background equivalent environment (sky, ground, and surroundings), Q_{loss} is the heat loss at the back of the PV panel, Q_e is the removed heat through evaporator. The effective solar radiation is given by:

$$G_{eff} = \alpha G_s A_p \quad (4. 2)$$

Where α is the absorptivity of the PV panel, G_s is the incoming solar irradiance, A_p is the solar panel surface area. The output electric power is given by:

$$E = G_s A_p \eta_{ref} (1 + \beta_{ref} (T_p - T_{ref})) \quad (4. 3)$$

Where η_{ref} is electrical efficiency of the panel at stand test conditions STC (airmass AM 1.5, irradiance 1000w/m², cell temperature 25°C), β_{ref} is temperature coefficient of output power given by manufacture, T_{ref} is 25°C. The convective heat exchange is given by:

$$Q_{conv} = h_{conv} (T_p - T_{amb}) A_p \quad (4. 4)$$

Where h_{conv} is the forced convection coefficient that can be approximated as a function of wind speed, which is given by:

$$h_{conv} = 2.8 + 3 \times v_{wind} \quad (4. 5)$$

Where v_{wind} is the wind speed. Actually, there are many different force convection equations(Armstrong and Hurley, 2010), the equation used here is proposed by Watmuff(Watmuff et al., 1977) which is widely used during the investigation of PV/T panel. The long-wave radiation heat exchange is given by:

$$Q_{rad} = \sigma \varepsilon_p (T_p^4 - T_{sky}^4) A_p + \sigma \varepsilon_f (T_p^4 - T_{amb}^4) A_f \quad (4. 6)$$

Where σ is the Stefan-Boltzmann's constant, ε_p is the emissivity of the panel, ε_f is the emissivity of the frame, A_f is the frame area, T_{sky} is the sky temperature that can be approximated as a function of ambient temperature, which is given by(Schott, 1985, Ji et al., 2008a):

$$T_{sky} = \begin{cases} 0.0552 \times T_{amb}^{1.5} \\ T_{amb} \end{cases} \quad \text{for overcast conditions} \quad (4. 7)$$

The heat loss at the back of the PV panel is given by:

$$Q_{loss} = \frac{T_p - T_{amb}}{\frac{\delta_{ins}}{\lambda_{ins}} + \frac{1}{h_{conv}}} A_p \quad (4.8)$$

Where δ_{ins} is the thickness of the insulation material, λ_{ins} is the thermal conductivity of the insulation material. The removed heat through evaporator is given by:

$$Q_e = \frac{T_p - T_{al}}{\frac{\delta_{gl}}{\lambda_{gl}} + \frac{\delta_{bs}}{\lambda_{bs}} + TCR} \quad (4.9)$$

Where T_{al} is the temperature of the aluminum plate, δ_{gl} is the thickness of the glass, λ_{gl} is the thermal conductivity of the glass, δ_{bs} is the thickness of the back sheet, λ_{bs} is the thermal conductivity of the back sheet, TCR(Sridhar, 1999) is the thermal contact resistance between the back sheet and the aluminum plate.

4.1.2 Compressor

The mass flow of the refrigerant is given by:

$$m_r = \rho_s \lambda_v \frac{V_{dis} \cdot RPM}{60} \quad (4.10)$$

Where ρ_s is the density of the suction gas, λ_v is the volumetric efficiency of the compressor, V_{dis} is the displacement of the compressor, RPM is the rotating speed of the motor. The theoretical power consumption of the compressor is given by:

$$N_{th} = \lambda_v V_{dis} \cdot RPM \cdot P_s \frac{k}{k-1} \left[\left(\frac{P_d}{P_s} \right)^{\frac{k-1}{k}} - 1 \right] \quad (4.11)$$

Where P_s is the suction gas pressure, P_d is the discharge gas pressure, k is adiabatic compression index. The input power consumption of the compressor is given by:

$$N_m = \frac{N_{th}}{\eta_i \eta_m \eta_{mo}} \quad (4.12)$$

Where η_i , η_m , η_{mo} are the indicated efficiency, mechanical efficiency and motor efficiency, respectively.

4.1.3 Evaporator

Turbulent flow and forced convection heat transfer are taking place in the evaporator tube with the internal diameter d_i and length L . The removed heat through evaporator can also written as:

$$Q_e = \pi d_i L h_e (T_w - T_r) \quad (4.13)$$

Where h_e is the average heat transfer coefficient of refrigerant, T_r is the refrigerant temperature, T_w is the wall temperature (the thermal contact resistance between the aluminum plate and copper tube is ignored, which means $T_w=T_{al}$). The following correlations (Chen, 1966, Shah, 1979, Shah, 1982, Cooper, 1984, Jung et al., 2004, Jingdan et al., 2012) can be used to determine the average heat transfer coefficient:

$$h_e = S \times h_{NB} + e \times h_l \quad (4.14)$$

$$h_{NB} = 55q^{0.67} M^{-0.5} P_r^m (-\log_{10} P_r)^{-0.55} \quad (4.15)$$

$$P_r = \frac{P}{P_{crit}} \quad (4.16)$$

$$m = 0.12 - 0.2 \log_{10} R_p \quad (4.17)$$

$$S = \frac{1}{1 + 2.53 \times 10^{-6} \times Re^{1.17}} \quad (4.18)$$

$$Re = Re_l e^{1.25} \quad (4.19)$$

$$e = \frac{2.35}{\left(\frac{1}{X_n} + 0.213\right)^{0.736}} \quad (4.20)$$

$$h_l = 0.023 Re_l^{0.8} Pr_l^{0.4} \frac{k_l}{d} \quad (4.21)$$

Where h_l is the heat transfer coefficient in liquid state, q is the heat flux, M is molecular weight of the refrigerant, P_r is the relative pressure, P is the pressure of the refrigerant, P_{crit} is the critical pressure of the refrigerant, R_p is the surface roughness (the approximate surface roughness of copper is $1 \mu\text{m}$), Re_l is the Reynolds number of the liquid phase, x is Inlet quality of refrigerant, μ_l , μ_g are the viscosity of the refrigerant in liquid and gas state, respectively, ρ_g , ρ_l are the density of the refrigerant in gas and liquid state, k_l is the conductivity of the refrigerant and d is the inner diameter of the pipe.

4.1.4 Thermostatic expansion valve

Thermostatic expansion valve can control the amount of refrigerant flow into the evaporator thereby controlling the superheat at the outlet of the evaporator. At condensing pressure P_c and evaporation pressure P_e ,

$$m_r = C_{TEV} (2\rho_l (P_c - P_e)) \quad (4.22)$$

Where C_{TEV} is the characteristic constant of the thermostatic expansion valve.

4.1.5 Water-cooled condenser

In the condenser, the refrigerant undergoes phase changes from superheated gas to sub-cooled liquid. The direction of change is opposite to what happens in the PV evaporator. The heat exchange at the water side is given by:

$$Q_c = C_w m_w (T_{o,w} - T_{i,w}) \quad (4.23)$$

Where Q_c is the condensing capacity, C_w is the specific heat capacity of the water, m_w is the mass flow of the water, $T_{o,w}$ and $T_{i,w}$ are outlet and inlet water temperature, respectively.

$$Q_c = \frac{LMTD}{\left(\frac{1}{h_w A} + R_{plate} + \frac{1}{h_r A} \right)} \quad (4.24)$$

Where LMTD is log-mean temperature difference, h_w and h_r are the heat transfer coefficients on the water side and refrigerant side, R_{plate} is the thermal resistance of the plate.

h_w can be calculated by using equation 3.5, h_r can be calculated by using equation 3.12.

The log-mean temperature difference is determined from a weighted average of the LMTDs for each segment of the heat exchanger; superheat, two-phase, and subcooled (Kedzierski, 1997). An alternate method for determining LMTD is to neglect the refrigerant subcooled and superheating and use the refrigerant saturation temperature instead of the actual refrigerant inlet and outlet temperature in the expression for LMTD. This approach may be reasonable for cases with small percentage of the overall heat transfer occurring in the subcooled and superheating regions. The expression for LMTD in this case are:

$$LMTD = \frac{(T_{sat} - T_{i,w}) - (T_{sat} - T_{o,w})}{\ln\left(\frac{T_{sat} - T_{i,w}}{T_{sat} - T_{o,w}}\right)} \quad (4.25)$$

4.2 Performance indicators

The most important performance indicators include heating capacity, PV output power, conversion efficiency, heat-collecting efficiency, heat pump's COP, average COP and energy generation factor of the whole system.

Heating capacity, PV output power is given by equation 4.23 and equation 4.3.

Conversion efficiency is given by:

$$\eta_c = \frac{E}{G_s A_p} \quad (4.26)$$

Heat-collecting efficiency is given by:

$$\eta_p = \frac{\int Q_c - N_{in}}{\int (G_s \cdot A_p)} \quad (4.27)$$

COP means coefficient of the performance which is given by

$$COP = \frac{Q_c}{N_{in}} \quad (4.28)$$

Average COP is given by:

$$COP_a = \frac{\int Q_c dt}{\int N_{in} dt} = \frac{C_w m_w (T_{h,w} - T_{l,w})}{\int N_{in} dt} \quad (4.29)$$

Where $T_{h,w}$ and $T_{l,w}$ are final and initial water temperature. This system generates thermal energy and electrical energy at the same time, so an energy generation factor of the system can be obtained from the definition of the COP of a heat pump system, the output power of PV panel is transformed into the equivalent thermal power through the use of the average electricity-generation efficiency of a coal-fired power plant, it is given by:

$$f_{en} = \frac{Q_c + E \eta_{inv} / \eta_{power}}{N_{in}} \quad (4.30)$$

Where η_{inv} is the efficiency of the grid tie inverter, the value given by the manufacture is 0.85. And a commonly used value of η_{power} is 0.38. Average $f_{en,a}$ is given by:

$$f_{en,a} = \frac{\int (Q_c + E \eta_{inv} / \eta_{power}) dt}{\int N_{in} dt} \quad (4.31)$$

4.3 Chapter summary

The mathematical model of the PV/T heat pump was built. The main performance indicators are heating capacity, PV power, conversion efficiency, heat-collecting efficiency, COP, energy generation factor.

5 Experimental investigation

In this chapter, the design of the test rig will be introduced in detail, including the working principle of the system, the components used and how they were connected. There is also information about how the test rig was built up and plans to do the experiment. Finally, experimental results and some problems during the test will be discussed.

5.1 Description of the test rig

5.1.1 Test rig design

The test rig is composed of a PV system and a heat pump water heater system. A schematic diagram of the test rig is shown in Fig. 5- 1. R290 was used as the refrigerant in this heat pump (refrigeration) system. The following describes the working principle of the test rig.

When the PV/T heat pump system operates, the superheated refrigerant gas from the PV evaporator enters the constant frequency compressor. With its pressure and temperature lifted up at the compressor, the refrigerant enters the condenser (brazed plate heat exchanger) where the refrigerant gas releases heat energy which is absorbed by the water, and the refrigerant gas condenses into liquid. The liquid refrigerant has a sudden pressure drop when passing through the thermostatic expansion valve, it becomes a low temperature two-phase fluid then enters the evaporator. The refrigerant absorbs heat energy which mainly comes for solar energy in the evaporator and fully evaporates. The superheated refrigerant gets into the compressor and starts another heat pump cycle. The electricity generated by the PV panel is injected to the power grid. Because of the direct solar energy absorption, the evaporating temperature and pressure in the PV evaporator are higher than those in evaporator of the conventional heat pump. This improves the energy performance and in cold winter, protects the evaporator from frosting. What's more, since the evaporator absorbs the majority of the thermal energy, the temperature of the PV panel is lower than the panel without cooling, which leads to a higher panel conversion efficiency.

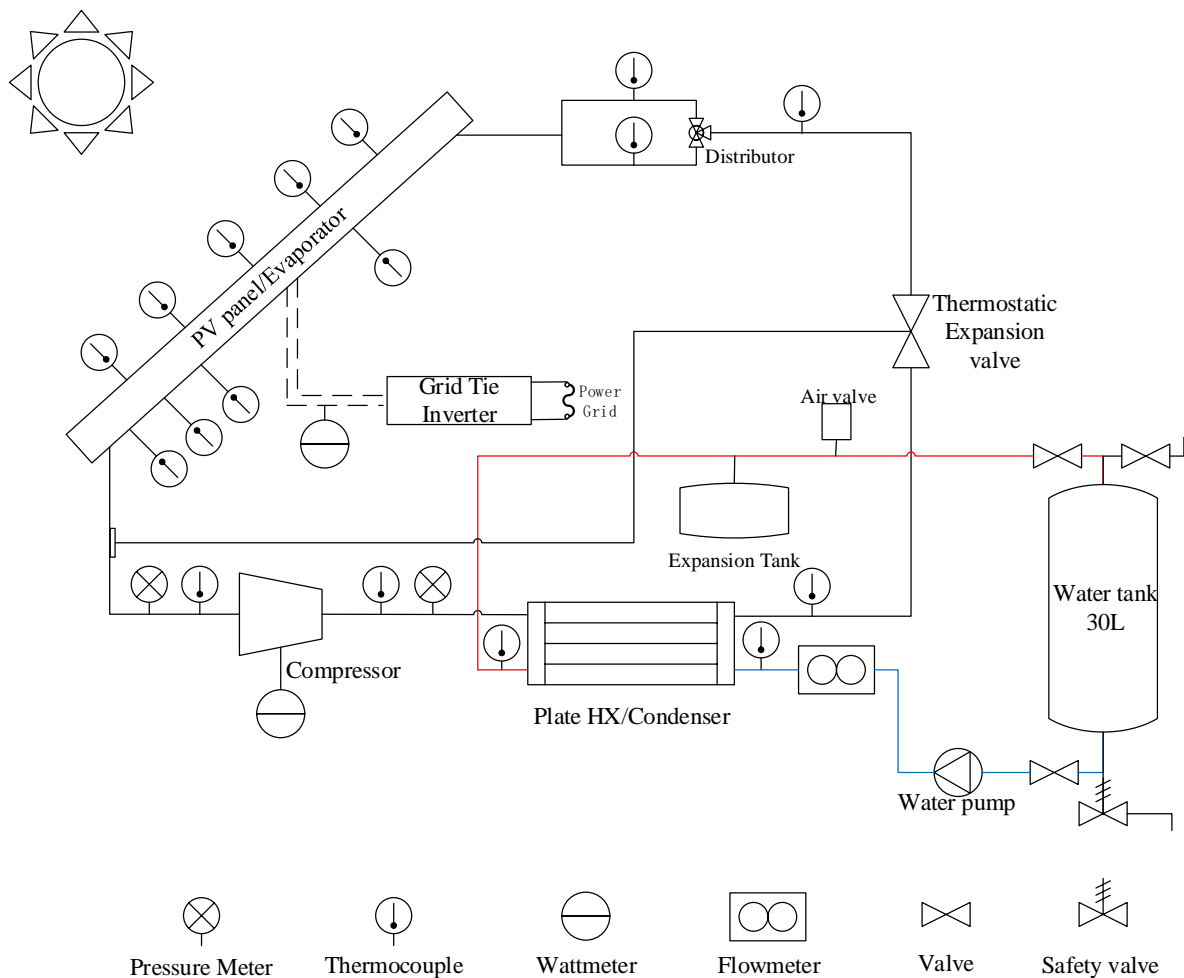


Fig. 5- 1 Schematic diagram of the test rig

The main components of the PV system are PV panel and grid tie inverter. The PV panel used in this test is REC260PE. Table 5- 1 shows the main information of the PV panel. More detailed information can be found in Appendix.

Table 5- 1 Specific features of the PV panel

Parameters	Value(unit)
Dimensions	1663.7mm×990.6mm
Area	1.64m ²
Weight	18kg
Nominal Power-P _{MPP}	260(W)
Nominal Power Voltage-V _{MPP}	30.7(V)
Nominal Power current-I _{MPP}	8.5(A)
Open circuit Voltage-V _{OC}	37.8(V)

Short circuit current-I _{sc}	9.01(A)
Electrical efficiency	15.8%
Nominal operating cell temperature	45.7°C(±2°C)
Temperature Coefficient of P _{MPP}	-0.40%/°C
Cell type	60RECPE multi-crystalline 3 strings of 20 cells with bypass diodes
Glass	1/8" solar glass with anti-reflection surface treatment
Frame	Anodized aluminum
Back sheet	Double layer highly resistant polyester

In most research, the photovoltaic system consists of PV panel (PV cells), PV controller, inverter, accumulator and load. PV controller is used to control the output voltage and current. An inverter is used to convert direct current into alternating current. Accumulators are used to store electrical energy. The load can be anything which can safely consume the energy, like big lamps, fans. However, it is difficult to buy all these stuffs in Norway and this project can't afford all of them because of the limited funds. Then another way which may meet the requirement was found. Since none of the components need to be supplied by the PV panel and it is not necessary to store the energy during the test, a grid tie inverter can be used.

Grid-tie inverter is a device which can convert direct current into an alternating current suitable for injecting into an electrical power grid. The grid-tie inverter can be directly connected with solar panel and power grid, the installation is shown in Fig. 5- 2. This kind of inverter has MPPT function, it can automatically find the max power point of the PV panel, which means the electricity generated by the PV panel can be fully utilized. Because of these characteristics, a controller or a load or an accumulator was not necessary to be used. It makes the PV system much cheaper, simpler and more efficient. What's more, the price of the electricity generated by the PV products is more expensive than the residential electricity price in China because of the current policy. This means injecting the electricity into the power grid is a wiser choice compared with using it directly. The stable efficiency of the inverter given by the manufacture is above 84%.

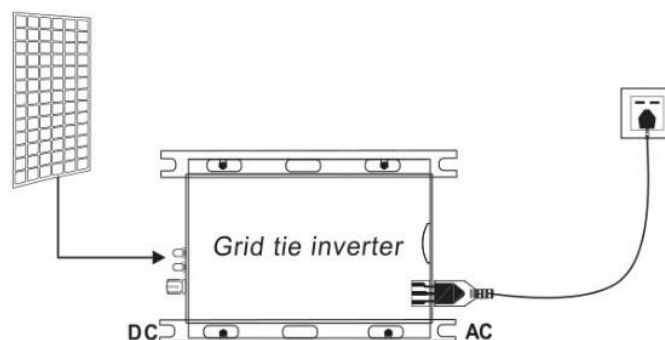


Fig. 5- 2 Installation of the grid tie inverter

The main components of the heat pump water heater system are compressor, evaporator, condenser, thermal expansion valve, water tank, water pump, and so on. They are shown in Table 5- 2. The specification of some important components like compressor can be found in Appendix.

Table 5- 2 Component list

Components	Type	Notes
Compressor	SECOP DLE5.7CN	For R290
Evaporator	Serpentuator	3/16" copper tube
Condenser	SWEP, B5TH*20	Plate heat exchanger
Expansion Valve	Danfoss, TUB 068U3702	Internally thermal expansion valve
Water tank	Flexi Benk RB 30	30L water tank
Water pump	ALPHA1 15-60 130	Max head: 6m
Expansion tank	A-Flex	Volume: 8L
Air valve	SYR 62	For safe purpose

The compressor is specially designed for R290, the Max. continuous condensing temperature given by the supplier is 55 °C, and the max condensing temperature can reach 65°C for short run. Considering the thermophysical properties of R290, the outlet water temperature of the heat pump is usually between 50°C and 60°C. Therefore, the chosen compressor can meet the requirement.

The evaporator is integrated with PV panel. The PV/T evaporator is designed by Mr. Magnus, the former student in charge of the project. The way it was made will be introduced in

next section. The construction of the PV/T panel is shown in Fig. 5- 3. Following are some features on the PV/T evaporator, a) the assembly, b) AluFlex aluminum profile, c) custom aluminum hub, d) 3-D printed (PLA-plastic) bracket, e) standard bolts, M6×40 and M5×20, f) copper tube (3/16”), g) 8mm thick aluminum back plate.

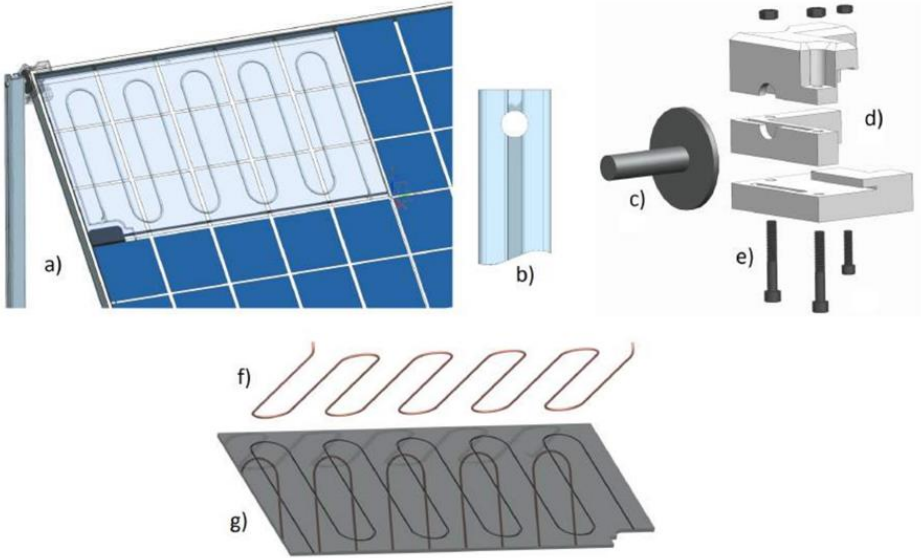


Fig. 5- 3 Diagram of the PV/T evaporator

There are 4 coils in total, in order to get a relatively low pressure drop and high heat transfer coefficient in evaporators, two of the coils are connected in series and then connect the coils in parallel. Hence, a distributor is necessary between the expansion valve and evaporator to distribute the two-phase flow. What’s more, considering getting better oil return, the refrigerant should go from the top to the bottom of the evaporator, so the high speed gas can bring the oil back to compressor.

The thermostatic expansion valve is approved for R290 by ignition source assessment in accordance to standard EN13463-3. It is an internally one, and the default superheat of this valve is 5°C according to the specification given by the supplier.

Brazed plate heat exchanger is used as condenser in this test rig. With its high heat transfer efficiency, the temperature difference between water and refrigerant is low. The simulated result of the performance of the plate heat exchanger was provided by the famous heat exchanger producer SWEP, which can be found in Appendix. Since without any Non-disclosure agreement, the company refused to provide the geometric characteristics of the plate heat exchanger. Some

geometric characteristics could be found on its website, others were found from other researchers' papers, and the rest of them were calculated according to the simulated results. They are shown in Table 5- 3.

Table 5- 3 Geometric characteristics of the brazed plate heat exchanger

Geometric characteristics	Value
Fluid flow plate length (mm)	154
Plate width (mm)	76
Area of the plate (mm ²)	0.012
Angle of the corrugation (°)	60
Corrugation amplitude (mm)	2
Plate thermal conductivity (w/m·k)	16
Number of plates	20
Number of plates effective in heat transfer	18
Number of channels on refrigerant side	9
Number of channels on water side	10

When 35L water (assuming the volume of the tubes and water pump is around 5L) is heated from 8°C to 55°C (since the final water temperature is over 50°C, so 55°C was chosen to do the calculation), the expansion volume is over 0.5L. Although the test rig already has a safety valve at the bottom of the water tank, we decided to add an expansion tank and an air valve on the water side. Hence, it's unnecessary to consider the drain during the experiment and it is safer.

The water pump can adjust its capacity during the operation, it only runs at minimum power and its power is around 10W. Usually, the economic flow velocity before the pump is 1-1.2m/s and the economic flow velocity after the pump is 1.5m/s to 2m/s. According to the design mass flow rate of the water, copper tubes with 15mm inner diameter were used in this test rig.

Fig. 5- 4 shows the draft of the test rig drawn by Unigraphics NX. It shows the frame of the rig and layout of the main components. The frame was made by aluminum profile. Since we have to do the experiments outside the Lab, 4 wheels were fixed on the test rig to make it movable. The position of the components is only for reference. The exact layout is determined

by the requirement during the process of building.

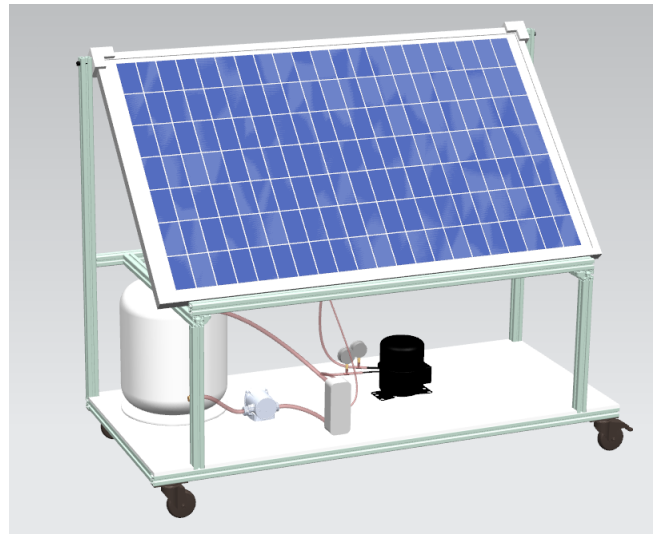


Fig. 5- 4 Draft of the test rig

5.1.2 Test rig build-up

The technicians and engineers from the Department of Power and Process Engineering helped build up the test rig. The Fig. 5- 5 a) shows the frame of the test rig. It is consisted of aluminum profiles, angle hinge brackets, two wheels with brake and two wheels without brake, and a wooden board. The movable horizontal profile on the frame is designed to fix the PV panel. The latitude of Trondheim is $63^{\circ}25'N$, and this test rig wasn't going to operate during the winter time in Norway, so the tilt angle of the PV panel should be the latitude minus the mean solar declination angle during the operation time. The mean solar declination angle during May, June and July is around 20° , so 45° was chosen as the tilt angle of the PV panel. Fig. 5- 5 b) shows the construction of the evaporator, it was made by the aluminum plate with the copper coils. The copper tubes were bended manually and embedded in the aluminum plate, they were also covered with aluminum tape. Considering it is necessary to make sure that each path of the evaporator gain the same heat, the four plates should be on the same plane, so they were fixed together as shown in Fig. 5- 5 c). Since the PV panel was borrowed from another institute and I was not supposed to do any destructive modifications, the PV panel and evaporators were fixed together by using a physical way. None thermal conductive grease was used between the aluminum plate and the back sheet of the PV panel, which was proven a mistake. The PV evaporator was covered with thermal insulator on the back. Fig. 5- 5 d) shows the main

components used to build the test rig. There is a compressor, a plate heat exchanger, a water pump, a water tank, some tubes on the table. From Fig. 5- 5 e), the layout of these components and the way they were connected can be seen. Fig. 5- 5 f) shows the Expansion tank and the air valve.

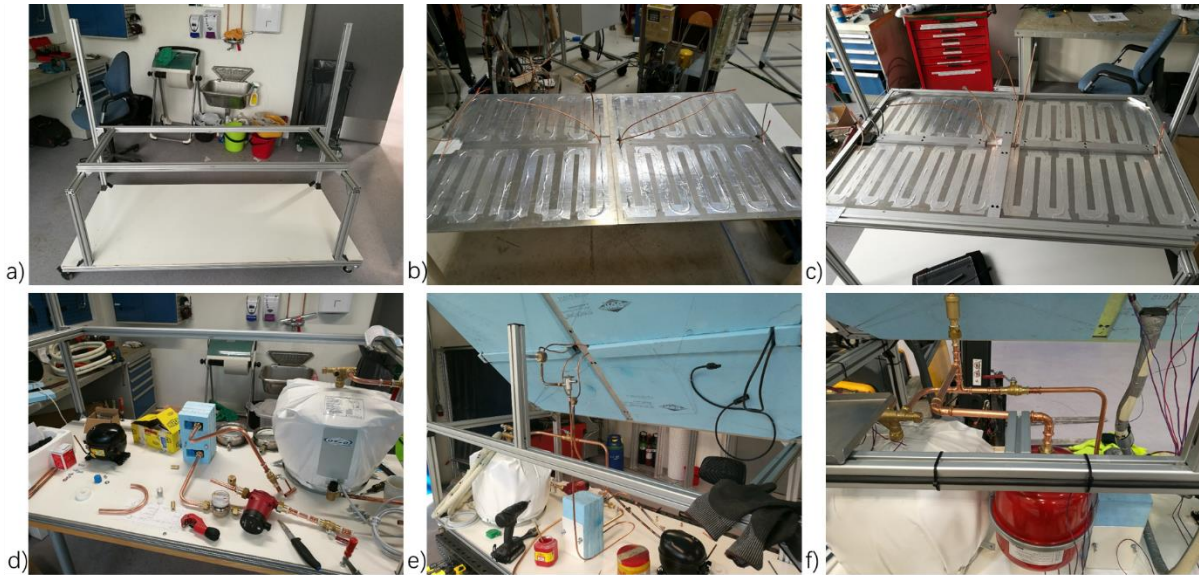


Fig. 5- 5 a) Frame of the test rig; b) Aluminum plate with copper coils;
 c) PV panel integrated with evaporator; d) Main components of the test rig;
 e) Connections between components; f) Expansion tank and air valve

The electric cabinet of the test rig is shown in Fig. 5- 6 a). The electric cabinet has two switches which are used to control the compressor and water pump. There are two cables at the bottom of the cabinet, one is connected with power grid and another is connected with water pump. There are two sockets on the right side of the cabinet, the top one is designed for the compressor, which means this socket is connected with the switch. And with the help of the socket, an energy meter can be used to measure the power consumption and energy consumption of the compressor. The bottom socket is designed for other electric devices like data logger, solar inverter and laptop. An extension socket with switch is connected with this socket. Fig. 5- 6 b) shows the grid tie inverter, it can eject the electricity generated by the PV panel to the power grid. The grid tie inverter also has a switch on it to make sure it will not work unless during the experiments.

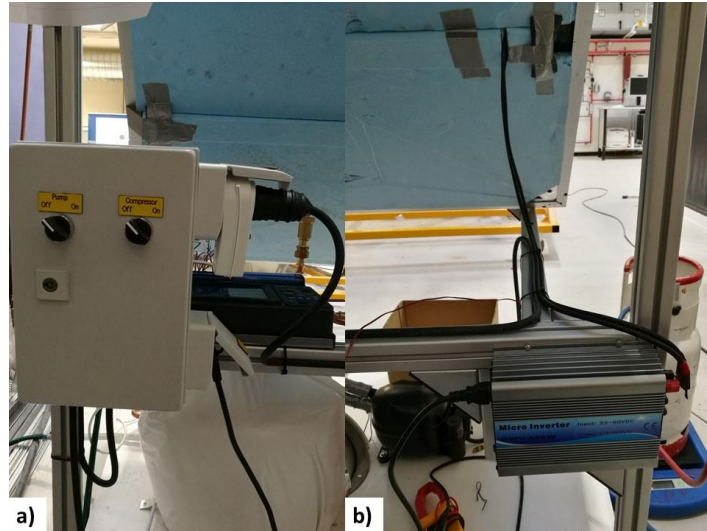


Fig. 5- 6 a) Electric cabinet b) Grid tie inverter

The tubes on refrigerant side were covered with insulator. It can not only reduce the heat convection between the tubes and environment but also improve the accuracy of temperature measurement. After air tightness detection and undergoing 26Bar pressure test, the heat pump system was vacuumed and refrigerant was charged into the system, which is shown in Fig. 5- 7. According to the estimation, the R290 charge weight is 98g and finally around 100g R290 was charged.

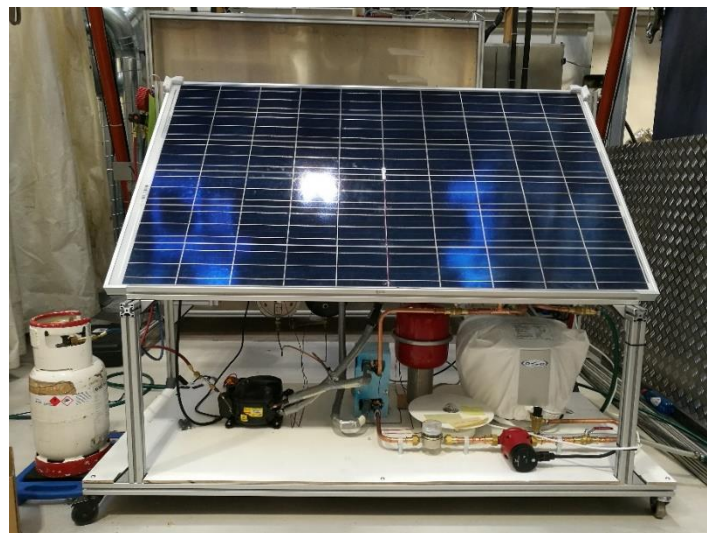


Fig. 5- 7 Refrigerant charge

5.1.3 Instrumentation

In this part, the instrumentation of the test rig will be introduced. Table 5- 4 shows the list of the instruments used during the experiment, the information of the range, resolution, accuracy is also included. The specification of some instruments can be found in Appendix.

The layout how the instruments were settled can be found in Fig. 5- 1. Some important instruments will be introduced next.

Table 5- 4 Instrument list

Instrument		Range	Resolution	Accuracy
Data logger	Temperature	-100-100°C	0.01°C	±0.6°C
	Voltage	-20-20mV	0.001mV	±0.02mV
	Energy meter	5-3680W	1W	±2%
	Pyranometer	0-4000W/m ²	0.1W/m ²	±10W/m ²
Clamp meter	Current	0-600A	0.1A	2%±5 digits
	Voltage	0-600V	0.1V	1%±5 digits
	Pressure gauge 1	-1-14Bar	0.05Bar	±5%
	Pressure gauge 2	-1-25Bar	0.5Bar	±5%
	Water meter	0-99999.999m ³	1L	±2%

A pyranometer is able to measure the solar radiation received by a plane surface from a 180° field of view angle. This quantity measured by a pyranometer is called “hemispherical” solar radiation, its unit is W/m². In an irradiance measurement by definition the response to “beam” radiation varies with the cosine of the angle of incidence; for example, it should have full response when the solar radiation hits the sensor perpendicularly (normal to the surface, sun at zenith, 0° angle of incidence), zero response when the sun is at the horizon (90° angle of incidence, 90° zenith angle), and 50 % of full response at 60° angle of incidence. The tilt angle of the PV panel is 45°, in order to directly measure the solar irradiance on PV panel, we should put the pyranometer at a tilt angle of 45°. By using a thermopile sensor, a pyranometer can generate a small output voltage proportional to the flux, it works completely passive. It can be only used in combination with a suitable measurement system, which is a data logger in this project. The pyranometer used during experiment is shown in Fig. 5- 8.

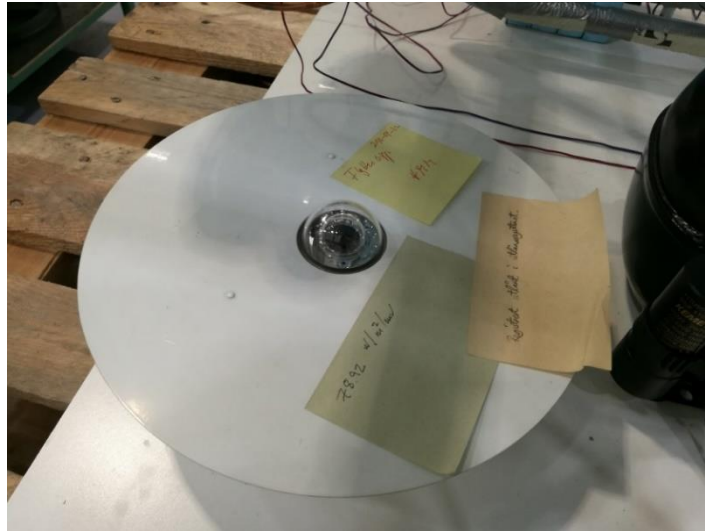


Fig. 5- 8 Hukseflux pyranometer

The data logger used here is HIOKI LR8400-20 data logger, which is shown in Fig. 5- 9. It is a high-speed data logger for recording multiple channels of voltage, temperature humidity and pulse signals, providing complete isolation between channels and strong noise resistance. It can log data at 10ms speeds across 30 channels simultaneously. During the experiment, it can be used to record the temperature data, voltage data from the pyranometer and pulse signals from water meter.



Fig. 5- 9 HIOKI LR8400-20 data logger

To get the output power of the PV panel, the output voltage and output current is necessary. After the discussion with technicians, a clamp meter was used to do the measurement during the experiment.

5.2 Experimental scheme

The tests were carried out in Trondheim, Norway located at 63°26'N and 10°24'E. The PV panel was set south-facing at 45° tilt angle and was exposed with natural sun light during the day at different ambient air temperatures, and in periods with no sun, was operated in the laboratory with light from an artificial sun.

5.2.1 Overall view of the test rig performance

The objective of the experiment is to know the performance of the PV system, heat pump water heater system and the whole system. The performance indicators are introduced in section 4.2.

The performance of the PV system is evaluated by the conversion efficiency, which can be calculated by the solar radiation and power of the PV panel. The solar radiation can be calculated by the output voltage of the pyranometer, which is recorded by the data logger. The PV power can be calculated by the voltage and current measured by the clamp meter.

The performance of the heat pump water heater is decided by the COP, which can be calculated by the power consumption of the compressor and heating capacity. The power consumption of the compressor can be measured directly by the energy meter. The heating capacity should be calculated by the water mass flow rate and temperature lift after plate heat exchanger.

With all the information above, the performance of the whole system can be evaluated.

However, more parameters are necessary to judge if the test rig works properly, following are the important parameters:

Temperature on the PV panel, back sheet and back plate: it is difficult to calculate the contact thermal resistance between back sheet and aluminum plate theoretically, with the help of this information, the mathematical model of the PV/T evaporator can be more accurate; what's more, this information can be used to judge whether the radiation from the artificial sun is even when the experiments were performed in the Lab according to the temperature distribution on the panel.

Suction pressure, suction temperature, inlet temperature of the evaporator: with the help of this information, the evaporating temperature, pressure drop in evaporator can be calculated;

The superheat temperature can also be calculated, and by adjusting the opening of the expansion valve, a suitable superheat can be obtained.

Discharge temperature and outlet temperature of condenser: with the help of this information, the sub cooling temperature of the heat pump system can be calculated to decide whether the condenser is chosen correctly.

Outlet temperature of two paths of the evaporator: if there is a big difference between the outlet temperature of the two paths, it means the distribution of the two-phase refrigerant is uneven. If too much liquid refrigerant goes into one path, the refrigerant cannot gain enough heat to evaporate, it may cause liquid hit if the worst happens, which can greatly damage the compressor.

5.2.2 Test procedure in laboratory

With the help of the artificial sun, it is possible to do the experiment in the lab. The artificial sun is shown in Fig. 5- 10. It has 7 lamps, the input power of each lamp is 2000W and it is nonadjustable. The number of the working lamps can be controlled to decide the radiation.



Fig. 5- 10 Artificial sun

By adjusting the angle of the lamps, the beam from the lamps hit the PV panel perpendicularly, Fig. 5- 11 shows the bird's eye view of the test facilities. Following are the detailed test steps:

- 1) Fill the water tank with tap water;

- 2) Switch on the data logger, then switch on the inverter;
- 3) Switch on the water pump, adjust the capacity of the water pump, wait for few minutes until it runs stable;
- 4) Switch on the artificial sun;
- 5) Start recording data, check the temperature data, make sure the inlet water temperature and outlet water temperature are the same;
- 6) After the lamps are fully heated up, switch on the compressor;
- 7) During the test, record the pressure, power consumption of the compressor, output voltage and current of the PV panel manually every 3 minutes (or shorter);
- 8) Switch off the compressor when the inlet water temperature is over 50°C, stop recording data;
- 9) Switch off the artificial sun;
- 10) Switch off the inverter, data logger and water pump, disconnect the power supply;
- 11) Drain the water tank.



Fig. 5- 11 Bird's eye view of the test facilities

The environment in the lab is stable, the room temperature is around 20°C, and there is almost no wind in the room. The investigation should be focused on the influence of the solar radiation. Tests should be done by using different number of lamps.

5.2.3 Test procedure outside laboratory

Tests were also carried out outside the lab, as shown in Fig. 5- 12. The test procedure outside lab is almost the same as the test procedure in the lab, only have to remove step 4 and 9. The test rig should be moved into Lab when it is not running for safety reasons.



Fig. 5- 12 Test rig outside Laboratory

The test rig has no rain-proof design, so it can't run on rainy days.

5.3 Experimental results and analysis

Some tests were performed in the Lab and outdoor. Experimental results and analysis will be introduced in this section. During the experiment, some problems were found and part of them were solved. These problems and ways to solve them will be discussed in this section.

5.3.1 Tests in laboratory

Several tests were performed in the lab with the help of the artificial sun. However, some problems occurred during these tests. After searching for some information, it turned out that this artificial sun was not suitable for our test rigs because of the following reasons.

- (1) The beam from the lamp is not parallel, so the radiation is uneven on the PV panel. The uneven radiation will cause the problem of mal-distribution of the refrigerant. And it is difficult to measure the solar irradiance on the PV panel. What's more, the temperature of some point on the PV panel will become very high while the operational temperature

of the PV panel on its specification is between -40°C and 85°C . This means doing experiments with artificial sun was not safe and may cause permanent damage to the PV panel.

- (2) Maybe because of the aging of the lamps, the radiation from different lamps were not the same. This guess can be verified by the uneven temperature distribution on PV panel. The heat pump system was not running then, so the temperature difference can be only caused by the artificial sun. It will also cause the mal-distribution problem.
- (3) The output power of the PV panel is much smaller than expected, only around 30W while the solar irradiance at some point is over $1000\text{W}/\text{m}^2$. One reason is the uneven radiation, most of the PV cells cannot get enough radiation; another reason may be the difference of the spectrum from the lamps and sun. The tests of the solar cell indoor have traditionally been performed using mostly Sulphur plasma lamps or xenon arc lamps (Bisaillon et al., 2000). But the lamps of the artificial sun are floodlights used for sports arenas and large public areas, which are not suitable for PV elements.

Therefore, in order to get real performance of the test rig, all the test results in the lab were given up, and the rest tests were done outside the lab. Experimental results discussed below are all from the tests done outdoor.

5.3.2 Experimental results before modification

Several tests were carried out on sunny days outdoor. The test results indicated some problems of the test rig and the main problem of the test rig was the mal-distribution of the refrigerant. The test results on May 11, 2017 will be introduced in detail.

Fig. 5- 13 shows the weather data on May 11, 2017. The solar irradiance was relatively steady that day and the value is around $850\text{W}/\text{m}^2\cdot\text{K}$, the ambient temperature was around 13°C . Since there is no anemometer in the Lab, the data of wind velocity was not recorded during the tests.

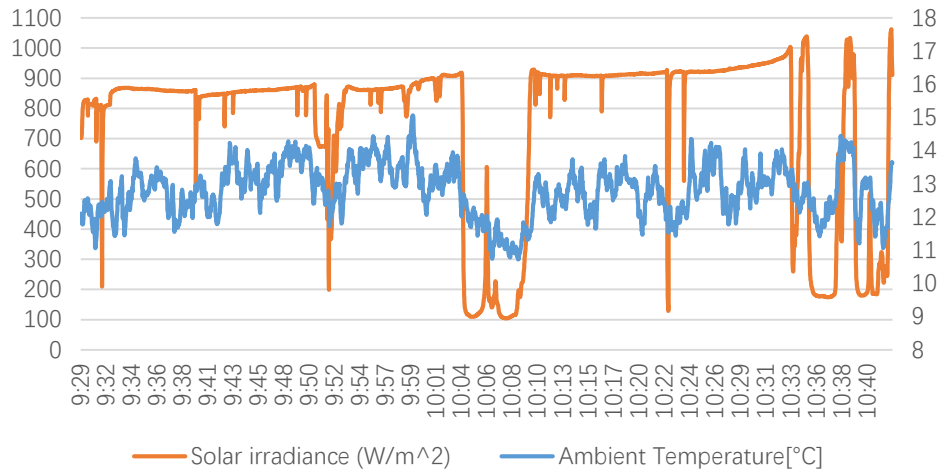


Fig. 5- 13 Weather data on May 11, 2017

Fig. 5- 14 shows the pulse signal from the pulse generator of the water meter. The pulse generator of the water meter generates one pulse every 10L water flowing through. According to the results of the linear fitting, the slope is 0.01702. So the flow rate of the water is about 0.17L/s. Since the temperature difference of water in condenser and power consumption of the compressor was measured, the heating capacity of the heat pump and COP of the heat pump system can be calculated.

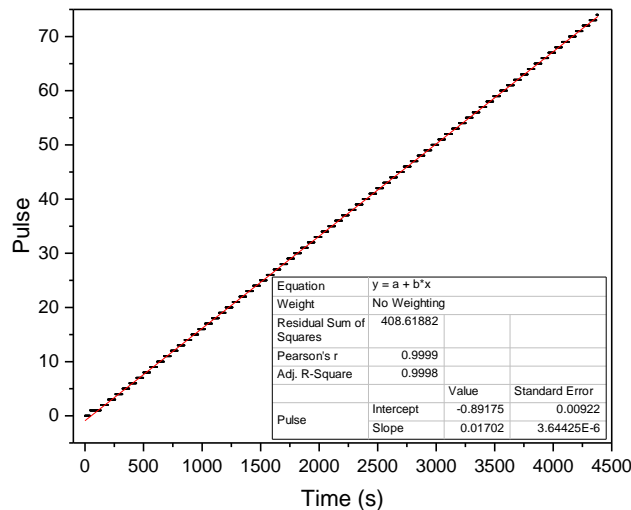


Fig. 5- 14 Pulse signal from the pulse generator water meter

The heating capacity was greatly influenced by solar irradiance and ambient temperature. As shown in Fig. 5- 15, it was cloudy between 10:03 and 10:10, the heating capacity decreased

greatly with a lag then. When the solar irradiance is small, the evaporator is not able to gain enough heat, the expansion valve will reduce the mass flow of the refrigerant to make sure the superheat, which decreases the heating capacity. The heating capacity after 10:10 was smaller than the heating capacity before 10:00 while the solar irradiance and ambient temperature was almost the same. According to my consideration, one reason was the increasing condensing temperature, another reason was mal-distribution in evaporator.

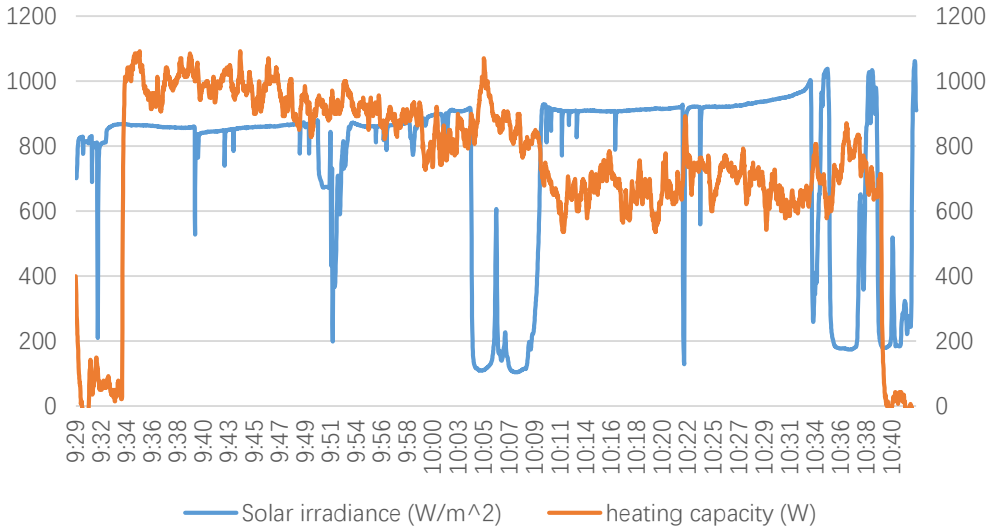


Fig. 5- 15 Variation of heating capacity and solar irradiance on May 11, 2017

Fig. 5- 16 shows the variation of condenser supply water temperature and power consumption of compressor. It can be seen that the compressor power was greatly affected by the inlet water temperature (condenser supply water temperature). From the experimental results, the compressor powers are determined as 198W, 229W, 257W for inlet water temperature at 20°C, 30°C, 40°C. A higher inlet water temperature means higher condensing pressure, which leads to a higher compression ratio and a higher compressor input power. An issue can be found in this figure: the inlet water temperature should always be increasing while there was decline between 10:00 and 10:10. This means the measured inlet water temperature was not accurate, and in fact, the value measured during the tests were higher than the actual one because the copper tube could absorb heat from solar radiation. A sunshade was used to cover the water tubes in the following tests.

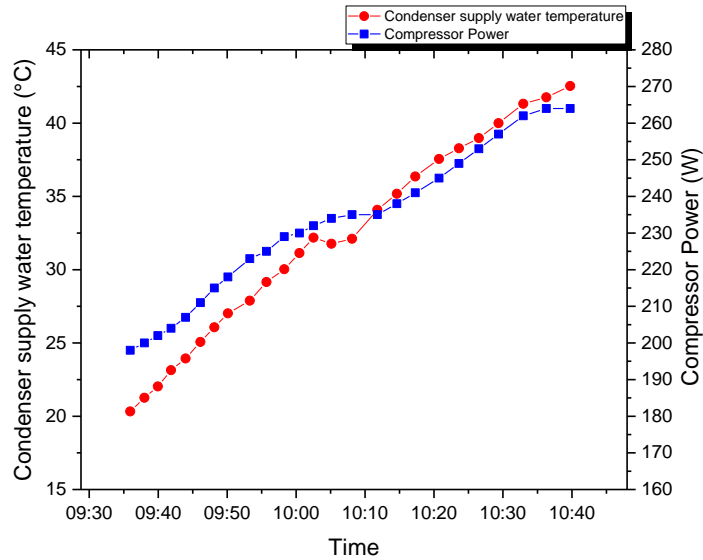


Fig. 5- 16 Variation of condenser supply water temperature and compressor power on May 11, 2017

Fig. 5- 17 shows the variation of PV electricity output and conversion efficiency. Comparing with the solar irradiance shown in Fig. 5- 13, it can be easily found out that a higher solar irradiance leads to a higher PV power output. Conversion efficiency is determined by cell temperature, which is influenced by solar irradiance, ambient temperature and cooling capacity of the heat pump system. Theoretically, a higher solar irradiance leads to a higher PV cell temperature, which is shown in Fig. 5- 18 (solar panel temperature 1, 2, 3, 4, 5 mean the temperature of detected point on panel shown in Fig. 5- 12 from left to right). And a higher PV cell temperature leads to a lower conversion efficiency. However, as shown in Fig. 5- 17, when the solar irradiance was smaller, the panel temperature was lower, and the conversion efficiency is smaller too. This is caused by the grid tie inverter according to my consideration. It is difficult for the inverter to find the max power point when the PV electricity output is very small. The output voltage of the PV panel was changing drastically while the solar irradiance is small. Meanwhile, the blue LED on the invert was flashing, which means the MPPT operating for tracking, adjusting for power output. Therefore, it existed some errors when voltage and current data was recorded. What's more, according to the specification of the PV panel, the conversion efficiency will reduce when the solar irradiance is lower than $200\text{W}/\text{m}^2$. The average conversion efficiency was only 14.1%, which is much lower than the value provided by the manufacture. One reason is that the cell temperature is higher than the nominal one, another reason is that the

max power point tracked by the inverter is not the accuracy one. The nominal max power voltage should be around 30V while the actual output voltage of the PV panel was around 28V.

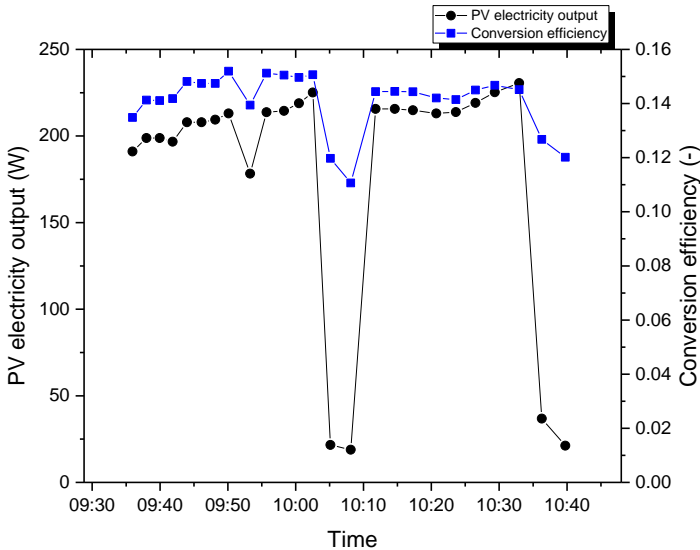


Fig. 5- 17 Variation of PV electricity output and conversion efficiency on May 11, 2017

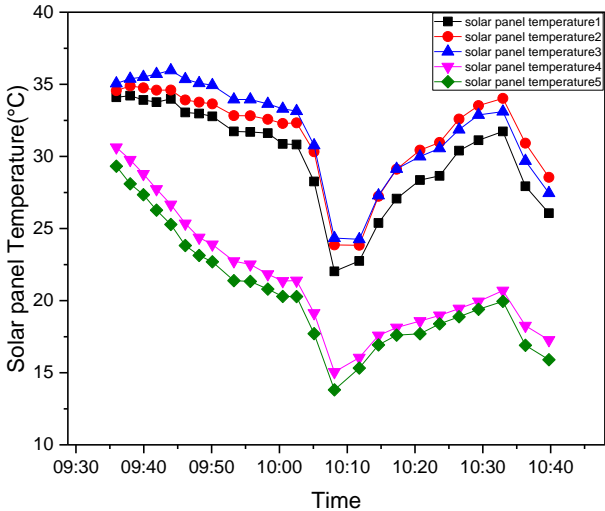


Fig. 5- 18 Variation of temperature of different points on PV panel on May 11, 2017

Fig. 5- 19 shows the variation of COP, average COP, f_{en} and $f_{en,a}$. The COP of the system is determined by the power consumption of the compressor and heating capacity. As mentioned above, the compressor power increases when the water temperature increases and the heating capacity was greatly influenced by the solar irradiance. These make the plot have a downward trend and fluctuation took place when the solar irradiance changed. The variation tendency of

the COP and energy generation factor was almost the same. The average COP of the system was only 3.5 when the water was heated from 20°C to 42°C. The energy generation factor was 5.2 during the whole operation.

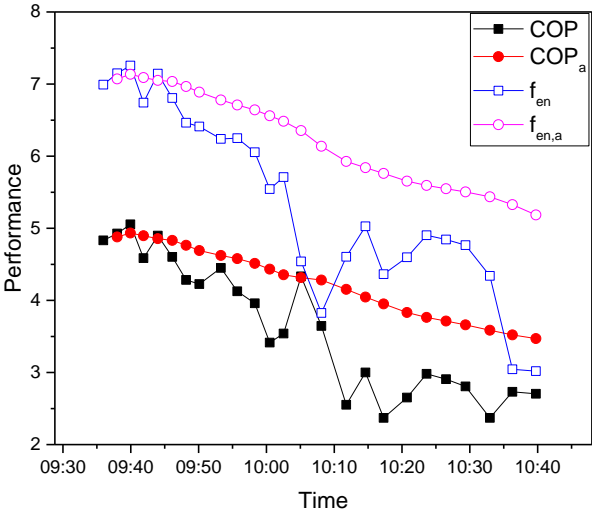


Fig. 5- 19 Variation of COP, average COP, f_{en} and $f_{en,a}$ of the system on May 11, 2017

The max continuous condensing temperature of the compressor is 55°C, and the condensing temperature can reach 65°C in a short period of time. Since a high efficiency plate heat exchanger was used as a condenser, the log mean temperature difference in condenser is about 4°C in design condition, it is easy and safe to get hot water over 50°C during experiment. The reason the water was only heated to 42°C on May 11 was mal-distribution of refrigerant in evaporator. Excessive refrigerant flowed in one of the evaporator paths and the cooling capacity might be reduced because the insufficient refrigerant flow in another path (Nakayama et al., 2000). What’s more, it was possible that some liquid refrigerant would flow into the compressor, which could cause great damage to compressor.

Some other tests were performed outdoor. However, the operation time was too short to get enough useful information because of the same problems mentioned above. The problems and modification of the test rig will be discussed in next section.

5.3.3 Problems and modification of the test rig

The test results shown above were not satisfying because the test rig had some problems. The most significant problems of the test rig are the design of the evaporator and the mal-distribution

in evaporator.

The diameter of the copper tube used in this test rig is very small, together with long tube length and big mass velocity (main caused by small sectional area of the tube), the pressure drop in evaporator is very big. Considering different refrigerants have different properties, especially the value of $\Delta t/\Delta p$ is quite different, it is difficult to judge the performance directly by pressure difference. So a temperature difference was used here to represent the pressure drop in evaporator. The temperature difference equals the inlet refrigerant temperature of the evaporator minus the saturation temperature under outlet pressure. The pressure drop should be lower than 2K while the test rig got a 4K pressure drop during experiment. The expansion valve used here is an internally one, the high pressure drop in evaporator leads to a high superheat, which is not good for the performance of the heat pump because it greatly limited the mass flow of the refrigerant. As shown in Fig. 5- 20, the average superheat of the heat pump could reach 12°C, which was obviously too high. The high superheat temperature can be controlled by adjusting expansion valve. However, it seemed impossible to solve the problem of pressure drop during the stay in Norway because there is no enough time to redesign and customize a new evaporator.

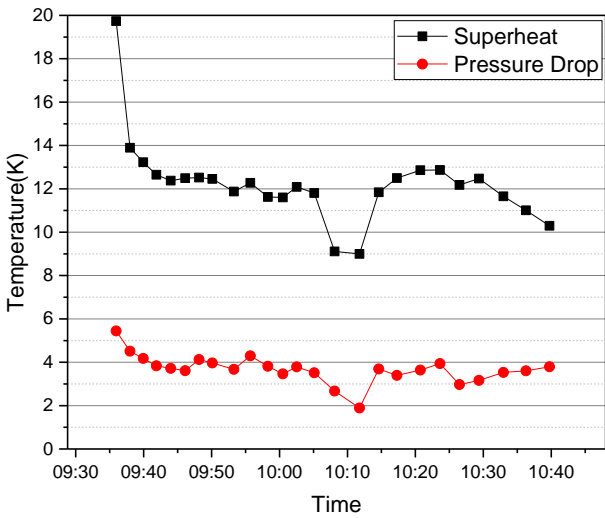


Fig. 5- 20 Superheat and pressure drop of the test rig before modification

Another problem of the test rig, which is also the most significant one, was the mal-distribution in evaporator. Fig. 5- 21 shows the refrigerant temperature after evaporator (test

results on May 11). The temperature difference was over 12°C and the outlet temperature of one path was abnormally high.

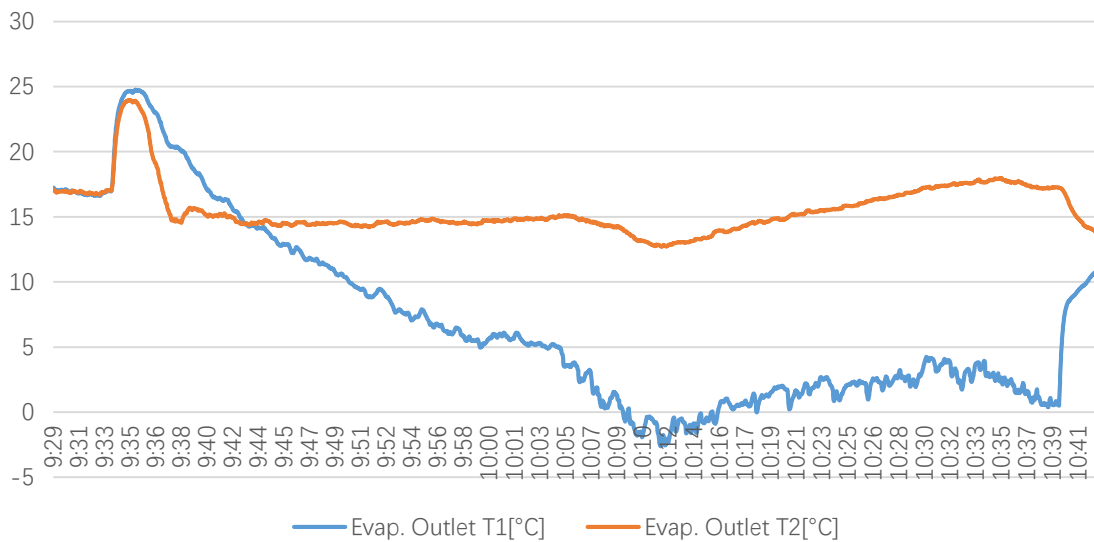


Fig. 5- 21 Variation of refrigerant temperature after evaporator before modification

There are several reasons for refrigerant mal-distribution: 1) Improper header, duct and circuit design; 2) Design defects of distributor; 3) Inclination of the distributor; 4) Fabrication tolerance; 5) Fouling and corrosion; 6) Uneven heat flux. Since the two paths of evaporator were the same and installed symmetrically, solar radiation on the panel should be even and fouling or corrosion should not be problems of a new test rig, the mal-distribution was very likely caused by design defects of distributor. Actually, the distributor used in this test rig was made by the technician in Lab because a suitable distributor for this system is hard to buy directly, it was a Y-shaped pipe which was not able to mix the refrigerant homogeneously. Nakayama (Nakayama et al., 2000) developed a new type of distributor to divide two-phase refrigerant equally into evaporator. A new distributor was customized based on his design. Fig. 5- 22 shows the section view of the new distributor, compared with the conventional distributor, the capillary mixing space is used to mix two-phase refrigerant instead of orifice. Therefore, the gas and liquid can be better mixed. According to Nakayama's experimental results, the length should be three times larger than the diameter of the mixing space and vertical installation is optimal option for distributor because of gravity.

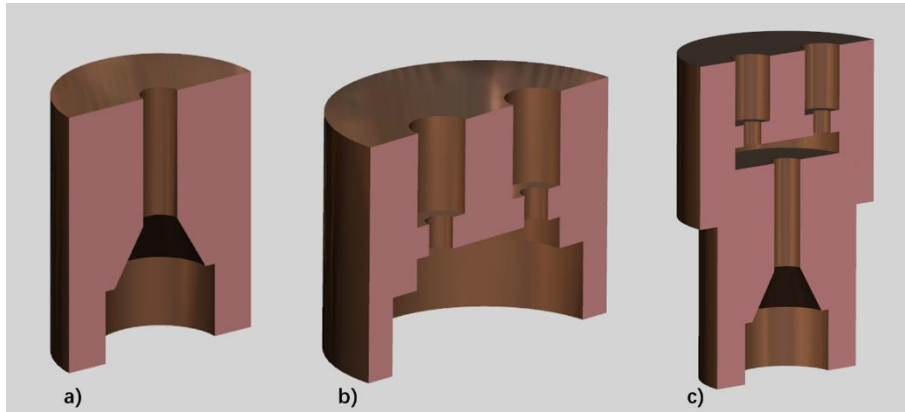


Fig. 5- 22 Section view of new distributor a) part1 b) part2 c) assembly

There are some control methods to optimize the refrigerant distribution in evaporator. A common one is individual refrigerant circuit control, which means each evaporator path needs one expansion valve. This way is not good because of its high cost. Another method is hybrid control, which optimizes distribution by controlling the inner diameter of feeder tubes or add throat valves after evaporator paths (Kim et al., 2009b). According to Kim's evaluation (Kim et al., 2009a), upstream control (controlling the inner diameter of feeder tubes) is a much better choice. The length of the feeder tube has a small impact on the performance of the refrigeration system while the inner diameter has a great impact. 3.92×0.71 mm capillary tubes were used as the feeder tube here.

Theoretically, a refrigeration system using distributor must use externally expansion valve because of the pressure drop in distributor and feeder tubes. However, using a new externally expansion valve means welding the pipe lines again. Along with delivery, pressure test and refrigerant charge, this plan really takes some time. What's worse is that the funds had already been run out then. Therefore, it's not worth replacing the expansion valve according to my consideration. Adjusting the expansion valve to control the superheat was the plan used during the experiment, which obviously not the best choice but an acceptable one. The default superheat of the expansion valve is 5°C and it was changed to 1°C by adjusting the position of the spring in valve. It can effectively increase the opening of the valve and reduce the superheat of the heat pump.

The test results after modification will be introduced in next section. However, the problem of mal-distribution in evaporator was not completely solved after modification according to the

test results. The new distributor and control strategy did do some help but the results are still not good enough. There must be some other reasons. After a period of observation, another possible explanation was raised and validated.

Uneven heat flux was not considered as a reason causing mal-distribution in the first place because of the symmetrical design. However, the test results after the modification proved the heat flux on the two sides are different, and the PV evaporator was not symmetrical. Before modification, only little refrigerant flowed into path 2, and of course the panel temperature above it was higher because of the small cooling capacity. After modification, more refrigerant flowed into path 2 instead of path 1, but the panel temperature above path 2 was still higher. A simple experiment was done to investigate this phenomenon. A thermal infrared imager was used to study the temperature distribution on PV panel. Fig. 5- 23 shows the photos taken by thermal infrared imager.

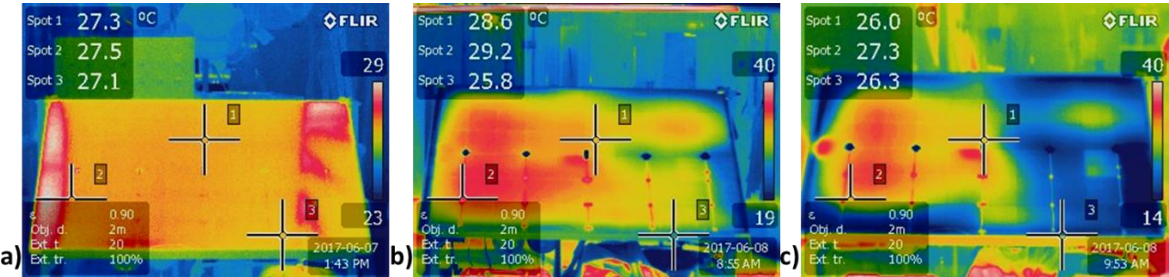


Fig. 5- 23 Temperature distribution on PV panel a) in the lab; b) outside when the heat pump wasn't running; c) outside when the heat pump was running.

Fig. 5- 23 a) shows that the temperature distribution on PV panel in the laboratory, without any radiation, it is uniform. However, after being exposed under the sun for a while, the temperature distribution on PV panel, which was shown in Fig. 5- 23 b), became uneven although the heat pump was not running. This indicates that the thermal contact resistance between the back sheet of PV panel and aluminum plate was different on two sides. This could be possible because none thermal conductive grease was used between. The 4 aluminum plates were fixed together to make them on the same plane, which is shown in Fig. 5- 5 c), but the PV panel itself is not flat. The glass and the back sheet of the panel is very thin and soft, and it would expand when heated. So air exited between the aluminum plate and PV panel. Different thermal resistance means different temperature lift between panel and evaporator, and the

evaporating temperature on the two sides are almost the same. This means the temperature on the one side of the panel was higher and this side had bigger convection and radiation. So the heat flux was different on the two sides. It is another design defect of the PV evaporator. However, it was found too late and the rest time is not enough to develop a new one.

5.3.4 Experimental results after modification

Several tests were done after the modification, the results and analysis is introduced in this section. The test results on May 29, 2017 will be discussed in detail and other results can be found in Table 5- 5.

As shown in Fig. 5- 24, weather condition was good and the test was performed in the afternoon. The solar irradiance is around 900W/m²·K and the value is very stable. Since the sun was always moving and the test was not moved during the experiment, the beam didn't always hit the panel perpendicularly. The solar radiation absorbed by the panel was decreasing with time because of the increasing angle between the beam and normal line of the panel. The average ambient temperature was around 18°C and the temperature difference was small. It's an ideal outdoor environment for performance tests.

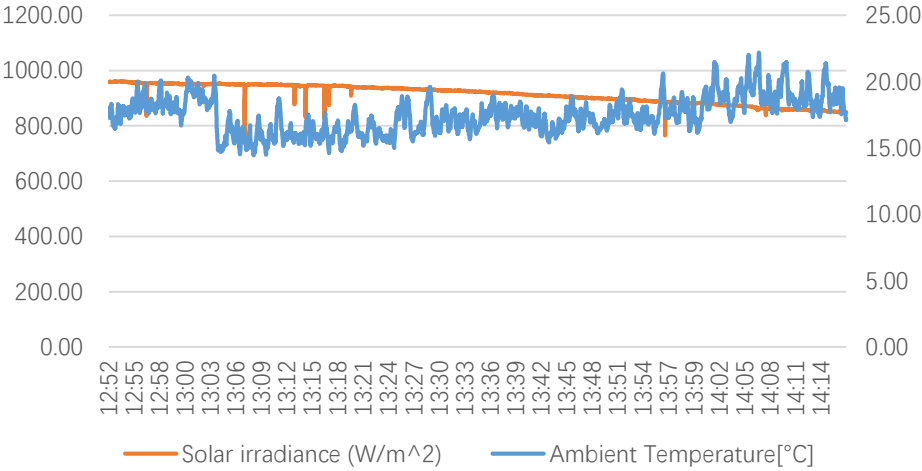


Fig. 5- 24 Weather data on May 29, 2017

Fig. 5- 25 shows the output power of the PV panel and its efficiency on May 29, 2017. The average efficiency during the test was 15.1%. The efficiency on this panel's specification was 15.8%, which is 4.6% higher than the test value. This can be caused by the different test methods and test conditions, so this value given by the supplier cannot be used as a standard in this study.

In order to know the performance improvement of the PV panel after combined with a cooling system, a contrast experiment was performed to test the performance of the PV panel without cooling. After exposed under the sun for over half an hour, the temperature of the PV panel was almost steady, and the conversion efficiency was 14.5% by then. Also, according to the specification of the PV panel, the nominal operating cell temperature is 45.7°C and the temperature coefficient of max power point power is -0.4%/°C. The nominal conversion efficiency is 14.5% calculated by the above information, and it is the same as the test result. So the PV conversion efficiency of this test rig increased around 4.1% during the test on May 29, 2017. Actually, the improvement could be bigger. After the test rig was moved outdoor, preparations needed to be done before starting experiment. These preparations took some time and the panel temperature was continuously increasing then. This explains the relatively low conversion efficiency at the beginning of the test. The output power of the PV panel was declining with the decreasing solar irradiance. It was around 220W, which is only a lot smaller than the power consumption of the compressor.

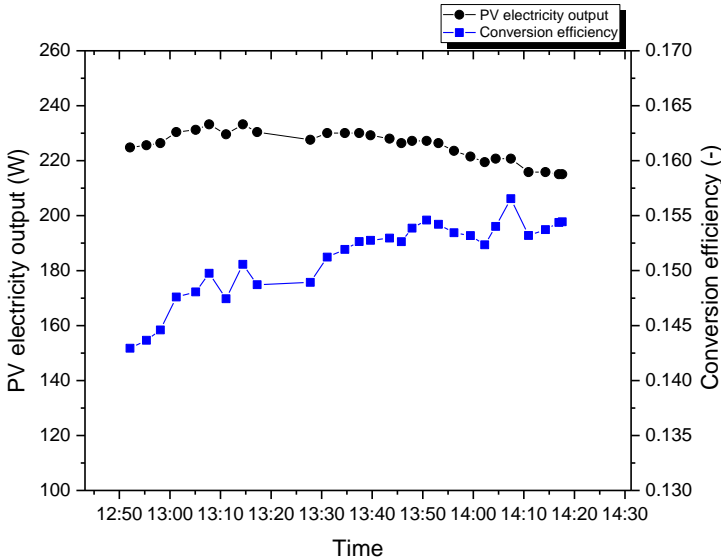


Fig. 5- 25 Variation of PV electricity output and conversion efficiency on May 29, 2017

Considering the heating power of the system, cyclic heating mode instead of instantaneous heating mode was used in this system. The temperature lift of the water was less than 2°C. 30L tap water was heated from 12.7°C to over 50°C during the experiment. The compressor powers are determined as 196W, 228W, 265W, 303W for inlet water temperature at 20°C, 30°C, 40°C,

50°C. The solar irradiance was stable during the test. It is difficult to tell its influence on the power consumption of compressor according to the experimental results. Theoretically, higher radiation means larger cooling capacity which leads to bigger mass flow of refrigerant. So, solar irradiance has a reverse effect on compressor power, but the influence should be a less extent than condenser supply water temperature.

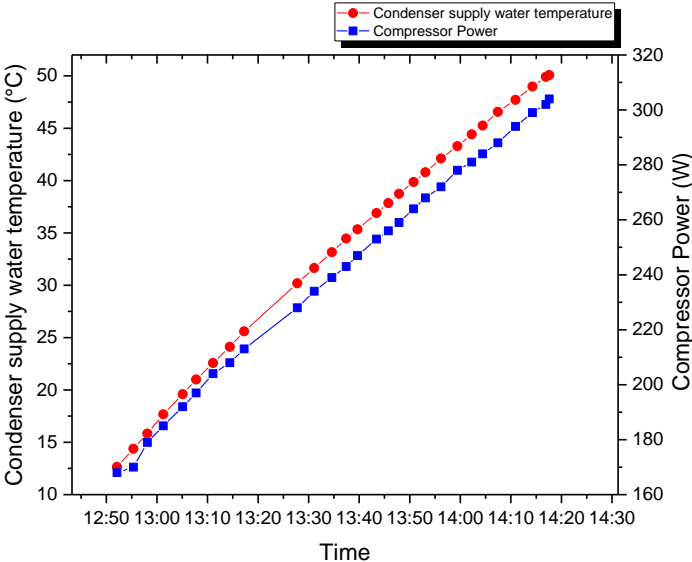


Fig. 5- 26 Variation of condenser supply water temperature and Compressor power on May 29, 2017

Fig. 5- 27 shows the performance of the system, including the COP, average COP, energy generation factor, average generation factor. The average COP of the heat pump was over 4 when the water was heated from 13°C to 50°C, and the energy generation factor of the system was 6.2. For cyclic heating system, COP is mainly influenced by condenser supply water temperature which determines the condensing temperature.

In order to study the performance of the system under different weather conditions, several tests were performed on cloudy days. The black curves in Fig. 5- 28 show the test results on Jun 7, 2017 and the red ones represent results on Jun 8, 2017. As shown in the graph, Jun 7 was cloudy and the solar irradiance was changing all the time, Jun 8 was sunny at the beginning of the test and then changing to overcast.

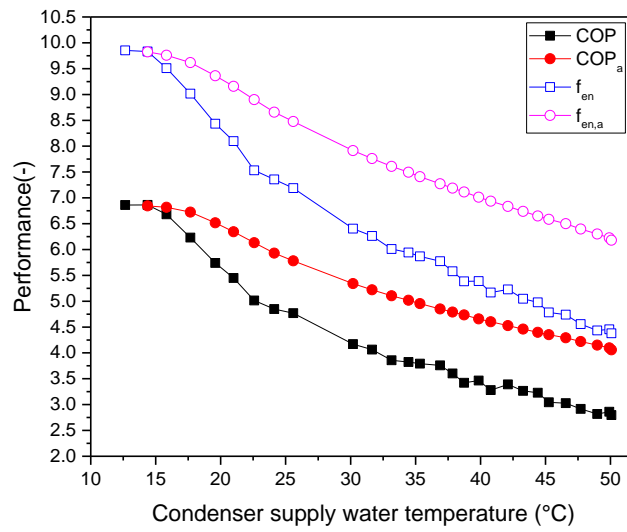


Fig. 5- 27 Variation of system performance with condenser supply water temperature on May 11, 2017

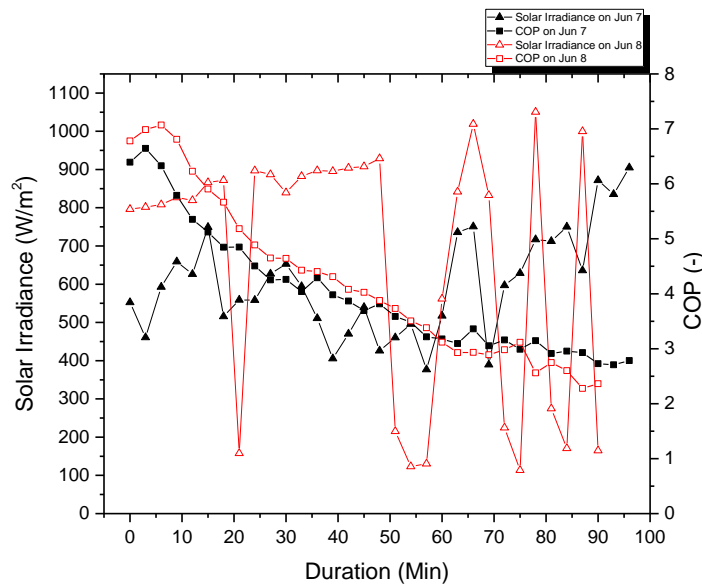


Fig. 5- 28 Variation of solar irradiance and COP on Jun 7, 2017 and Jun 8, 2017

Besides condenser supply water temperature, solar irradiance is another significant influence factor of the heat pump performance. The initial water temperatures on Jun 7 and Jun 8 were very close, so were the heating capacities. So there is only a small difference between these two days' condenser supply water temperatures with the same operating time. However, in the first half of the tests, the COP on Jun 8 was obviously higher than the COP on Jun 7 because Jun 8 had a higher solar irradiance. When the solar irradiance started increasing at the

end of the test on Jun 7, the COP stopped decreasing although the condensing temperature was increasing with time and became higher than the COP on Jun 8. A higher irradiance leads to a higher evaporating temperature and pressure, and the COP also increases.

Table 5- 5 Experimental results on different days

	May 29	May 30	Jun 2	Jun 7	Jun 8	Jun 15
Solar irradiance/W/m ²	915	693	939	586	674	876
Ambient temperature/°C	17.5	13.5	16.1	23.2	22.4	24.2
Initial water temperature/°C	12.7	14.3	15.7	16.1	16.7	14.8
Final water temperature/°C	50.2	50.1	50.8	50.9	50.0	50.6
Duration/min	85	98	87	96	87	81
Average panel temperature/°C	33.6	24.9	31.2	24.1	28.2	35.9
Conversion efficiency	0.151	0.150	0.148	0.155	0.150	0.153
Heat-collecting efficiency	0.49	0.61	0.45	0.77	0.67	0.56
PV output power/W	226	169	227	153	165	222
COP _a	4.06	3.95	3.90	3.82	4.12	4.30
f _{en,a}	6.18	5.61	6.01	5.25	5.67	6.32

Table 5- 5 shows the experimental results on different days. The average panel temperature here represents the mean value of the data measured by the five thermocouples on panel. It does not equal to cell temperature because the thermocouples were put on the glass instead of the PV cells. And the solar radiation also had impact on the temperature results. Therefore, the average panel temperature, which cannot be used as PV cell temperature, is only for reference here. The conversion efficiency in the table is the mean value of the experimental results calculated by the manually recorded data. It was influenced by many different factors like solar radiation, ambient temperature, angle of incidence. A higher solar radiation may lead to a lower efficiency because it may increase the cell temperature. The conversion efficiency reached 15.5% on Jun 7, which indicates a 6.9% increase.

At a time when the solar radiation is weak, the evaporating temperature is low and the PV

evaporator can absorb heat not only from the solar energy but also from the environment. So, a lower solar irradiance usually leads to a higher heat-collecting efficiency. The heat-collecting efficiency ranged from 0.45 to 0.77 in the tests.

The test conditions were very close on May 29 and Jun 15, they had similar solar irradiance, initial water temperature, operating time, but the ambient temperature is higher on Jun 15. A higher ambient temperature leads to a higher evaporating temperature, and a higher evaporating temperature means a higher COP. Different from the COP, average COP is not only influenced by the condenser supply water temperature, ambient temperature, solar irradiance as mentioned above, but also influenced by the initial water temperature because of the cyclic heating mode. A lower initial water temperature leads to a higher average COP. The average COP on Jun 15 reached 4.3 when the water was heated from 14.8°C to 50.6°C.

5.3.5 Error analysis

Error analysis of the measurement system is given in this part. For a directly measured quantity, there are two different specifications: the standard deviation and the reading error. Both of them are describing the precision of the measurement. It is always the case that one of this two is much larger than the other, and in this case, the larger one is the error of the directly measured quantity. The resolution and accuracy of the instruments used for measurement is shown in Table 5- 4. The reading error can be ignored except the measurement of high pressure.

Often, the results cannot be directly measured. Two or more measured quantities are combined arithmetically to get the results. Assume the directly measured quantities are x_1, x_2, \dots, x_n , their errors are $\Delta x_1, \Delta x_2, \dots, \Delta x_n$, and the result y is decided by:

$$y = f(x_1, x_2, \dots, x_n) \quad (5.1)$$

The errors of these directly measured quantities will propagate to an error in the result:

$$|\Delta y| = \left| \frac{\partial f}{\partial x_1} \Delta x_1 \right| + \left| \frac{\partial f}{\partial x_2} \Delta x_2 \right| + \dots + \left| \frac{\partial f}{\partial x_n} \Delta x_n \right| = \sum_{i=1}^n \left| \frac{\partial f}{\partial x_i} \Delta x_i \right| \quad (5.2)$$

The fractional error is the value of the error divided by the value of the quantity: $\Delta x/x$. So the fractional error of the result is:

$$\left| \frac{\Delta y}{y} \right| = \sum_{i=1}^n \left| \frac{1}{y_i} \frac{\partial f}{\partial x_i} \Delta x_i \right| \quad (5.3)$$

The fractional error of the results, which include PV power, conversion efficiency, COP, can be calculated based on this theory. The directly measured quantities used here are voltage, current, solar irradiance, compressor power, water temperature lift.

Therefore, the fractional errors of the PV power, conversion efficiency, Compressor power, heating capacity, COP are 3%, 5%, 2%, 3.2%, 5.2%.

5.4 Chapter summary

Based on the theories in Chapter 4, a test rig of PV/T heat pump system was designed and built. Experimental researches were taken under summer weather conditions of Trondheim. According to the experimental results, the conversion efficiency of the PV panel can reach 15.5% in the best case, it was increased by 6.9% compared with the nominal value. The efficiency was influenced by solar radiation, ambient temperature and angle of incidence. A higher ambient temperature leads to a lower efficiency. The influence of the solar irradiance is complicated, ordinarily, a higher solar radiation may cause a decline in efficiency. The PV evaporator can absorb heat both from solar radiation and environment, the heat collecting efficiency ranged from 0.45 to 0.77 in the tests. The COP of the heat pump is greatly influenced by the condenser supply water temperature. COP decreases with the increasing condenser supply water temperature. Solar radiation and ambient temperature have a positive impact on COP. The average COP of the heat pump can reach 4.3 when the water was heated from 14.8°C to 50.6°C. The fractional errors of the conversion efficiency, COP are 5% and 5.2%.

6 Simulation

In this chapter, a simulation model of PV/T heat pump system was built by EES. The simulation tool and computation method will be introduced. The mathematical model was modified based on the experimental results. The simulated results were compared with the experimental results to demonstrate the effectiveness of the model. Then, the model was used to predict the daily performance of the PV/T heat pump system in Shanghai. Annual performance in three different cities was also discussed.

6.1 Simulation tool EES

EES is a general equation-solving program that can numerically solve thousands of coupled non-linear algebraic and differential equations. It is an acronym for engineering equation solver. The program can also be used to solve differential and integral equations, do optimization, provide uncertainty analyses, perform linear and non-linear regression, convert units, check unit consistency, and generate publication-quality plots. A major feature of EES is the high accuracy thermodynamic and transport property database that is provided for hundreds of substances in a manner that allows it to be used with the equation solving capability.

EES utilizes equations rather than the assignments that are used in a formal programming language. So it is not necessary for users to develop their own iterative technique for solving a set of non-linear equations. The built-in libraries include a lot of models of heat transfer, fluid flow and components which can be used in a thermodynamic model.

6.2 Computation method

The study and the simulation of the PV/T heat pump system was based on the following assumptions: 1) the temperature distribution of the refrigerant in the evaporator vertical to flow direction is even; 2) the solar radiation on the panel is homogeneous; 3) the contact thermal resistance between the aluminum plate and PV panel is uniform (actually, it is not uniform according to the experimental results); 4) mal-distribution of refrigerant is not taken into consideration in the simulation; 5) the thickness of the copper tube wall is very small, so the

thermal resistance of the tube wall is ignored in the simulation; 6) the information of the PV panel from the specification is correct; 7) condenser supply water temperature equals average water temperature in water tank.

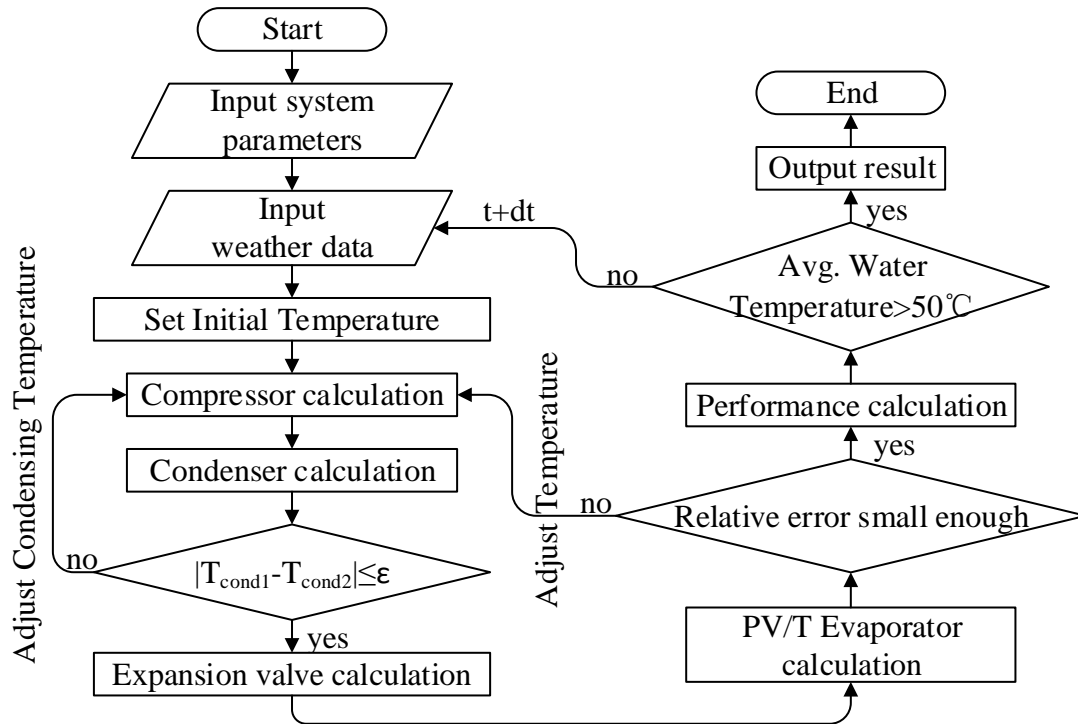


Fig. 6- 1 Flow chart of the computation process for system model

Fig. 6- 1 shows the flow chart of the computation process for this system. Following explains some steps of the procedure. System parameters mean the necessary parameters of all the components used in the test rig, like the Geometric characteristics of the heat exchanger, rotation of the compressor, time step. Weather data includes solar irradiance, ambient temperature, wind speed. Wind speed was not recorded during the test, so information from the weather forecast was used here. Initial evaporating temperature, condensing temperature, panel temperature should be set according to the before calculation. The mathematical model used in compressor calculation, condenser calculation, expansion valve calculation and PV/T evaporator calculation has been introduced in Chapter 4. If the relative error is not small enough after PV/T evaporator calculation, evaporating temperature and panel temperature should be adjusted. The procedure ends when the average water temperature in the 30L water tank reaches

50°C.

This simulation model is used to calculate the daily performance of the PV/T heat pump system. The results of this simulation contain the COP of heat pump, conversion efficiency of the PV panel, compressor power, average water temperature and others.

In Europe, the domestic hot water temperature should be over 70°C, so it can kill the legionella, which is a kind of bacteria, instantly. The standard of domestic hot water temperature is much lower in China, it's usually between 50-55°C. Considering the critical temperature of the propane is relatively lower than other working fluid, R290 is usually used to provide moderate outlet water temperature from 50°C to 60°C for standard pressure (28bar). Along with the Max. continuous condensing temperature of compressor is 55°C. 50°C is determined as the final water temperature.

6.3 Simulation model validation

The simulated results were compared with the experimental results to demonstrate the effectiveness of the mathematical model.

Fig. 6- 2 shows the variation of compressor power and average water temperature on May 29, 2017. The weather data can be found in Fig. 5- 24. For both sets of the results, the compressor power was increasing during the whole duration because of the growing water temperature. The actual power consumption of the compressor was a little bigger than the simulated results at the beginning. It may be caused by the starting current of the motor. The simulated data of water temperature matches the experimental results well, which means the heating capacities of both sets are very close.

Fig. 6- 3 shows the variation of COP and average COP on May 29, 2017. The simulated results match the experimental results well. The simulated average COP is 4.16, 2.5% bigger than the measured value.

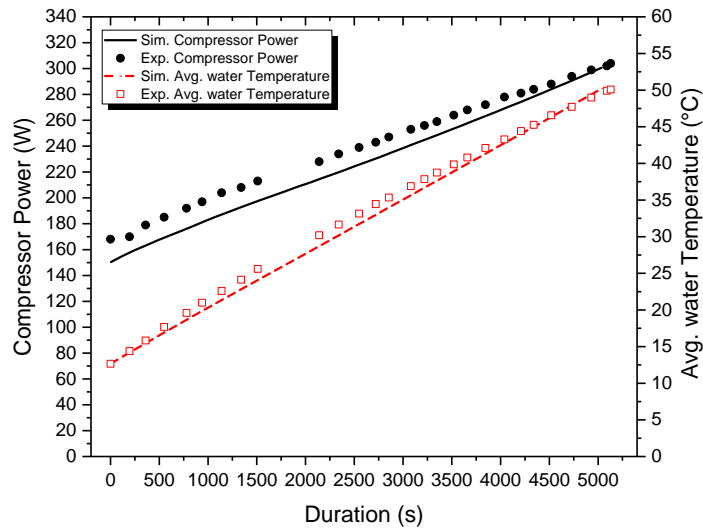


Fig. 6- 2 Measured and simulated data of compressor power and avg. water temperature on May 29, 2017

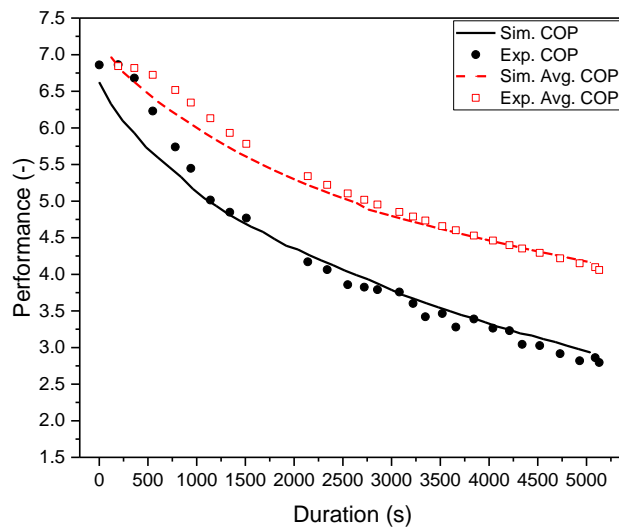


Fig. 6- 3 Measured and simulated data of COP and average COP on May 29, 2017

Fig. 6- 4 shows the variation of the PV output power and conversion efficiency on May 29, 2017. There is a big difference between experimental results and simulated results in the first half of the duration. This phenomenon was caused by two main reasons. When the tests were performed outdoor, some preparations need to be done before turning on the compressor. The PV panel was exposed under the sun without cooling for a while and the cell temperature increased immediately. So the conversion efficiency was low at the beginning. However, this

period of time was not taken into consideration when running the simulation. What's more, equation 4.3, in which the efficiency at standard test conditions equals 15.8%, was used to calculate the conversion efficiency in this simulation. It is almost impossible to reach this value under intended uses. So the simulated value is higher than the actual one.

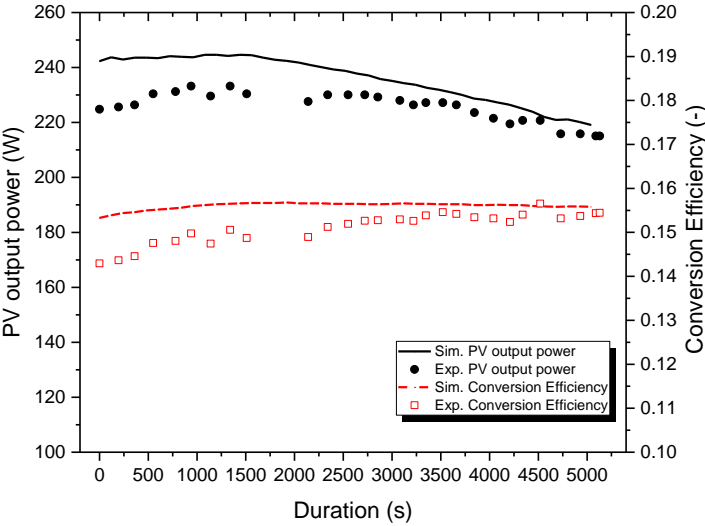


Fig. 6- 4 Measured and simulated data of PV power and PV efficiency on May 29, 2017

Table 6- 1 shows the comparison between simulated results and experimental results on different days. The test conditions can be found in Table 5- 5. In overcast conditions, the influence of convection is much bigger. However, the wind velocity was not measured during the tests. The simulated convective heat transfer coefficient on the PV panel was not correct enough without wind speed data. This affected the calculation of panel temperature and absorbed heat. As shown in Table 6- 1, the error is relatively small on sunny days like May 29, Jun 15 and the error is big on cloudy days like May 30.

Table 6- 1 Comparison between experimental results and simulated results

Date	Average COP			Conversion Efficiency		
	Exp.	Sim.	Error	Exp.	Sim.	Error
05/29	4.06	4.16	2.5%	15.1%	15.6%	3.3%
05/30	3.95	3.75	5.1%	15.0%	16.1%	7.3%
06/02	3.90	3.99	2.3%	14.8%	15.6%	5.4%
06/07	3.82	3.64	4.7%	15.5%	15.9%	2.6%

Date	Average COP			Conversion Efficiency		
	Exp.	Sim.	Error	Exp.	Sim.	Error
06/08	4.12	4.03	2.2%	15.0%	15.6%	4.0%
06/15	4.30	4.35	1.2%	15.3%	15.4%	0.7%

The biggest error of average COP is 5.1% and the biggest error of the conversion efficiency is 7.3%. In general, the error is in an acceptable range and this model has a reference value in guiding the experimental investigation on PV/T heat pump system.

6.4 Performance analysis in different cities

In order to study the performance of PV/T heat pump system at different places, analysis based on this simulation was done in this section. The daily performance in Shanghai and the annual performance in Oslo, New Delhi and Shanghai will be introduced.

6.4.1 Daily performance in Shanghai

Shanghai, located at 31°13' north latitude and 121°28' east longitude, is one of the biggest city in China. It is located in the Yangtze River Delta and bounded on the east by the east china sea. It has a completely different climate with Trondheim. It is good to know how the PV/T heat pump system performs in Shanghai.

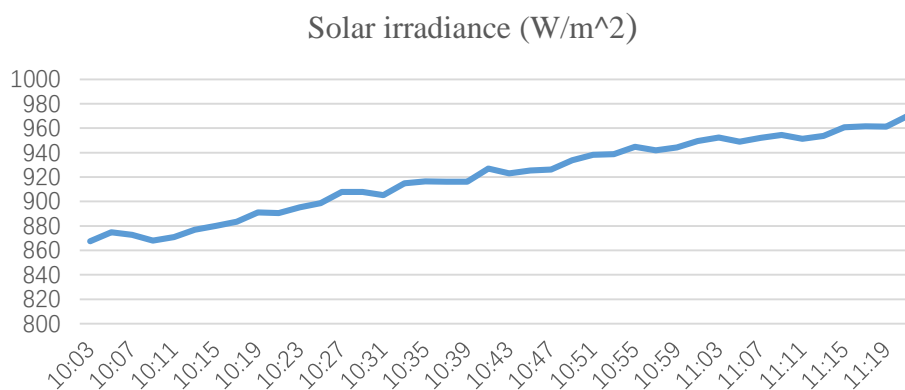


Fig. 6- 5 Solar irradiance data on Apr 30, 2017 in Shanghai

Weather data on April 30, 2017 in Shanghai was used to run the simulation. The data was provided by Guanqun Li from Shanghai Jiao Tong University. The average temperature was 28°C on that day. The wind speed on that day was not measured either and a speed of 2m/s was

used in the simulation. The solar irradiance, which is shown in Fig. 6- 5, was recorded by a pyranometer. The average value in that morning was 920W/m².

Since tap water temperature was not measured, the average city water temperature found on the internet was used as the initial water temperature. The water temperature changes dramatically year round. The temperature ranges from 6.2°C in February up to 27.6°C in the month of August, as shown in Fig. 6- 6. The initial water temperature used in simulation was 12.4°C and the final temperature was 50°C.

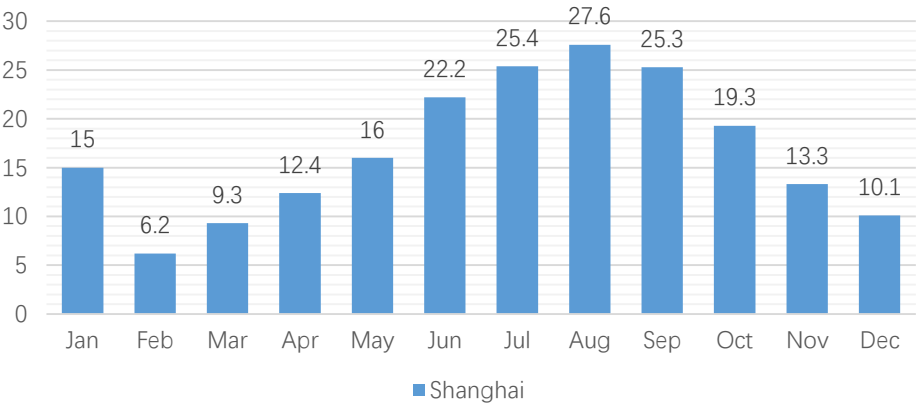


Fig. 6- 6 Monthly average water temperature in Shanghai

Simulated data of COP, average COP and conversion efficiency was shown in Fig. 6- 7. The conversion efficiency increased quickly at the beginning because the panel was cooled by the evaporator. It then declined slowly because of the increasing solar irradiance. The COP was decreasing all the time because of the increasing condenser supply water temperature. The average conversion efficiency was 15.1% and the average COP was 4.8 when the water was heated from 12.4°C to 50.5°C. As shown in Table 6- 2, the test conditions except ambient temperature are very close in these two different cities. Since the latitude of Shanghai is 30 degrees lower, Shanghai has a much higher environmental temperature in the same season. The heat pump has a better performance while the PV panel efficiency is lower in Shanghai. The energy generation factor was used here to judge the performance of the PV/T heat pump system. The simulated value is 7.12 in Shanghai while the simulated value is 6.50 in Trondheim. When the ambient temperature increased 10°C, the conversion efficiency decreased 3.2% but the average COP increased 15% according to the simulated results. This means a higher ambient temperature contributes a better performance of the whole system although conversion

efficiency is lower in this situation.

Table 6- 2 Performance comparison in Trondheim and Norway

	Exp. May 29, Trondheim	Sim. May 29, Trondheim	Sim. Apr 30, Shanghai
Solar irradiance/W/m ²	915	915	920
Ambient temperature/°C	17.5	17.5	28
Initial water temperature/°C	12.7	12.7	12.4
Final water temperature/°C	50.2	50.2	50.5
Duration/min	85	84	76
Conversion efficiency	0.151	0.156	0.151
Average COP	4.06	4.16	4.78
$f_{en,a}$	6.18	6.50	7.12

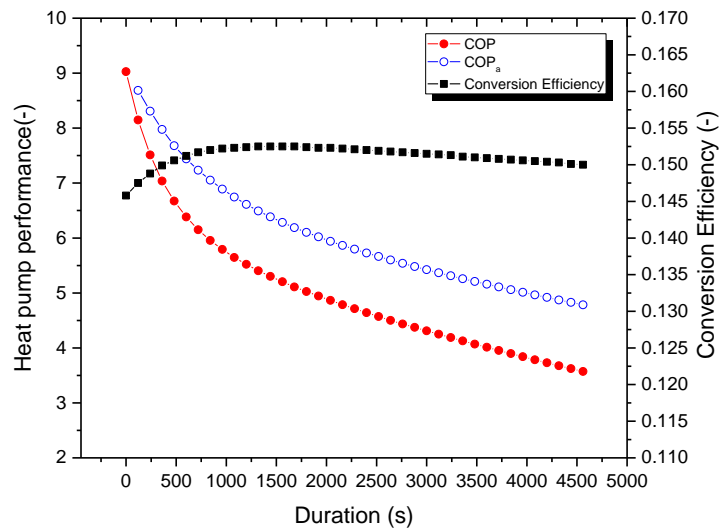


Fig. 6- 7 Variation of COP and conversion efficiency on Apr 30, 2017 in Shanghai

Hence, the PV/T heat pump system has a better comprehensive performance when the ambient temperature is higher.

6.4.2 Annual performance analysis

The experiments were mainly done in May and June in Trondheim, Norway. In order to study the performance of PV/T heat pump system in different months at different places. The operation of the system in Oslo, Norway, Shanghai, China, New Delhi, India was simulated.

Monthly average water temperature shown in Fig. 6- 6 was found on the internet. The water

temperature in Oslo is obviously lower than other cities’.

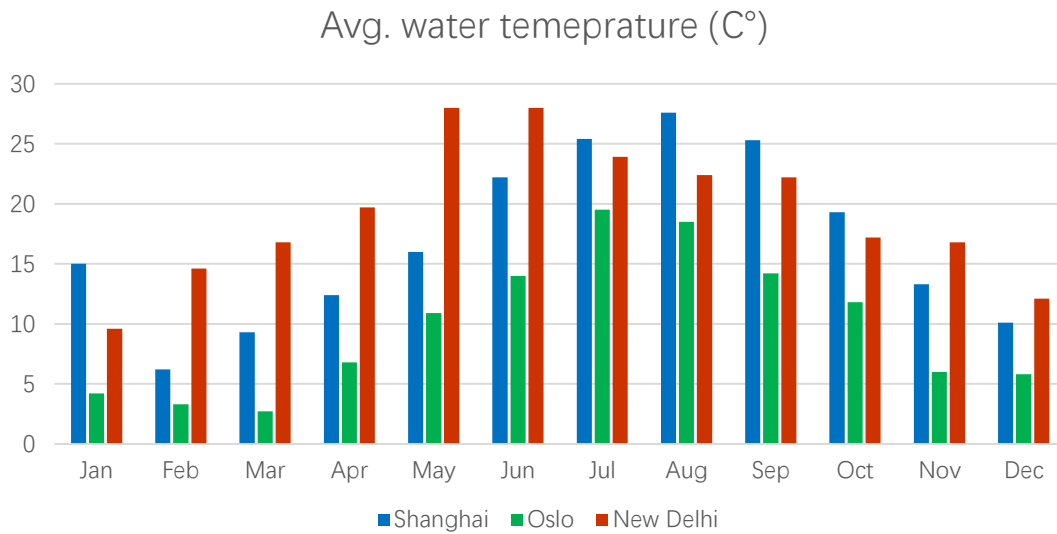


Fig. 6- 8 Monthly average water temperature in different cities

Weather data in three different cities are required when running the simulation. The data was exported from as software named Meteonorm. This software has a global database, it can generate accurate and representative typical years for any place on earth. More than 30 different weather paramiters like temperature, wind speed, wind direction, air pressure, solar radiation can be found in the database.

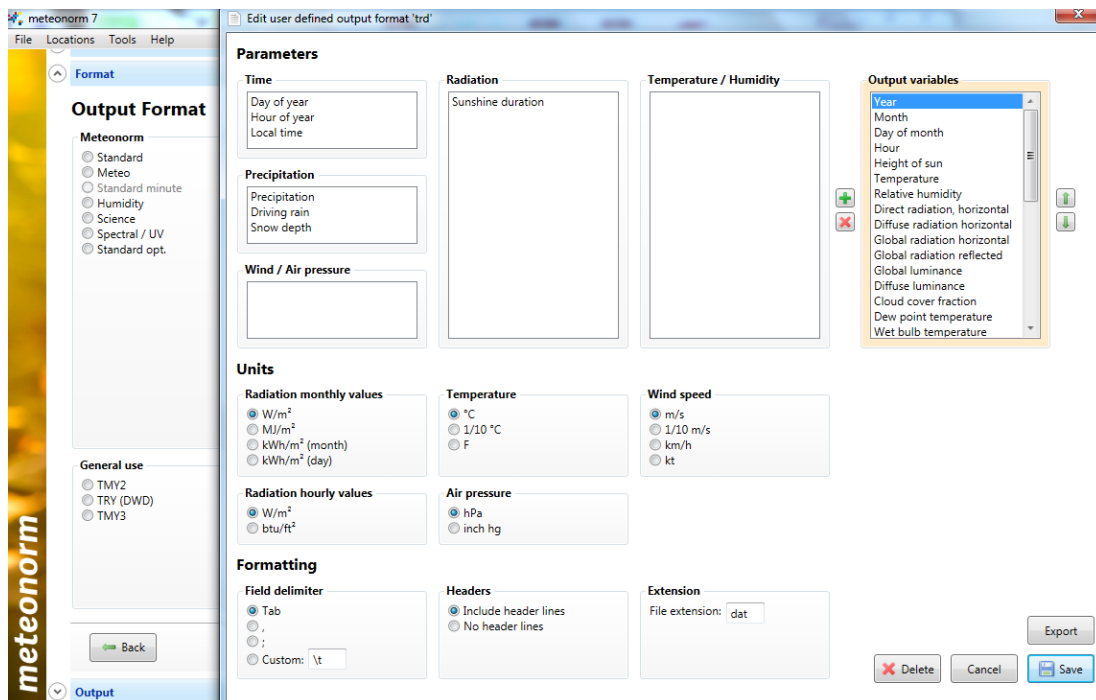


Fig. 6- 9 Operating interface of the software named meteonorm

The monthly average weather data, including global solar irradiance, ambient temperature and wind speed, during the daytime in three different cities was shown in Fig. 6- 10, Fig. 6- 11 and Fig. 6- 12. The daytime here ranged from 10 a.m. to 3 p.m. considering the polar night during the winter in Oslo.

The climates in these three cities are quite different. The climate of New Delhi is a monsoon-influenced humid subtropical climate bordering a hot semi-arid climate. It has a long summer, extending from early April to October. The resource of solar energy is very rich in New Delhi. The temperature is quite high throughout the year. The annual mean value is 25°C and it's even higher during the day time.

Shanghai has a humid subtropical climate and four distinct seasons. Although it has a very similar latitude with New Delhi, the average solar radiation in shanghai is much lower because it has much more precipitation days (average 120.8 precipitation days a year in Shanghai while New Delhi has average 54 rainy days). The wind is strong because of its location.

Oslo has a slightly mild humid continental climate. The temperature is much lower compared with the other two cities and there are only few sunshine hours in the winter. It's not an ideal city for solar energy development.

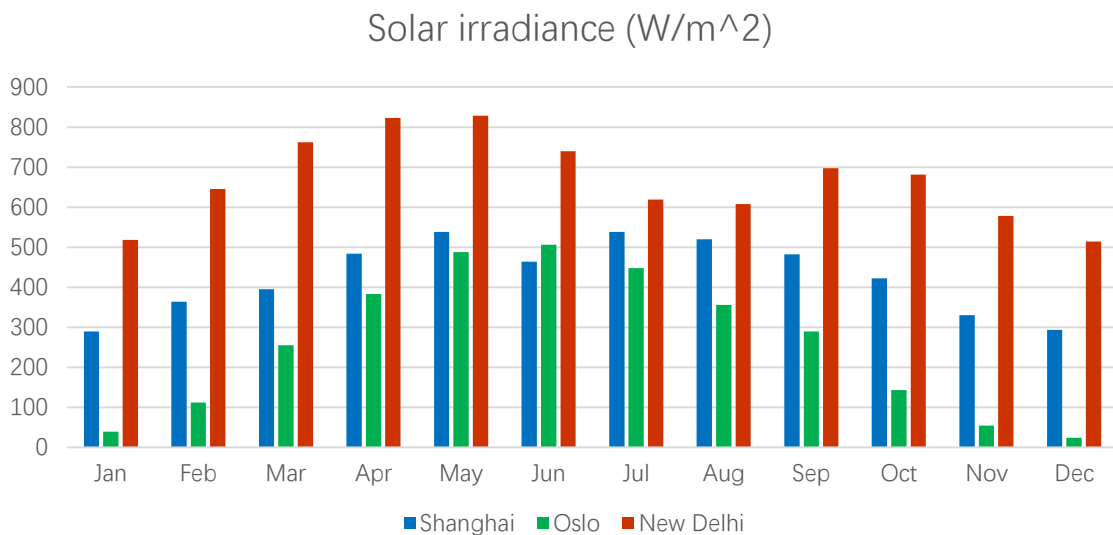


Fig. 6- 10 Monthly average Solar irradiance in different cities

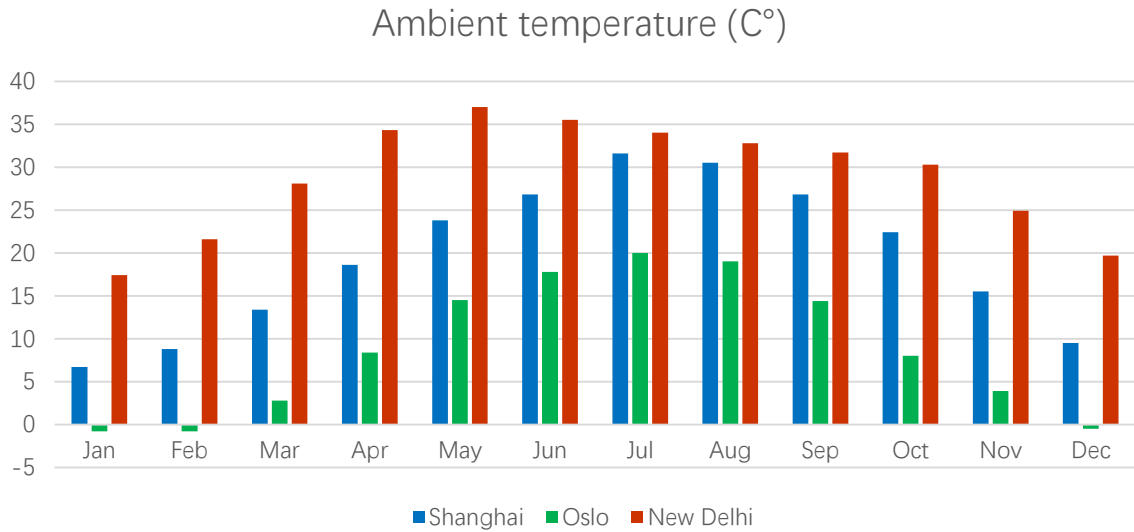


Fig. 6- 11 Monthly average ambient temperature in different cities

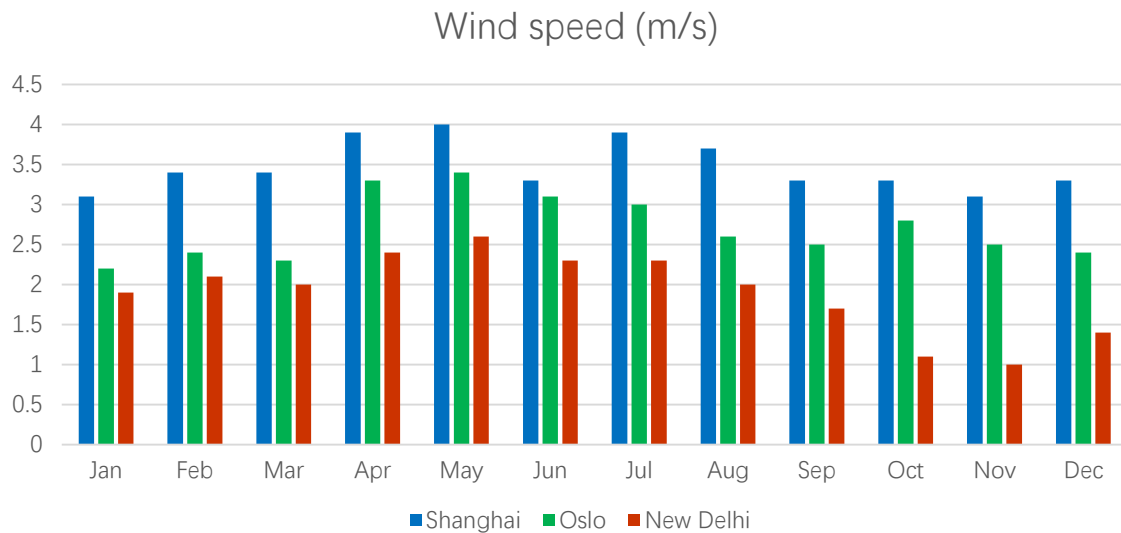


Fig. 6- 12 Monthly average wind speed in different cities

The simulated results of average COP, conversion efficiency, energy generation factor were shown in Fig. 6- 13 and Fig. 6- 14. The average COP in Shanghai ranged from 2.72 to 4.15 and the mean value is 3.51. Although the latitude of Shanghai is around 30 degrees, solar energy resources are not rich enough for good performance of the system. As mentioned before, the COP is mainly influenced by solar radiation and ambient temperature. The temperature in Shanghai is high but the average solar irradiance is not big, which leads to a low COP. There are about 120 precipitation days in Shanghai a year, and droplets on the panel may enhance the heat transfer. This was not taken into consideration in the simulation, so the actual performance

may be better than simulated results.

The average COP in New Delhi ranged from 3.67 to 5.06 and the mean value is 4.40. Both the temperature and solar irradiance is high in New Delhi, which makes it a perfect place for the operation of the PV/T heat pump system.

The average COP in Oslo ranged from 2.12 to 3.58 and the mean value is 2.81. The temperature is very low in Oslo and the sunshine duration is short in winter because of the polar night. Actually, in November, December and January, the solar irradiance is less than 100W/m² and the temperature is around 0°C, the PV/T heat pump system is likely unable to run under such bad weather conditions. The average COP is over 3 during the summer and the experimental results shown in Chapter 5 prove the performance of the system is not bad in sunny days.

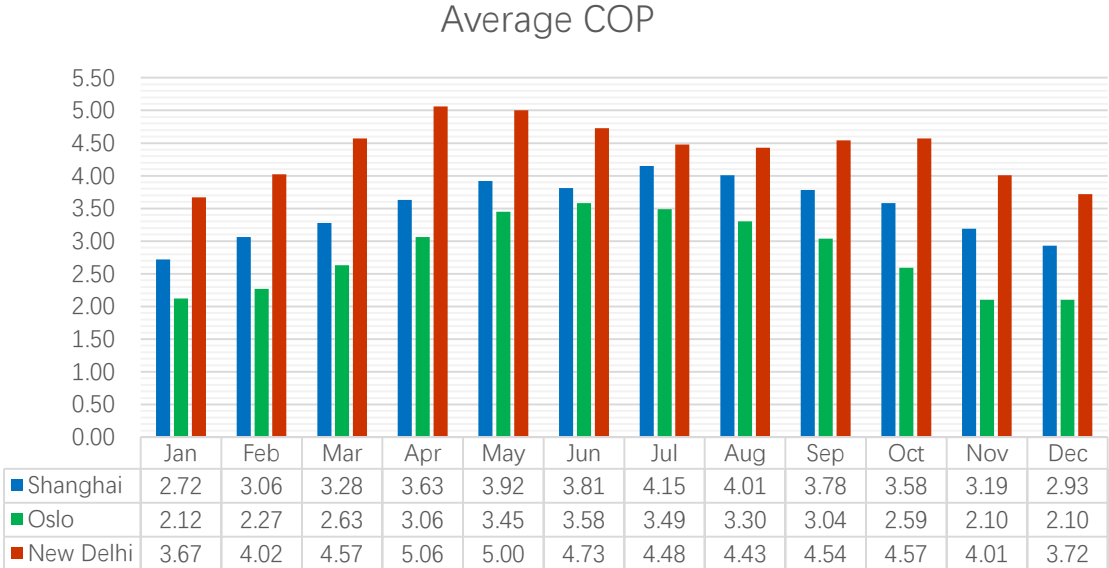


Fig. 6- 13 Monthly average COP_a in different cities

Different from the COP, low temperature contributes high conversion efficiency. The annual average conversion efficiency in Oslo is 17.3% while the value in Shanghai and New Delhi is 16.4% and 15.5%. New Delhi has the best comprehensive performance throughout the year. Some modification should be done based on the current system for year-round application in cold environment with weak sunshine.

Here are some possible schemes to improve the performance of the system: An air evaporator can be connected with PV evaporator in parallel. At a time when the sunshine is

weak, the air evaporator will start to work to absorb heat from the environment; An inverter compressor can be used in the system. The mass flow of the refrigerant can be adjusted according to the environmental parameters and the system can always run with high efficiency.

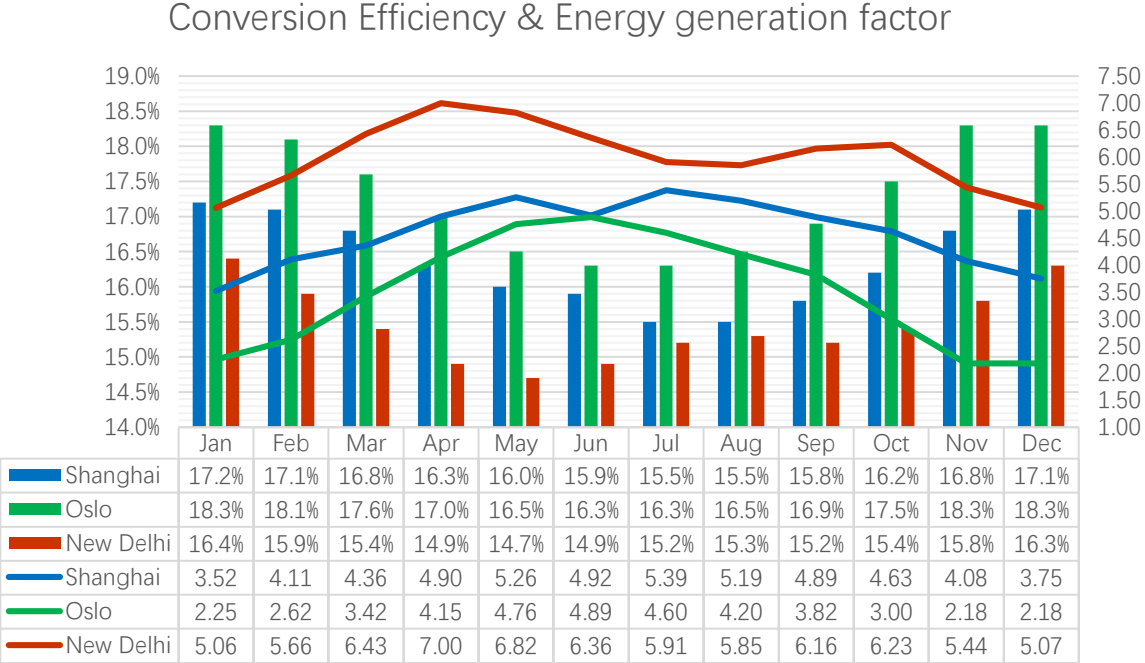


Fig. 6- 14 Monthly average conversion efficiency and energy generation factor

6.5 Chapter summary

Simulation of the test rig was made by EES to study the performance of PV/T heat pump system at different places and climates. The effectiveness of the simulation was validated by comparing the simulated results and experimental results. The error is in an acceptable range and the simulation can be used for further study. Daily performance analysis on April 30 in Shanghai was done, and it indicated that a higher air temperature leads to a better comprehensive performance. Annual operation simulated results in Shanghai, Oslo, New Delhi were analyzed. Monthly average value of air temperature, solar radiation and wind speed was adopted as the rated condition for annual performance evaluation. The annual average COP in Shanghai, Oslo, New Delhi are 3.5, 2.8 and 4.4, respectively. And the annual average conversion efficiency in Shanghai, Oslo, New Delhi are 16.4%, 17.3%, 15.5%. In order to improve the performance in cold environment without sufficient sunlight, an air evaporator in parallel and an inverter compressor can be used.

7 Discussions

The discussions will highlight what problems exist now and what improvements should be done regards to the experimental investigation and simulation of PV/T heat pump system.

7.1 Problems and improvements of the experiment

There are several problems with the design of the test rig. Some of the problems have been solved, and the rest of them and possible ways to solve them are as follows:

- 1) The diameter of the copper coils used as evaporator was too small. The pressure drop in it was very big and it had a negative impact on the performance of heat pump. A new evaporator with proper length and diameter should be designed.
- 2) The contact thermal resistance between PV panel (back sheet) and the evaporator (aluminum plate) was big. And the distribution of the thermal resistance was uneven. This caused the mal-distribution of refrigerant in evaporator. Thermal conductive grease should be used between them.
- 3) The aluminum plate was too thick. It was heavy and a waste of money. A thinner plate should be used.

There are also some problems with the measurement during the test:

- 1) The precision of some measurement instruments is not high enough, especially the pressure gauge. A pressure transmitter is a much better choice.
- 2) Some data like compressor power, PV output current, PV output voltage, pressure was recorded manually. It was difficult to read all of them in a very short time, and this means they were not recorded at the same time. This increased the error of the system. A data logger system which can continuously monitor during the operation should be used for measurement.

Some improvements can be done about the experimental scheme:

- 1) A contract experiment of the PV panel's performance should be done by measuring the conversion efficiency of a same PV panel without any modification at the same time.

- 2) More tests should be done in different seasons.

7.2 Problems and improvements of the simulation

Building a simulation model by EES is great learning. But there is still some difference between simulated results and measured results. The mathematical model of the PV evaporator is not accurate enough. More investigation can be focused on it and CFD analysis may help a lot. Also, a framework of PV/T heat pumps should be built. Then, it is more easy to design a new system and conduct further investigation.

7.3 The feasibility for commercial use

From environmental point of view, this system is able to reduce building energy consumption. With the development of passive house, the hot water heating demand will account for more than 50% of total annual heating demand in the future, and heat pump is a more and more widely used technology to provide hot water. This means this system has a wide market perspective. What's more, the refrigerant used in this system is propane, whose ODP is 0 and GWP is 3. From consumers' point of view, cost and reliability are very important. By saying reliability, it means the system can provide hot water when costumers need it. One of the drawbacks of this system is that it almost doesn't work without solar radiation, so a backup heating from electricity or gas is necessary to handle the peaks during bad weathers. Typically, a person needs 50L hot water a day, and 150L (or bigger) water tank is necessary for family use. The water tank used here is 30L, and the area of the PV panel is 1.65m². If the system is designed to cover the whole hot water demand, it will need a much bigger PV panel. The investment cost is relatively high, but if the electricity generated by the PV panel can be used wisely, the payback period will become shorter. To sum up, this system is suitable for the region with good solar radiation and relatively high electricity price.

8 Conclusion

This thesis investigated the PV/T heat pump system using propane as refrigerant. A PV panel was combined with heat pump system to improve the conversion efficiency and produce hot water at the same time. Experimental investigation of the system was done in Trondheim, Norway. A simulation model was established to study the performance in different climate zones. The main conclusions of this research include:

- (1) According to the experimental results, the conversion efficiency of the PV panel can reach 15.5% in the best case, it was increased by 6.9% compared with the nominal value. A higher ambient temperature leads to a lower efficiency and a higher solar radiation may cause a decline in conversion efficiency.
- (2) According to the experimental results, the average COP of the heat pump can reach 4.3 when the water was heated from 14.8°C to 50.6°C. COP decreases with the increasing condenser supply water temperature. Solar radiation and ambient temperature have a positive impact on COP.
- (3) According to the simulated results, a higher ambient temperature leads to a better comprehensive performance of PV/T heat pump system.
- (4) According to the simulated results, the annual average COP in Shanghai, Oslo, New Delhi are 3.5, 2.8 and 4.4, respectively. And the annual average conversion efficiency in Shanghai, Oslo, New Delhi are 16.4%, 17.3%, 15.5%.

9 Further work

Based on the findings, investigations and conclusions in this thesis, following tasks can be taken into consideration regarding PV/T heat pump system.

- (1) Build a data logger system which can continuously monitor during the operation. More tests should be done under different weather conditions.
- (2) Investigate the influence of the refrigerant charge. A new system using different refrigerant can be developed to make a comparison.
- (3) Investigate different PV evaporator designs, like designs with heat pipes.
- (4) Use inverter compressor and electronic expansion valve, develop optimal control strategy to improve the performance of the system under different operating conditions.
- (5) Develop a specific roadmap with concrete tasks for the development of PV/T heat pump.

Reference

- ARMSTRONG, S. & HURLEY, W. G. 2010. A thermal model for photovoltaic panels under varying atmospheric conditions. *Applied Thermal Engineering*, 30, 1488-1495.
- BASKIN, E. 1991. Applicability of plate heat exchangers in heat pumps. *ASHRAE Transactions*, 97, 305-308.
- BISAILLON, J. C., CUMMINGS, J. R., CULIK, J. S., LESKO, J. D., SIMS, P. E. & RAND, J. A. Non-traditional light sources for solar cell and module testing. Conference Record of the Twenty-Eighth IEEE Photovoltaic Specialists Conference - 2000 (Cat. No.00CH37036), 2000 2000. 1498-1501.
- CHEN, J. C. 1966. Correlation for boiling heat transfer to saturated fluids in convective flow. *Industrial & engineering chemistry process design and development*, 5, 322-329.
- CHEN, J. F., ZHANG, L. & DAI, Y. J. 2018. Performance analysis and multi-objective optimization of a hybrid photovoltaic/thermal collector for domestic hot water application. *Energy*, 143, 500-516.
- CHUA, K. J., CHOU, S. K. & YANG, W. M. 2010. Advances in heat pump systems: A review. *Applied Energy*, 87, 3611-3624.
- CLAESSON, J. Performance of compact brazed plate heat exchanger operating as condenser in domestic heat pump system: An experimental investigation. 8th IEA Heat Pump Conference, 2005.
- COOPER, A. Condensation of steam in plate heat exchangers. AIChE Symposium, 1974. 172-177.
- COOPER, M. 1984. Heat flow rates in saturated nucleate pool boiling-a wide-ranging examination using reduced properties. *Advances in heat transfer*, 16, 157-239.
- DU, Y., FELL, C. J., DUCK, B., CHEN, D., LIFFMAN, K., ZHANG, Y., GU, M. & ZHU, Y. 2016. Evaluation of photovoltaic panel temperature in realistic scenarios. *Energy Conversion and Management*, 108, 60-67.
- DUBEY, S., SARVAIYA, J. N. & SESHADRI, B. 2013. Temperature Dependent Photovoltaic (PV) Efficiency and Its Effect on PV Production in the World – A Review. *Energy Procedia*, 33, 311-321.
- EVANS, D. L. 1981. Simplified method for predicting photovoltaic array output. *Solar Energy*, 27, 555-560.
- FERNANDEZ-SEARA, J., PI EIRO, C., ALBERTO DOPAZO, J., FERNANDES, F. & SOUSA, P. X. B. 2012. Experimental analysis of a direct expansion solar assisted heat pump with integral storage tank for domestic water heating under zero solar radiation conditions. *Energy Conversion and Management*, 59, 1-8.
- FERNANDEZ-SEARA, J., UH A, F. J., SIERES, J. & CAMPO, A. 2007. A general review of the Wilson plot method and its modifications to determine convection coefficients in heat exchange devices. *Applied Thermal Engineering*, 27, 2745-2757.
- FOCKE, W. W., ZACHARIADES, J. & OLIVIER, I. 1985. The effect of the corrugation inclination angle on the thermohydraulic performance of plate heat exchangers. *International Journal of Heat and Mass Transfer*, 28, 1469-1479.
- FU, H. D., PEI, G., JI, J., LONG, H., ZHANG, T. & CHOW, T. T. 2012. Experimental study of a

- photovoltaic solar-assisted heat-pump/heat-pipe system. *Applied Thermal Engineering*, 40, 343-350.
- HAYES, N. & JOKAR, A. 2009. Dynalene/Water Correlations to Be Used for Condensation of CO₂ in Brazed Plate Heat Exchangers. *ASHRAE Transactions*, 115, 599-616.
- HAYES, N., JOKAR, A. & AYUB, Z. H. 2011. Study of carbon dioxide condensation in chevron plate exchangers; heat transfer analysis. *International Journal of Heat and Mass Transfer*, 54, 1121-1131.
- HUANG, B. J., LIN, T. H., HUNG, W. C. & SUN, F. S. 2001. Performance evaluation of solar photovoltaic/thermal systems. *Solar Energy*, 70, 443-448.
- ITO, S., MIURA, N. & TAKANO, Y. 2005. Studies of heat pumps using direct expansion type solar collectors.(Author Abstract). *Journal of Solar Energy Engineering*, 127, 60.
- ITO, S., MIURA, N., WANG, J. Q. & NISHIKAWA, M. 1997. Heat Pump Using a Solar Collector With Photovoltaic Modules on the Surface. *Journal of Solar Energy Engineering*, 119, 147-151.
- JI, J., LIU, K., CHOW, T.-T., PEI, G., HE, W. & HE, H. 2008a. Performance analysis of a photovoltaic heat pump. *Applied Energy*, 85, 680-693.
- JI, J., PEI, G., CHOW, T.-T., LIU, K., HE, H., LU, J. & HAN, C. 2008b. Experimental study of photovoltaic solar assisted heat pump system. *Solar Energy*, 82, 43-52.
- JIANG, C. & DAI, Y. 2016. Direct expansion solar assisted heat pump using novel fin-tube collector/evaporator. *Huagong Xuebao/CIESC Journal*, 67, 318-325.
- JINGDAN, G., GUOLIANG, D., WEI, W., YIFENG, G. & JI, S. Optimal Design Principle for Air Conditioner with Refrigerant R290. *Chinese Journal of Refrigeration Technology*, 2012. 23-26.
- JONES, A. D. & UNDERWOOD, C. P. 2001. A thermal model for photovoltaic systems. *Solar Energy*, 70, 349-359.
- JUNG, D., LEE, H., BAE, D. & OHO, S. 2004. Nucleate boiling heat transfer coefficients of flammable refrigerants. *International Journal of Refrigeration*, 27, 409-414.
- KEDZIERSKI, M. A. 1997. Effect of inclination on the performance of a compact brazed plate condenser and evaporator. *heat transfer engineering*, 18, 25-38.
- KIM, J.-H., BRAUN, J. E. & GROLL, E. A. 2009a. Evaluation of a hybrid method for refrigerant flow balancing in multi-circuit evaporators. *International Journal of Refrigeration*, 32, 1283-1292.
- KIM, J.-H., BRAUN, J. E. & GROLL, E. A. 2009b. A hybrid method for refrigerant flow balancing in multi-circuit evaporators: Upstream versus downstream flow control. *international journal of refrigeration*, 32, 1271-1282.
- KONG, X. Q., ZHANG, D., LI, Y. & YANG, Q. M. 2011. Thermal performance analysis of a direct-expansion solar-assisted heat pump water heater. *Energy*, 36, 6830-6838.
- LONGO, G. A. 2010. Heat transfer and pressure drop during hydrocarbon refrigerant condensation inside a brazed plate heat exchanger. *International Journal of Refrigeration*, 33, 944-953.
- LONGO, G. A. 2011. The effect of vapour super-heating on hydrocarbon refrigerant condensation inside a brazed plate heat exchanger. *Experimental Thermal and Fluid Science*, 35, 978-985.
- LORENTZEN, G. 1995. The use of natural refrigerants: a complete solution to the CFC/HCFC

- predicament. *International Journal of Refrigeration*, 18, 190-197.
- MOHANRAJ, M., JAYARAJ, S. & MURALEEDHARAN, C. 2009. Performance prediction of a direct expansion solar assisted heat pump using artificial neural networks. *Applied Energy*, 86, 1442-1449.
- MOLINAROLI, L., JOPPOLO, C. M. & DE ANTONELLIS, S. 2014. Numerical Analysis of the Use of R-407C in Direct Expansion Solar Assisted Heat Pump. *Energy Procedia*, 48, 938-945.
- MORENO-RODR GUEZ, A., GONZ LEZ-GIL, A., IZQUIERDO, M. & GARCIA-HERNANDO, N. 2012. Theoretical model and experimental validation of a direct-expansion solar assisted heat pump for domestic hot water applications. *Energy*, 45, 704-715.
- MULEY, A. & MANGLIK, R. M. 1999. Experimental Study of Turbulent Flow Heat Transfer and Pressure Drop in a Plate Heat Exchanger With Chevron Plates. *Journal of Heat Transfer*, 121, 110-117.
- NAKAYAMA, M., SUMIDA, Y., HIRAKUNI, S. & MOCHIZUKI, A. 2000. Development of a Refrigerant Two-Phase Flow Distributor for a Room Air Conditioner.
- PALM, B. & CLAEISSON, J. 2006. Plate Heat Exchangers: Calculation Methods for Single and Two-Phase Flow. *Heat Transfer Engineering*, 27, 88-98.
- PALMER, S. C., PAYNE, W. V. & DOMANSKI, P. A. 2000. *Evaporation and condensation heat transfer performance of flammable refrigerants in a brazed plate heat exchanger*, Citeseer.
- PEI, G., JI, J., HAN, C. & FAN, W. 2009. Performance of Solar Assisted Heat Pump Using Pv Evaporator Under ` Different Compressor Frequency. In: GOSWAMI, D. Y. & ZHAO, Y. (eds.) *Proceedings of ISES World Congress 2007 (Vol. I – Vol. V): Solar Energy and Human Settlement*. Berlin, Heidelberg: Springer Berlin Heidelberg.
- RUSSELL, M. C. & KERN, E. C. J. 1979. *Optimization of photovoltaic/thermal collector heat pump systems*, ; Massachusetts Inst. of Tech., Lexington (USA). Lincoln Lab.
- SCHOTT, T. Operation temperatures of PV modules: a theoretical and experimental approach. EC Photovoltaic solar energy conference. 6, 1985. 392-396.
- SHAH, M. M. 1979. A general correlation for heat transfer during film condensation inside pipes. *International Journal of Heat and Mass Transfer*, 22, 547-556.
- SHAH, M. M. 1982. Chart correlation for saturated boiling heat transfer: equations and further study. *ASHRAE Trans.:(United States)*, 88.
- SKOPLAKI, E. & PALYVOS, J. A. 2009. On the temperature dependence of photovoltaic module electrical performance: A review of efficiency/power correlations. *Solar Energy*, 83, 614-624.
- SPORN, P. & AMBROSE, E. The heat pump and solar energy. Proc. of the World Symposium on Applied Solar Energy. Phoenix, US, 1955.
- SRIDHAR, L. 1999. *Investigation of thermal contact resistance at a plastic-metal interface in injection molding*. New Jersey Institute of Technology, Department of Mechanical Engineering.
- SUN, X., DAI, Y., NOVAKOVIC, V., WU, J. & WANG, R. 2015. Performance Comparison of Direct Expansion Solar-assisted Heat Pump and Conventional Air Source Heat Pump for Domestic Hot Water. *Energy Procedia*, 70, 394-401.
- SUN, X., WU, J., DAI, Y. & WANG, R. 2014. Experimental study on roll-bond collector/evaporator with optimized-channel used in direct expansion solar assisted heat pump water

- heating system. *Applied Thermal Engineering*, 66, 571-579.
- TSAI, H.-L. 2015. Modeling and validation of refrigerant-based PVT-assisted heat pump water heating (PVTA-HPWH) system. *Solar Energy*, 122, 36-47.
- WATMUFF, J., CHARTERS, W. & PROCTOR, D. 1977. Solar and wind induced external coefficients-solar collectors. *Cooperation Mediterraneenne pour l'Energie Solaire*, 1, 56.
- XU, G., ZHANG, X. & DENG, S. 2011. Experimental study on the operating characteristics of a novel low-concentrating solar photovoltaic/thermal integrated heat pump water heating system. *Applied Thermal Engineering*, 31, 3689-3695.
- XU, G., ZHANG, X. & YANG, L. 2008. Performance evaluation of PV/T integrated heat pump using two different collector/evaporators. *CIESC Journal*, 59, 224-229.
- YAN, Y.-Y., LIO, H.-C. & LIN, T.-F. 1999. Condensation heat transfer and pressure drop of refrigerant R-134a in a plate heat exchanger. *International Journal of Heat and Mass Transfer*, 42, 993-1006.
- YANG, J., JACOBI, A. & LIU, W. 2017. Heat transfer correlations for single-phase flow in plate heat exchangers based on experimental data. *Applied Thermal Engineering*, 113, 1547-1557.
- ZONDAG, H. A. 2008. Flat-plate PV-Thermal collectors and systems: A review. *Renewable and Sustainable Energy Reviews*, 12, 891-959.

Appendix 1



DLE5.7CN Energy-optimized LBP/MBP Compressor R290 220-240V 50Hz

General

Code number	102H4653
Approvals	EN 60335-2-34 w. Annex AA
Compressors on pallet	100

Application

Application	LBP/MBP	
Frequency	Hz	50 60
Evaporating temperature	°C	-35 to 7.2 -
Voltage range	V	198 to 254 -
Max. condensing temperature continuous (short)	°C	55 (65) -
Max. winding temperature continuous (short)	°C	125 (135) -

Cooling requirements

Frequency	Hz	50			60		
Application		LBP	MBP	HBP	LBP	MBP	HBP
32°C		F ₂	F ₂	-	-	-	-
38°C		F ₂	F ₂	-	-	-	-
43°C		F ₂	F ₂	-	-	-	-

Remarks on application:

For evaporation temperatures higher than 0 °C do not run compressor at condensing temperatures higher 50 °C in steady state operation.

Motor

Motor type	CSIR/RSIR/RSCR	
LRA (rated after 4 sec. UL984), HST LST	A	8.8 7.4
Cut in Current, HST LST	A	8.8 11.9
Resistance, main start winding (25°C)	Ω	13.5 14.3

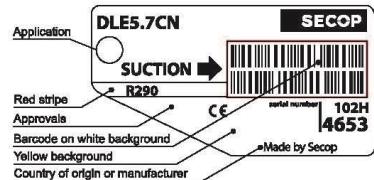
Design

Displacement	cm ³	5.70
Oil quantity (type)	cm ³	230 (polyolester)
Maximum refrigerant charge	g	150
Free gas volume in compressor	cm ³	1465
Weight without electrical equipment	kg	8.0

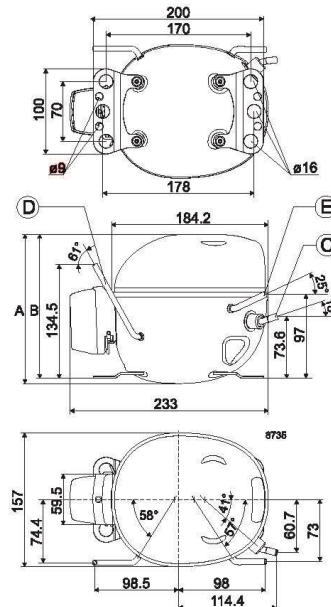
Dimensions

Height	mm	A	175
		B	169
		B1	-
		B2	-
Suction connector	location/I.D. mm angle	C	8.2 18°
	material comment		Copper Rubber plug
Process connector	location/I.D. mm angle	D	6.2 61°
	material comment		Copper Rubber plug
Discharge connector	location/I.D. mm angle	E	6.2 25°
	material comment		Copper Rubber plug
Oil cooler connector	location/I.D. mm angle	F	-
	material comment		-
Connector tolerance	I.D. mm		±0.09

Remarks:



- S = Static cooling normally sufficient
- O = Oil cooling
- F₁ = Fan cooling 1.5 m/s
(compressor compartment temperature equal to ambient temperature)
- F₂ = Fan cooling 3.0 m/s necessary
- SG = Suction gas cooling normally sufficient
- = not applicable in this area



EN 12900 LBP

220V, 50Hz, CSIR/RSIR, fan cooling F₂

Evap. temp. in °C	-45	-40	-35	-30	-25	-23.3	-20	-15	-10	-6.7	-5	0	5	7.2	10	15	20
Capacity in W			169	215	267	287	328	400	483	547	582	697	832	897			
Power cons. in W			145	162	179	184	194	208	222	230	234	245	256	260			
Current cons. in A			1.13	1.17	1.21	1.23	1.25	1.30	1.34	1.36	1.38	1.42	1.45	1.47			
COP in W/W			1.17	1.33	1.50	1.56	1.69	1.92	2.18	2.38	2.49	2.84	3.25	3.45			

EN 12900 MBP

220V, 50Hz, CSIR/RSIR, fan cooling F₂

Evap. temp. in °C	-45	-40	-35	-30	-25	-23.3	-20	-15	-10	-6.7	-5	0	5	7.2	10	15	20
Capacity in W			158	203	252	271	309	376	454	513	546	654	780	841			
Power cons. in W			148	167	184	190	201	218	233	243	248	262	276	281			
Current cons. in A			1.13	1.18	1.23	1.24	1.27	1.32	1.37	1.40	1.42	1.47	1.52	1.54			
COP in W/W			1.07	1.22	1.37	1.42	1.54	1.73	1.95	2.11	2.20	2.49	2.83	2.99			

ASHRAE LBP

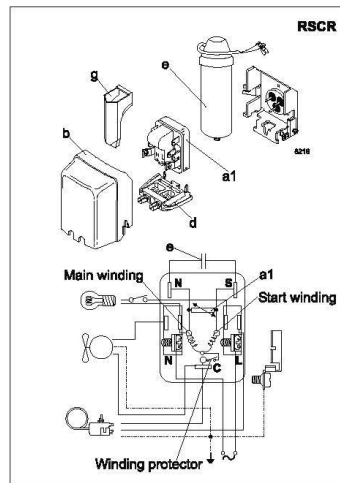
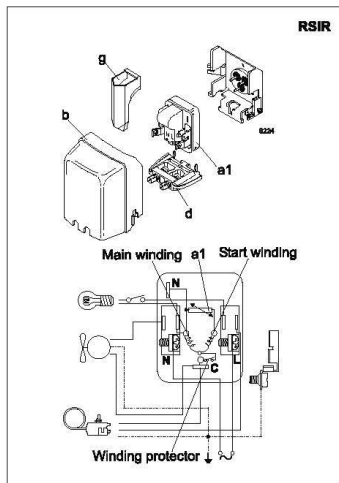
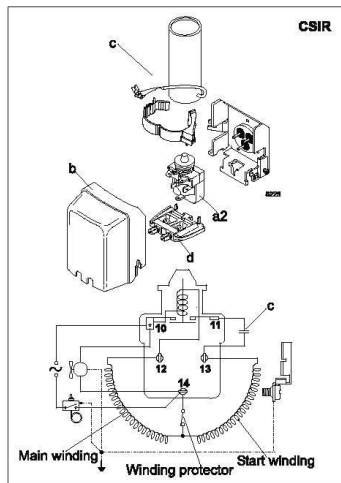
220V, 50Hz, CSIR/RSIR, fan cooling F₂

Evap. temp. in °C	-45	-40	-35	-30	-25	-23.3	-20	-15	-10	-6.7	-5	0	5	7.2	10	15	20
Capacity in W			168	220	277	298	341	415	501	566	603	722	862	930			
Power cons. in W			149	169	188	195	208	227	245	258	264	282	300	308			
Current cons. in A			1.15	1.20	1.26	1.28	1.32	1.38	1.45	1.50	1.52	1.59	1.67	1.70			
COP in W/W			1.12	1.30	1.47	1.53	1.64	1.83	2.04	2.20	2.28	2.56	2.87	3.03			

ASHRAE MBP/HBP

220V, 50Hz, CSIR/RSIR, fan cooling F₂

Evap. temp. in °C	-45	-40	-35	-30	-25	-23.3	-20	-15	-10	-6.7	-5	0	5	7.2	10	15	20
Capacity in W			150	197	247	266	304	370	447	505	537	643	766	827			
Power cons. in W			148	167	186	193	205	224	243	255	261	279	296	304			
Current cons. in A			1.15	1.20	1.26	1.28	1.32	1.38	1.45	1.50	1.52	1.59	1.67	1.70			
COP in W/W			1.02	1.18	1.33	1.38	1.48	1.65	1.84	1.98	2.06	2.31	2.59	2.72			



Accessories for	DLE5.7CN	Figure	Code number
PTC starting device	6.3 mm spade connectors	a1	-
	4.8 mm spade connectors		-
ePTC starting device	4.8 mm spade connectors	a2	103N0050
Starting relay	6.3 mm spade connectors	a2	117U7015
Start. capacitor 80 µF	6.3 mm spade connectors	c	117U5015
Cover		b	103N0491
Run capacitor 5 µF (optional)	6.3 mm spade connectors	e	-
	4.8 mm spade connectors	e	117-7129
Cord relief		d	103N1010
Protection screen for PTC		g	-

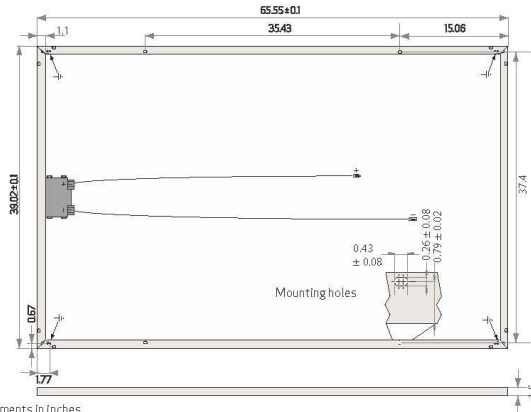
Test conditions	EN 12900		ASHRAE	
	LBP	MBP	LBP	MBP
Condensing temperature	40°C	45°C	54.4°C	54.4°C
Ambient temperature	32°C	32°C	32.2°C	35°C
Suction gas temperature	20°C	20°C	32.2°C	35°C
Liquid temperature	no subcooling		32.2°C	46.1°C

Mounting accessories		Code number
Bolt joint for one comp.	Ø: 16 mm	118-1917
Bolt joint in quantities	Ø: 16 mm	118-1918
Snap-on in quantities	Ø: 16 mm	118-1919

Secop can accept no responsibility for possible errors in catalogues, brochures and other printed material. Secop reserves the right to alter its products without notice. This also applies to products already on order provided that such alterations can be made without subsequential changes being necessary in specifications already agreed. All trademarks in this material are property of the respective companies. Secop and the Secop logotype are trademarks of Secop GmbH. All rights reserved. www.secop.com

Appendix 2

REC PEAK ENERGY BLK SERIES



All measurements in inches

ELECTRICAL DATA @ STC	REC240PE BLK	REC245PE BLK	REC250PE BLK	REC255PE BLK	REC260PE BLK	REC265PE BLK
Nominal Power - P_{MPP} (Wp)	240	245	250	255	260	265
Watt Class Sorting - (W)	0/+5	0/+5	0/+5	0/+5	0/+5	0/+5
Nominal Power Voltage - V_{MPP} (V)	29.7	30.1	30.2	30.5	30.7	30.9
Nominal Power Current - I_{MPP} (A)	8.17	8.23	8.30	8.42	8.50	8.58
Open Circuit Voltage - V_{OC} (V)	36.8	37.1	37.4	37.6	37.8	38.1
Short Circuit Current - I_{SC} (A)	8.75	8.80	8.86	8.95	9.01	9.08
Panel Efficiency (%)	14.5	14.8	15.1	15.5	15.8	16.1

Analysed data demonstrates that 99.7% of panels produced have current and voltage tolerance of $\pm 3\%$ from nominal values. Values at standard test conditions STC (airmass AM 1.5, irradiance 1000 W/m², cell temperature 25°C). At low irradiance of 200 W/m² (AM 1.5 and cell temperature 25°C) at least 97% of the STC panel efficiency will be achieved.

ELECTRICAL DATA @ NOCT	REC240PE BLK	REC245PE BLK	REC250PE BLK	REC255PE BLK	REC260PE BLK	REC265PE BLK
Nominal Power - P_{MPP} (Wp)	183	187	189	193	197	202
Nominal Power Voltage - V_{MPP} (V)	27.7	28.1	28.3	28.5	29.0	29.4
Nominal Power Current - I_{MPP} (A)	6.58	6.64	6.68	6.77	6.81	6.90
Open Circuit Voltage - V_{OC} (V)	34.4	34.7	35.0	35.3	35.7	36.0
Short Circuit Current - I_{SC} (A)	7.03	7.08	7.12	7.21	7.24	7.30

Nominal operating cell temperature NOCT (800 W/m², AM 1.5, windspeed 1 m/s, ambient temperature 20°C).

CERTIFICATION



UL 1703, IEC 62716 (ammonia resistance) & IEC 61701 (salt mist corrosion - severity level 6).

WARRANTY

10 year product warranty.
25 year linear power output warranty (max. degradation in performance of 0.7% p.a.).

16.1% EFFICIENCY
10 YEAR PRODUCT WARRANTY
25 YEAR LINEAR POWER OUTPUT WARRANTY
DUTY*FREE US IMPORT DUTY FREE

TEMPERATURE RATINGS

Nominal Operating Cell Temperature (NOCT)	45.7°C ($\pm 2^\circ\text{C}$)
Temperature Coefficient of P_{MPP}	-0.40 %/ $^\circ\text{C}$
Temperature Coefficient of V_{OC}	-0.27 %/ $^\circ\text{C}$
Temperature Coefficient of I_{SC}	0.024 %/ $^\circ\text{C}$

GENERAL DATA

Cell Type:	60 REC PE multi-crystalline 3 strings of 20 cells with bypass diodes
Glass:	1/8" mm solar glass with anti-reflection surface treatment
Back Sheet:	Double layer highly resistant polyester
Frame:	Anodized aluminum (black)
Junction Box:	IP67 rated 4 mm ² solar cable, 35" + 47"
Connectors:	Multi-Contact MC4 (4 mm ²)
Origin:	Made in Singapore

MAXIMUM RATINGS

Operational Temperature:	-40 ... +85°C
Maximum System Voltage:	600 V
Design Load:	75.2 lbs/ft ² (3600 Pa)* 33.4 lbs/ft ² (1600 Pa)* *Refer to installation manual
Max Series Fuse Rating:	15 A
Max Reverse Current:	15 A

MECHANICAL DATA

Dimensions:	65 1/2 x 39 x 1 1/2 in
Area:	17.76 ft ²
Weight:	39.6 lbs

Note! All given specifications are provisional data only and subject to change without notice at any time.

Ref: NE-05-04-R-1213

REC is a leading global provider of solar energy solutions. With more than 15 years of experience, we offer sustainable, high performing products, services and investments for the solar industry. Together with our partners, we create value by providing solutions that better meet the world's growing energy needs. Founded in Norway, REC is listed on the Oslo Stock Exchange (ticker: RECSOL) and headquartered in Singapore. Our 1,500 employees worldwide generated revenues of NOK 4.1 billion in 2012.



Appendix 3



Risk Assessment Report

PV-T R290 heat pump test rig


Prosjektnavn	Improved Energy Efficiency with Solar Panels in Combinations with Cooling / Heating System
Apparatur	PV-T R290 heat pump test rig
Enhet	NTNU
Apparaturansvarlig	Trygve M. Eikevik
Prosjektleder	Trygve M. Eikevik
HMS-koordinator	Morten Grønli
HMS-ansvarlig (linjeleder)	Olav Bolland
Plassering	Refrigeration Lab
Romnummer	C159
Risikovurdering utført av	Chengyang Jiang, Håvard Rekstad, Lars Konrad Sørensen

Approval:

Apparatur kort (UNIT CARD) valid for:	12 months
Forsøk pågår kort (EXPERIMENT IN PROGRESS) valid for:	12 months

Rolle	Navn	Dato	Signatur
Prosjektleder	Trygve M. Eikevik	19/4-2017	
HMS koordinator	Morten Grønli		
HMS ansvarlig (linjeleder)	Olav Bolland		

ATTACHMENT E: PROCEDURE FOR RUNNING EXPERIMENTS

Prosjekt Improved Energy Efficiency with Solar Panels in Combinations with Cooling / Heating System		
Apparatur PV/T R290 heat pump test rig	Dato	Signatur
Prosjektleder Trygve M. Eikevik	19/4-2017	


	Completed
Conditions for the experiment:	
Experiments should be run in normal working hours, 08:00-16:00 during winter time and 08.00-15.00 during summer time. Experiments outside normal working hours shall be approved.	
One person must always be present while running experiments, and should be approved as an experimental leader.	
An early warning is given according to the lab rules, and accepted by authorized personnel.	
Be sure that everyone taking part of the experiment is wearing the necessary protecting equipment and is aware of the shut down procedure and escape routes.	
Preparations	Carried out
Post the "Experiment in progress" sign.	
<i>Start up procedure</i> 1. Check the connection of the electric parts; 2. Switch on the inverter; 3. Fill up the water tank; 4. Switch on the water pump to circulate the water to condenser; 5. Data logger ready to log experiment; 6. Switch on the compressor; 7. Check standstill conditions for temperature and pressure.	
During the experiment 1. Data logger autosave the data; 2. Regulate the flow rate of the water circulation 3. Check the pressure every 5 minutes	
<i>Control of temperature, pressure e.g.</i>	
End of experiment 1. Switch off the compressor; 2. Stop the data logger; 3. Switch off the water pump; 4. Switch off the inverter; 5. Empty the water tank.	
<i>Shut down procedure</i>	
Remove all obstructions/barriers/signs around the experiment.	
Tidy up and return all tools and equipment.	
Tidy and cleanup work areas.	

	Return equipment and systems back to their normal operation settings (fire alarm)	
	To reflect on before the next experiment and experience useful for others	
	Was the experiment completed as planned and on scheduled in professional terms?	
	Was the competence which was needed for security and completion of the experiment available to you?	
	Do you have any information/ knowledge from the experiment that you should document and share with fellow colleagues?	

Operator(s):

Navn	Dato	Signatur
Chengyang Jiang	18.4. 2017	Chengyang Jiang


ATTACHMENT F: TRAINING OF OPERATORS

Prosjekt Improved Energy Efficiency with Solar Panels in Combinations with Cooling / Heating System		
Apparatur PV/T R290 heat pump test rig	Dato	Signatur
Prosjektleder Trygve M. Eikevik	19/4-2017	

Knowledge about EPT LAB in general	
Lab	
<ul style="list-style-type: none"> • Access • routines and rules • working hour 	
Knowledge about the evacuation procedures.	
Activity calendar for the Lab	
Early warning, iept-experiments@ivt.ntnu.no	
Knowledge about the experiments	
Procedures for the experiments	
Emergency shutdown.	
Nearest fire and first aid station.	

I hereby declare that I have read and understood the regulatory requirements has received appropriate training to run this experiment and are aware of my personal responsibility by working in EPT laboratories.

Operator(s):

Navn	Dato	Signatur
Chengyang Jiang	18.4.2017	

Appendix 4

\$tabstops 0.2 0.4 0.6 0.8 7 in

\$unitsystem SI Mass kJ kg C Degree

//Solar panels in combination with cooling/heating system (PV/T heat pump system)

//Function used to calculate convective boiling heat transfer

Function **evap**(Fluid\$, T_sat, G, d, x, q``)

{ \$evap

This function calculates the convective boiling heat transfer coefficient in tubes using Gao(2012) and Shah(1982) correlation.

inputs:

Fluid\$=Fluid name

T_sat = saturation temperature [C,K,F,R]

G = mass velocity [kg/m²-s] or [lbm/ft²-hr]

d = inner tube diameter [m]

x = quality (0 to 1)

q`` = heat flux [W/m²] or [Btu/hr-ft²] }

If (x<0) or (x>1) **Then Call error**('quality must be between 0 and 1.')

If (G<0) **Then Call error**('The mass flow rate must be a finite positive value.')

If (x<=0.001) **Then**

x=0.001 "approximate value of quality--substituted because the Lockhart-Martinelli parameter is undefined at x=0"

If (x>0.999) **Then**

x=0.999 "approximate value of quality--substituted because the two-phase multiplier is undefined at x=1"

rho_l=**density**(Fluid\$, T=T_sat, x=0)

"density of saturated liquid"

rho_v=**density**(Fluid\$, T=T_sat, x=1)

"density of saturated vapor"

k_v=**conductivity**(Fluid\$, T=T_sat, x=1)

"thermal conductivity of saturated vapor"

k_l=**conductivity**(Fluid\$, T=T_sat, x=0)

"thermal conductivity of saturated liquid"

mu_v=**viscosity**(Fluid\$, T=T_sat, x=1)

"viscosity of saturated vapor"

mu_l=**viscosity**(Fluid\$, T=T_sat, x=0)

"viscosity of saturated liquid"

Pr_l=**prandtl**(Fluid\$, T=T_sat, x=0)

"Prandtl of saturated liquid"

Pr_v=**prandtl**(Fluid\$, T=T_sat, x=1)

"Prandtl of saturated vapor"


```

P_c=p_crit(Fluid$)
P_sat=p_sat(Fluid$,T=T_sat)
P_red=P_sat/P_c
X_tt=((1-x)/x)^0.9*(rho_v/rho_l)^0.5*(mu_l/mu_v)^0.1
omega=-log10(P_red)
R_p=1
    "roughness (um)"
m=0.12-0.2*log10(R_p)
M_r=44.1
    "molecular weight of the refrigerant(R290)"
h_NB=55*q``^0.67*M_r^(-0.5)*P_red^m*omega^(-0.55)
Re_l=G*(1-x)*d/mu_l
e=2.35/(1/X_tt+0.213)^0.736
Re=Re_l*e^1.25
S=1/(1+2.53*10^(-6)*Re^1.17)
h_l=0.023*Re_l^0.8*Pr_l^0.4*k_l/d
h_e=S*h_NB+e*h_l
evap=h_e
End

```

Function evap_avg(Fluid\$, T_sat, G, d, x_1, x_2, q`)

{\$evap_avg

This function calculates the average convection boiling heat transfer coefficient in tubes.

inputs:

Fluid\$=Fluid name

T_sat = saturation temperature [C,K,F,R]

G = mass velocity [kg/m²-s] or [lbm/ft²-hr]

d = inner tube diameter [m]

x_1 = minimum quality (0 to 1)

x_2 = maximum quality

q` = heat flux [W/m²] or [Btu/hr-ft²] }

N=50

SumH=0

If (x_1<0) or (x_1>1) **Then Call error**('quality must be between 0 and 1')

If (x_2<0) or (x_2>1) **Then Call error**('quality must be between 0 and 1')

i=0

Repeat

 x=x_1+(x_2-x_1)*(i/N)

 h_x=evap(Fluid\$, T_sat, G, d, x, q`)

 SumH=SumH+h_x

 i=i+1

Until (i>=N+0.1)

evap_avg=SumH/(N+1)

End

//Function used to calculate the convection condensation heat transfer coefficient

Function cond_bphx(Fluid\$, T_sat, G, D_h, x)

{\$cond_bphx

This function calculates the convection condensation heat transfer coefficient using the Yan. Yi (1999) correlation.

Inputs:

Fluid\$ = Fluid name

T_sat = saturation temperature, here means the condensing temperature [C, K]

G = mass flux [kg/m²-s] or [lbm/ft²-hr]

D_h = Hydraulic diameter [m]

x = quality (0-1) }

If (x<0) or (x>1) **Then Call error**('quality must be between 0 and 1.')

If (G<0) **Then Call error**('The mass flow rate must be a finite positive value.')

If (x<=0.001) **Then**

x=0.001 "approximate value of quality--substituted because the Lockhart-Martinelli parameter is undefined at x=0"

If (x>0.999) **Then**

x=0.999 "approximate value of quality--substituted because the two-phase multiplier is undefined at x=1"

rho_l=**density**(Fluid\$, T=T_sat, x=0)

rho_g=**density**(Fluid\$, T=T_sat, x=1)

k_l=**conductivity**(Fluid\$, T=T_sat, x=0)

mu_l=**viscosity**(Fluid\$, T=T_sat, x=0)

mu_g=**viscosity**(Fluid\$, T=T_sat, x=1)

Pr_l=**prandtl**(Fluid\$, T=T_sat, x=0)

P_c=**p_crit**(Fluid\$)

P_sat=**p_sat**(Fluid\$, T=T_sat)

P_red=P_sat/P_c

{the correlation for heat transfer of refrigerant in a brazed plate heat exchanger, Yan Yi (1999).}

{G_eq=G*(1-x+x*(rho_l/rho_g)^{0.5})

Re_eq=G_eq*D_h/mu_l

h_m=4.118*Re_eq^{0.4}*Pr_l^{0.3333}*k_l/D_h}

{the correlation for heat transfer of refrigerant in a brazed plate heat exchanger, Palmer(2000).}

X_tt=((1-x)/x)^{0.9}*(rho_g/rho_l)^{0.5}*(mu_l/mu_g)^{0.1}

phi=(1+12/X_tt+1/X_tt/X_tt)^{0.5}

omega=-**log10**(P_red)

Ga=rho_l*(rho_l-rho_g)*9.8[m/s²]*D_h³/mu_l²

Re_l=G*(1-x)*D_h/mu_l

{from focke 1985}

If(Re_l<=150) **Then**

Nu_l=1.89*Re_l^{0.46}*Pr_l^{0.5}

```

Else
  If(Re_l<=600) Then
    Nu_l=0.57*Re_l^0.7*Pr_l^0.5
  Else
    Nu_l=1.112*Re_l^0.6*Pr_l^0.5
  Endif
Endif
Nu_r=Nu_l^0.387*phi^0.0824*Ga^0.346*P_red^1.5*omega^1.5
h_m=Nu_r*k_l/D_h
cond_bphx=h_m
End

```

Function cond_bphx_avg(Fluid\$, T_sat, G, D_h, x_1, x_2)

{cond_bphx_avg

This function determine the average heat transfer coefficient for condensation in a brazed plate heat exchanger.

inputs:

Fluid\$ = Fluid name

T_sat = saturation temperature, here means the condensing temperature [C, K]

G = mass flux [kg/m²-s] or [lbm/ft²-hr]

D_h = Hydraulic diameter [m]

x_1 = minimum quality

x_2 = maximum quality }

N=50

SumH=0

If (x_1<0) or (x_1>1) Then Call error('quality must be between 0 and 1')

If (x_2<0) or (x_2>1) Then Call error('quality must be between 0 and 1')

i=0

Repeat

x=x_1+(x_2-x_1)*(i/N)

h_x=cond_bphx(Fluid\$, T_sat, G, D_h, x)

SumH=SumH+h_x

i=i+1

Until (i>=N+0.1)

cond_bphx_avg=SumH/(N+1)

End

//function used to calculate the pressure in evaporator

Function dp\dz_2phase_horiz(Fluid\$,m_dot\A,P,d,x)

{dp\dz_2phase_horiz

dp\dz_2phase_horiz returns the pressure gradient in a horizontal tube in which a fluid is evaporating

Inputs:

Fluid\$ is the name of the real fluid that is evaporating

$m_{\dot{V}}$ is the mass flow rate divided by the cross-sectional area

P is the saturation pressure

d is the inner diameter of the tube

x is the local quality

UP\$=unitsystem\$('Pressure')

P=P*convert(Pa,UP\$)

rho_L=density(Fluid\$,P=P,x=0)

mu_L=viscosity(Fluid\$,P=P,x=0)

rho_g=density(Fluid\$,P=P,x=1)

mu_g=viscosity(Fluid\$,P=P,x=1)

If (unitsystem('SI')=0) **Then**

rho_L=rho_L*convert(lb_m/ft^3,kg/m^3)

rho_g=rho_g*convert(lb_m/ft^3,kg/m^3)

mu_L=mu_L*convert(lb_m/ft-hr,kg/m-s)

mu_g=mu_g*convert(lb_m/ft-hr,kg/m-s)

Endif

Re_L= $m_{\dot{V}}d/\mu_L$

f_L=0.079/Re_L^0.25

Re_g= $m_{\dot{V}}d/\mu_g$

f_g=0.079/Re_g^0.25

a=f_L^2* $m_{\dot{V}}^2/(d\rho_L)$

b=f_g^2* $m_{\dot{V}}^2/(d\rho_g)$

G=a+2*(b-a)*x

$dp/dz_{2phase_horiz}=G*(1-x)^{1/3}+b*x^3$

End

Function **deltap_2phase_horiz**(Fluid\$, G, P_i, d, L, x_in, x_out)

{ DELTAP_2phase_horiz

Function DELTAP_2phase_horiz calculates DELTAP, the pressure drop in horizontal tubes in which there is two-phase heat transfer

Inputs:

Fluid\$ is a real fluid in the EES data base

G is the mass velocity, i.e., the mass flow rate of fluid through the tube divided by the cross-sectional area of the tube

P_i is the entering pressure

d is the tube diameter

x_in and x_out are the entering and exiting qualities, respectively}

UP\$=unitsystem\$('Pressure')

If (unitsystem('SI')=1) **Then**

UMF\$='kg/s'

UG\$='kg/m^2-s'

UL\$='m'

Else

```

UMF$='lbm/hr'
UG$='lbm/hr-ft^2'
UL$='ft'

```

Endif

```

G=G*convert(UG$,'kg/m^2-s')
P_i=P_i*convert(UP$,'Pa')
d=d*convert(UL$,'m')
L=L*convert(UL$,'m')

```

```

m_dot\A=G
x_1=x_in
P=P_i
ict=1
N=10

```

Repeat

```

x_2=x_in+(x_out-x_in)/N *ict
ict=ict+1
x=(x_2+x_1)/2
P_1=P
dP=dp\dz_2phase_horiz(Fluid$,m_dot\A,P,d,x)*L/N
P_2=P_1-dp
P_2=P_1-dp-(m_dot\A^2*(mterm(Fluid$,m_dot\A,x_2,P_2)-mterm(Fluid$,m_dot\A,x_1,P_1)))
P_avg=(P_1+P_2)/2

```

```

dp=dp\dz_2phase_horiz(Fluid$,m_dot\A,P_avg,d,x)*L/N

```

```

P=P-dp-(m_dot\A^2*(mterm(Fluid$,m_dot\A,x_2,P_2)-mterm(Fluid$,m_dot\A,x_1,P_1)))
x_1=x_2

```

Until (ict>N+0.5)

```

deltap_2phase_horiz=abs(P_i-P)*convert('Pa',UP$)

```

End

//caculation

Procedure

```

pvthp(T_amb,T_iw,T_ap0,m_dot_w,G_s,v_wind,dt:T_e,T_c,T_p,T_ap,P_e,P_c,Q_e,Q_c,T_w,W_com
,E,eta_p,COP)

```

{\$PVTHP

This procedure is the main program to simulate the performance of the PV/T heat pump system.

The parameters of the main components were included in this procedure.

inputs:

```

T_amb = ambient temperature [C]
T_iw = inlet water temperature [C]
T_ap0 = initial aluminum plate temperature [C]

```

$m_{\dot{w}}$ = mass flow rate of water [kg/s]

G_s = global solar irradiance [W/m^2]

v_{wind} = wind speed [m/s]

dt = time step [s]

outputs:

T_e = evaporation temperature

T_c = condensing temperature

T_p = plate temperature

T_{ap} = aluminum plate temperature

P_e = evaporation pressure

P_c = condensing pressure

Q_e = evaporation power

Q_c = condensing power

T_w = average water temperature in water tank

W_{com} = power consumption of compressor

E = PV electricity power

η_{p} = electricity efficiency of PV panel

COP = coefficient of performance}

"!Specification of The PV/T Heat pump system"

"refrigerant"

$R\$$ ='Propane'

"refrigent"

"Information of PV panel"

L_p =1.664

"length of the solar panel"

b_p =0.991

"width of the solar panel"

h_p =0.0381

"Thickness of frame of the solar panel"

A_p =1.65

"Area of the solar panel"

$A_f=(L_p+b_p)*2*h_p$

"Area of the frame"

η_{pth} =0.158

"panel efficiency at a standard test condition"

β_p =-

0.004 "teperature coefficient of P_{MPP} "

r_{gl} =0.04

"glass relectivity"

r_c =0.08

"PV cell relectivity"

ϵ_{gl} =0.85

"glass emissivity"

epsilon_aal=0.77
 "anodized aluminum emissivity"
 I_sc=8.95
 "short circuit current"
 U_oc=37.8
 "open circuit voltage"
 I_mpp=8.42
 "max power current"
 U_mpp=30.5
 "max power voltage"
 E_mpp=260
 "max output power"
 sigma_ins=0.025
 "thickness of the insulation plate"
 lambda_ins=0.04
 "heat conductivity of the insulation plate"
 sigma_bs=0.0005
 "thickness of the back sheet"
 lambda_bs=0.17
 "heat conductivity of the back sheet (polyester)"
 sigma_g=0.0032
 "thickness of the glass"
 lambda_g=1.05
 "heat conductivity of the glass"
 m_p=30[kg]
 "weight of the aluminum plate"
 C_al=0.88[kJ/kg-
 C] "thermal capacity of aluminum"
 "Evaporator"
 L_e=9
 "length of the copper tube"
 N_e=2
 "number of tubes"
 d_oe=3/16***convert**(inch,m)
 "outer diameter"
 sigma_e=0.76***convert**(mm,m)
 "thickness of tube"
 d_ie=d_oe-
 2*sigma_e "inner diameter"
 sigma_bp=8***convert**(mm,m)
 "backplate thickness"
 "Compressor DLE5.7CN"
 RPM=2900
 "RPM of the compressor"

```

V_dis=5.7e-
6      "displacement volume"
V_swept=V_dis*RPM*convert(m^3-rev/min-
rev,m^3/s) "swept volume"
lambda_v=0.8
      "volumetric efficiency"
eta_is=0.64
      "isentropic efficiency"
k=1.4
      "polytropic exponent"
      "Thermostatic Expansion Valve"
T_sh=9
      "super heat (internally expansion valve)"
      "BPHX condenser"
D_h=0.004
[m]    "Hydraulic diameter"
s_w=0.0014782
[m^2]  "Sectional area on water side"
s_r=0.0013304
[m^2]  "Sectional area on refrigerant side"
R_p=7.478e-4
[k/w]  "Thermal resistance of the plate"
s_plate=0.216
[m^2]  "Total heat exchange area of the plate heat exchanger"

"! Calculation"
"Step 1, assume initial Evaporating T and Condensing T and Panel T"
  T_e=T_amb-
10[C]  "Evaporating Temperature (assumed)"
  T_c=T_iw+5[C]
      "Condensing Temperature(assumed)"

"Step 2, Compressor Calculation"
01:
T_icom=T_e+T_sh
      "!01:inlet temperature of compressor"
P_icom=p_sat(R$, T=T_e)
      "inlet pressure of compressor"
P_ocom=p_sat(R$, T=T_c)
      "outlet pressure of the compressor"
rho_icom=density(R$, T=T_icom, P=P_icom)
      "inlet density of propane"
m_dot_r=rho_icom*V_swept*lambda_v
      "mass flow of propane"

```


$W_{com} = \lambda v_{swept} P_{icom} k / (k-1) * ((P_{ocom} / P_{icom})^{(k-1)/k} - 1) / 0.9 + 0.1$ [kW] "compressor power"
 $G_{r_e} = 4 * m_{dot_r} / (\pi * d_{ie}^2) / N_e$
 "mass velocity of propane in evaporator"
 $G_{r_c} = m_{dot_r} / s_r$
 "mass velocity of propane in condenser"
 $s_{icom} = \text{entropy}(R, T=T_{icom}, P=P_{icom})$
 "inlet entropy of propane"
 $h_{icom} = \text{enthalpy}(R, T=T_{icom}, P=P_{icom})$
 "inlet enthalpy of propane"
 $h_{is} = \text{enthalpy}(R, P=P_{ocom}, s=s_{icom})$
 "isentropic enthalpy of compressor"
 $h_{ocom} = h_{icom} + (h_{is} - h_{icom}) / \eta_{is}$ "outlet enthalpy of the compressor"
 $T_{ocom} = \text{temperature}(R, P=P_{ocom}, h=h_{ocom})$
 "outlet enthalpy of the compressor"

"Step 3, Condenser calculation"

$T_{sc} = 2$
 "subcooling temperature"
 $P_c = P_{ocom}$
 "condensing pressure"
 $T_{icond} = T_{ocom}$
 "inlet temperature of condenser"
 $h_{icond} = h_{ocom}$
 "inlet enthalpy of condenser"
 $T_{ocond} = T_c - T_{sc}$
 T_{sc} "outlet temperature of condenser"
 $h_{ocond} = \text{enthalpy}(R, P=P_c, T=T_{ocond})$
 "outlet enthalpy of condenser"
 $Q_c = (h_{ocond} - h_{ocom}) * m_{dot_r}$
 "heating capacity"
 $T_{ow} = T_{iw} + Q_c / (m_{dot_w} * 4.2)$ [kJ/kg-C]
 "outlet water temperature of condenser"
 $h_{r_c} = \text{cond_bphx_avg}(R, T_c, G_{r_c}, D_h, 0)$
 1) "heat transfer coefficient of Refrigerant"
 $G_w = m_{dot_w} / s_w$
 "mass velocity of water in condenser"
 $T_{w_avg} = (T_{iw} + T_{ow}) / 2$
 "average water temperature"
 $P_w = 101$ [kPa]
 "assume the water pressure is 1 atm"

```

mu_w=viscosity(Water,T=T_w_avg,P=P_w)
Re_w=G_w*D_h/mu_w
"Renold number on water side"
Pr_w=prandtl(Water,T=T_w_avg,
P=P_w) "Prandtl number"
k_w=conductivity(Water,T=T_w_avg,P=P_w)
"Conductivity"
{the correlation for heat transfer of water in a brazed plate heat exchanger, Yan Yi (1999).}
N_U_w=0.2121*Re_w^0.78*Pr_w^0.333
h_w=N_U_w*k_w/D_h
"heat transfer coefficient of water"
LMTD= Q_c*convert(kW,W)*(1/(s_plate*h_r_c)+1/(s_plate*h_w)+R_p)
"log-mean temperature difference"
C_c=2.718282^(T_ow-
T_iw)/LMTD) "constant used in the following equation"
T_c2=(C_c*T_ow-T_iw)/(C_c-1)
T_c:=(T_c+T_c2)/2
"correction of condensing temperature"
if(abs(T_c-T_c2)>0.01) Then Goto
01 !"judge1"

"Step 4, EXV calculation"
// The constant of the valve is unknown
h_ievap=h_ocond
"assume isoenthalpy"

"Step 5 Evaporator calculation"
P_e=P_icom
"evapration temperature"
x=quality(R$,T=T_e,h=h_ievap)
"inlet quality of the propane"
h_oevap=h_icom
"outlet enthalpy of the evaporator"
Q_e=(h_oevap-
h_ievap)*m_dot_r
"evaporation capacity"
{W_com=Q_c-
Q_e+0.07[kW]} "Compressor power"}
Q_tot=G_s*A_p*(1-r_gl)*(1-
r_c) "total energy gain"
//T_sky=T_amb
"Sky T indoor"
$checkunits off
T_sky=0.0552*(T_amb+T_zero#)^1.5-

```

```

T_zero# "sky temperature"
h_bar_p=2.8+3*v_wind
$checkunits on
T_p=0[C]
"Initial panel temperature"
02: T_p:=T_p+0.01
If (T_p>80) Then Call error('ERROR')

T_pk=converttemp(C,K,T_p)
"solar plate Temperature in K"
T_skyk=converttemp(C,K,T_sky)
"sky Temperature in K"
T_ambk=converttemp(C,K,T_amb)
"ambient Temperature in K"
Q_rad=(sigma#*epsilon_g*(T_pk^4-T_skyk^4)*A_p+sigma#*epsilon_aal*(T_sky^4-
T_ambk^4)*A_f)*convert(W,kW)
"Radiation power"
E=G_s*A_p*eta_pth*(1+beta_p*(T_p-
25[C])) "electricity power"
eta_p=eta_pth*(1+beta_p*(T_p-
25[C])) "solar panel efficiency"
Q_conv=h_bar_p*A_p*(T_p-
T_amb)*convert(W,kW)
"front panel convection power"
Q_loss=A_p*(T_p-
T_amb)/(1/h_bar_p+sigma_ins/lambda_ins)*convert(W,kW)
"panel back heat loss"
if(Q_loss<0) Then Q_loss=0
T_ap=T_p-Q_e*A_p*10[C-
m^2/kW] "aluminum plate temperature"
Q_al=m_p*c_al*(T_ap-T_ap0)/dt
if(abs(Q_tot/(Q_E+E+Q_rad+Q_conv+Q_loss+Q_al)-1)>0.001) Then Goto
02 "!!judge2"
q``=Q_e/(pi#*d_ie*L_e*N_e)*convert(kW/m^2,W/m^2)
"heat flux"
h_bar=evap_avg(R$, T_e, G_r_e, d_ie, x, 1,
q``)"heat transfer coefficient"
T_wall=T_ap-Q_e*convert(kW,W)/A_p*(sigma_bs/lambda_bs+sigma_g/lambda_g+0.01[C-
m^2/W]) "caculating the wall temperature"
T_e2=T_wall-
Q_e*convert(kW,W)/(h_bar*pi#*d_ie*L_e*N_e)

T_e:=(T_e+T_e2)/2
if(abs(T_e-T_e2)>0.01) Then Goto

```

01 "Ijudge3"

//Output Data

T_c:=T_c

T_p:=T_p

T_ap:=T_ap

P_e:=P_e

P_c:=P_c

Q_e:=Q_e

Q_c:=(-

h_ocond+h_ocom)*m_dot_r

"condenser capacity"

T_w:=Q_c*dt/(30[kg]*4.2[kj/kg-
C])+T_iw "average water

temperature"

W_com:=W_com

"Compressor power"

E:=E

eta_p:=eta_p

COP:=Q_c/W_com

End

// Input data

"Environmental Data"

{Array T_amb}

T_amb[1..39]=[22.49,22.62,22.84,22.54,22.87,23.02,23.17,23.13,23.33,23.17,23.38,23.40,23.56,23.4
0,23.59,23.91,24.14,24.46,24.58,24.31,24.69,24.54,24.75,24.59,24.61,24.83,25.20,25.32,25.64,25.53,
25.62,25.90,26.19,26.33,25.96,26.14,26.51,26.49,26.08]

{Array T_amb end}

{Array G_s}

G_s[1..39]=[0.84981056,0.91752392,0.91065788,0.8152436,0.8164274,0.85217816,0.88343048,0.88
934948,0.92202236,0.92028612,0.90978976,0.92565268,0.92075964,0.9186288,0.89013868,0.8962
1552,0.8866662,0.88224668,0.80009096,0.88879704,0.876012,0.72669536,0.812876,0.76726024,0.
90931624,0.94380428,0.8211626,0.93772744,0.92210128,0.92959868,0.92549484,0.91799744,0.90
292372,0.89913556,0.89779392,0.8823256,0.82716052,0.77917716,0.75692172]

{Array G_s end}

v_wind=2[m/s]

"water tank"

T_iw[1]=14.81[C]

"initial water T"

m_dot_w=0.1735[kg/s]

dt=120[s]

"step time"

T_ap0[1]=T_amb[1]

"initial aluminum plate temperature"

time[1]=0[s]

Call

pvthp(T_amb[1],T_iw[1],T_ap0[1],m_dot_w,G_s[1],v_wind,dt:T_e[1],T_c[1],T_p[1],T_ap[1],P_e[1],P_c[1],Q_e[1],Q_c[1],T_w[1],W_com[1],E[1],eta_p[1],COP[1])

Duplicate i=2,39

time[i]=dt*(i-1)

T_iw[i]=T_w[i-1]

T_ap0[i]=T_ap[i-1]

Call

pvthp(T_amb[i],T_iw[i],T_ap0[i],m_dot_w,G_s[i],v_wind,dt:T_e[i],T_c[i],T_p[i],T_ap[i],P_e[i],P_c[i],Q_e[i],Q_c[i],T_w[i],W_com[i],E[i],eta_p[i],COP[i])

End